https://ntrs.nasa.gov/search.jsp?R=19940006466 2020-06-16T21:26:28+00:00Z

NASA CONTRACTOR REPORT 191171

SPACE STORABLE

ROCKET TECHNOLOGY PROGRAM

SSRT

FINAL REPORT – OPTION 1 PROGRAM

AUGUST 1993

Prepared for:
NASA–LeRC
Cleveland, Ohio 44135
Contract NAS 3–26246

Prepared by:
M.L. Chazen, T. Mueller, T. Rust
TRW Applied Technology Division
Redondo Beach, California 90278

Approval:

Melvin Chazen
Program Manager

Albert Solbes, Manager
Combustion and Energy Technology Department

TRW Applied Technology Division
Space & Electronics Group

One Space Park
Redondo Beach, CA 90278
310.812.4321

SN 56372
K030-93-SRH-133
5 August 1993

National Aeronautics and Space Administration
Lewis Research Center
21000 Brookpark Road
Cleveland, Ohio 44135

Attention: Mr. James Biaglow, M/S SPTD-1

Subject: Contract NAS3-26246
Space Storable Rocket Technology (SSRT)
Option 1 Program Final Report

Dear Mr. Biaglow:

In accordance with the subject contract, enclosed are twenty-five (25) copies of the Final Report for the SSRT Option 1 Program. Distribution has been made as indicated on the attached distribution list.

This concludes the exciting Option 1 Program which demonstrated operation of the L02-N2H4 high performance engine. We expect the Option 2 program to be as exciting with even greater results.

Sincerely,

Saundra R. Hill
Contracts Manager
Applied Technology Division

cc: Mr. Wayne Girard, NASA-LeRC, M/S 500-305 (letter only)
Mel Chazen, 01/1170

DISTRIBUTION LIST FOR FINAL REPORT NAS3-26246

	No. of Copies
National Aeronautics & Space Administration Lewis Research Center 21000 Brookpark Road Cleveland, OH 44135	
Attn: Contracting Officer, M.S. 500-305	1
S.B. Foust, M.S. SPTD-1	2
Technology Utilization Office, M.S. 7-3	1
Report Control Office, M.S. 60-1	1
AFSC Liaison Office, M.S. 501-3	2
Library, M.S. 60-3	2
Office of Reliability & Quality Assurance, M.S. 500-211	1
T.L. Labus, M.S. 500-103	1
D.E. Sokolowski, M.S. 500-103	1
S.J. Schneider, M.S. SPTD-1	1
J.A. Biaglow, M.S. SPTD-1	25
National Aeronautics & Space Administration Headquarters Washington, DC 20546	
Attn: OFFICE OF AERONAUTICS & EXPLORATION TECHNOLOGY	
E. VanLandingham/RP	1
F. Curran/RM	1
G.M. Reck/RS	1
OFFICE OF SPACE FLIGHT	
Dir. Advanced Program Development/MD	1
National Aeronautics & Space Administration Ames Research Center Moffett Field, CA 94035	
Attn: Library	1
National Aeronautics & Space Administration Dryden Flight Research Center Edwards, CA 93523	
Attn: Library	1
National Aeronautics & Space Administration George C. Marshall Space Flight Center Huntsville, AL 35812	
Attn: Library	1
L.W. Jones/EP53	1
National Aeronautics & Space Administration Goddard Space Flight Center Greenbelt, MD 20771	
Attn: Library	1
National Aeronautics & Space Administration John F. Kennedy Space Center Kennedy Space Center, FL 32899	
Attn: Library	1

National Aeronautics & Space Administration
Lyndon B. Johnson Space Center
Houston, TX 77001

Attn: Library	1
C.A. Vaughan/EP	1
R.J. Taeuber/EP11	1
J.W. Griffin/EP42	1
R.A. Delventahl/EP42	1
W.C. Boyd/EP43	1

National Aeronautics & Space Administration
Langley Research Center
Langley Station
Hampton, VA 23365

Attn: Library	1
D.C. Freeman/367	
L.B. Garrett/288	

NASA Scientific & Technical Information Facility
P.O. Box 8757
Baltimore-Washington International Airport
Baltimore, MD 21240

Attn: Philip N. French	25

Jet Propulsion Laboratory
4800 Oak Grove Drive
Pasadena, CA 91103

Attn: Library	1
M.W. Dowdy/125-224	1

Defense Documentation Center
Cameron Station
Building 5
5010 Duke Street
Alexandria, VA 22314

Attn: TISIA	1

Defense Advanced Research Projects Agency
1400 Wilson Blvd.
Washington, DC 22209

Attn: Library	1

Aeronautical System Division
Air Force Systems Command
Wright-Patterson Air Force Base
Dayton, OH

Attn: Library	1
NAZ/Capt. T.K. Roberts	1

Dept. of the Air Force
OLAC, Phillips Laboratory (AFSC)
Edwards AFB, CA 93523
Attn: Library 1
RKLC/B.R. Bornhorst 1
RKLC/D. Barland 1

Space Division
Los Angeles Air Force Station, CA 90009
Attn: Library 1

Bureau of Naval Weapons
Department of Navy
Washington, DC 20546
Attn: Library 1

Picatinny Arsennal
Dover, NJ 07801
Attn: Library 1

U.S. Naval Research Laboratory
Washington, DC 20390
Attn: Library 1

Marquardt Coporation
16555 Saticoy Street
Box 2013 South Annex
Van Nuys, CA 91409
Attn: Library 1
R.C. Stechman 1

Martin Marietta Corporation
P.O. Box 179
Denver, CO 80201
Attn: Library 1

McDonnell Douglas Astronautics
5301 Bolsa Avenue
Huntington Beach, CA 92647
Attn: Library 1
T. Shumate 1

Pratt & Whitney Aircraft Group
United Technologies Corporation
P.O. Box 2691
West Palm Beach, FL 33402
Attn: Library 1

Rocketdyne Division
Rockwell International
6633 Canoga Avenue
Canoga Park, CA 91304
Attn: Library 1
G.L. Briley 1
R.S. Iacabucci 1

Space Systems Division
Rockwell International
12214 Lakewood Blvd
Downey, CA 90241
Attn: Library 1
D.L. Gerhardt 1

Rocket Research Corporation
Willow Road at 116th Street
Redmond, WA 98052
Attn: Library 1

Boeing Aerospace Company
P.O. Box 3999
Seattle, WA 98124
Attn: Library 1
J.S. Meserole/M.S. 82-23

John Hopkins University
Applied Physics Laboratory
John Hopkins Road
laurel, MD 20810
Attn: Library 1

General Dynamics/Convair
P.O. Box 80847
San Diego, CA 92138
Attn: Library 1

Curtiss-Wright Corporation
One Passaic St.
Woodridge, NJ 07075
Attn: Library 1

General Electric Company
Valley Forge Space Center
P.O. Box 8555
Philadelphia, PA 19101
Attn: Library 1

Grumman Aerospace Corporation
Bethpage, NY 11714
Attn: Library 1

Atlantic Research Corporation
P.O. Box 300 LPO
Niagara Falls, NY 14304
Attn: Library 1
R. Canny 1

Hughes Aircraft Company
Space & Communications Group
P.O. Box 92919
Los Angeles, CA 90009
Attn: Library 1

Lockheed Missiles & Space Company
P.O. Box 504
Sunnyvale, CA 94087
Attn: Library 1

U.S. Army Missile Command
Redstone Scientific Information Center
Redstone Arsenal, AL 35808
Attn: Document Section 1

U.S. Naval Missile Center
Point Mugu, CA 93041
Attn: Technical Library 1

U.S. Weapons Center
China Lake, CA 93557
Attn: Library 1

Aerospace Corporation
2350 E. El Segundo Blvd.
Los Angeles, CA 90245
Attn: Library 1

Garrett Turbine Engine Co.
402 South 36th Street
Phoenix, AZ 85034
Attn: Library 1

Gencorp Aerojet Propulsion Division
P.O. Box 13222
Sacramento, CA 95813
Attn: Library 1

Avco Systems Division
201 Lowell Street
Wilmington, MA 01887
Attn: Library 1

Sundstrand Aviation Mechanical
2421 Eleventh Street
Rockford, IL 61101
Attn: Library 1

TRW Systems Group
1 Space Park
Redondo Beach, CA 90278
Attn: Library 1
M.L. Chazen 1

Vought Corporation
3811 Van Dyke Avenue
Sterling Heights, MI 48077
Attn: Library 1

TABLE OF CONTENTS

		Page
1.0	SUMMARY	1
2.0	INTRODUCTION	3
3.0	ANALYSIS	5
	3.1 Performance	5
	3.1.1 Injector Mixing/Atomization Analysis	
	3.1.2 TKD Performance Model	
	3.2 Thermal Analysis	7
	3.2.1 Injector Thermal Analysis	
	3.2.2 Thrust Chamber Thermal Analysis	
4.0	HOT FIRE TEST RESULTS	12
	4.1 Design Approach	12
	4.2 Hardware Design Description and Fabrication	17
	4.3 Test Summary	19
	4.3.1 Test Plan	
	4.3.2 Performance Mapping Test Series	
	4.3.3 Injector Cooling Evaluation Testing	
	4.4 Option 2 Critical Experiment Tests	38
	4.4.1 Test Approach and Hardware Modifications	
	4.4.2 Critical Experiment Hot Fire Tests	
5.0	RHENIUM TECHNOLOGY	52
	5.1 Material Property Definition	52
	5.1.1 Materials Testing	
	5.1.2 Microscopy Analysis of Tensile Specimens	
	5.1.3 Microscopy Analysis of Samples Prior to Materials Test	
	5.2 Joint Design	67
	5.2.1 Methods of Attachment	67
6.0	CONCLUSIONS	78
7.0	RECOMMEDATIONS	79

LIST OF FIGURES

		Page
Figure 3.1	Injector Thermal Model Nodes	8
Figure 3.2	Location of Injector TC Probes	10
Figure 3.3	SINDA Model Results for Test HA2A-4099.	11
Figure 3.4	Q/A vs. T_{wall} for LO_2 in Injector	11
Figure 3.5	Copper Chamber Throat Temperatures	13
Figure 3.6	Copper Chamber Model Anchored to Test HA2A-4099 Data	13
Figure 3.7	Predicted Steady State Columbium Chamber Wall Temperature	14
Figure 3.8	Predicted Steady State Rhenium Chamber Wall Temperature	14
Figure 4.1	SSRT Engine Assembly (Film Cooling) ...	18
Figure 4.2	SSRT Engine Assembly (Thermal Block) ..	20
Figure 4.3	Heavy Wall Copper Chamber	21
Figure 4.4	SSRT Injector Oxidizer Geometry Modifications	22
Figure 4.5	Test Facility Schematic	24
Figure 4.6	-11 Element Testing, 1992 vs. 1991 Results	30
Figure 4.7	-11, -12 and -13 Performance vs. Ox Gap	30
Figure 4.8	-12 and -13 Performance vs. Fuel Gap ..	32
Figure 4.9	-11 Hybrid and -12 Hybrid Performance vs. Momentum Ratio	32
Figure 4.10	-11 Hybrid Element Performance vs. Mixture Ratio	34
Figure 4.11	Performance vs. Total Flow for -11 Hybrid Element	34
Figure 4.12	Performance Trends, Cooled vs. Uncooled	37
Figure 4.13	Injector Face Temperature vs. Momentum Ratio	37
Figure 4.14	Performance vs. % Film Cooling	39
Figure 4.15	SSRT Engine Assembly, GO_2 Injection Thermal Block	41
Figure 4.16	SSRT Engine Assembly, Thermal Block - No Splash Plate	42
Figure 4.17	SSRT Engine Assembly, Splash Plate	44
Figure 4.18	Performance vs. GO_2 Flow Rate	46
Figure 4.19	C^* Increase Due to GHe Injection	46
Figure 4.20	TIS Temperature Increase Due to GHe Injection	49
Figure 4.21	C^* vs. Momentum Ratio for -13a Hybrid Element	49
Figure 5.1-1	Rhenium Tensile Specimen	53
Figure 5.1-2	Rhenium Chamber Model	54
Figure 5.1-3	Rhenium Chamber Model	55
Figure 5.1-4	Ultimate Strength - Rhenium	56
Figure 5.1-5	Elongation - Rhenium	57
Figure 5.1-6	Reduction of Area - CVD Rhenium	58

Page

Figure 5.1.2-1	SEM View of Fracture in Tensile Specimen 1-1, 75F, as Deposited. 20X..	59
Figure 5.1.2-2	SEM View of Fracture in Tensile Specimen 1-2, 75F, Annealed. 20X.....	59
Figure 5.1.2-3	SEM View of Fracture in Tensile Specimen 1-3, 75F, Annealed 20X.....	60
Figure 5.1.2-4	SEM View of Fracture in Tensile Specimen 1-4, 75F, Annealed. 20X	60
Figure 5.1.2-5	SEM View of Fracture in Tensile Specimen 1-5, 1500F, as Deposited. 20X	61
Figure 5.1.2-6	SEM View of Fracture in Tensile Specimen 1-6, 3400F, Annealed. 20X....	61
Figure 5.1.2-7	SEM View of Fracture in Tensile Specimen 1-7, 1500F, Annelaed. 20X....	62
Figure 5.1.2-8	SEM View of Fracture in Tensile Specimen 1-8, 1500F, Annealed. 20X....	62
Figure 5.1.2-9	SEM View of Fracture in Tensile Specimen 1-9, 2200F, Annealed. 20X....	63
Figure 5.1.2-10	SEM View of Fracture in Tensile Specimen 1-10, 3400F, Annealed. 20X...	63
Figure 5.1.2-11	SEM View of Fracture in Tensile Specimen 1-11, 2800F, Annealed. 20X...	64
Figure 5.1.2-12	SEM View of Fracture in Tensile Specimen 1-13, 2800F, Annealed. 20X...	64
Figure 5.1.2-13	SEM View of Fracture in Tensile Specimen 1-14, 3400F, Annealed. 20X...	65
Figure 5.1.2-14	SEM View of Fracture in Tensile Specimen 1-15, 3400F, Annealed. 20X...	65
Figure 5.1.3-1	Micrograph of Tensile Specimen 1-2 After Annealing Showing Combination of Columnar and Recrystallized Layers. 40X.....	68
Figure 5.1.3-2	Micrograph of Tensile Specimen 1-4 After Annealing Showing Completely Recrystallized Structure. 40X.....	68
Figure 5.1.3-3	Micrograph of Tensile Specimen 1-6 Before Annealing Showing Columnar Structure as Deposited. 50X.....	69
Figure 5.1.3-4	Micrograph of Tensile Specimen 1-8 After Annealing Showing Combination of Columnar and Recrystallized Layers. 50X.....	69
Figure 5.1.3-5	Micrograph of Tensile Specimen 1-10 Showing Combination of Columnar and Recrystallized. 50X.....	70
Figure 5.1.3-6	Micrograph of Tensile Specimen 1-13 Showing Completely Recrystallized Structure. 50X.....	70
Figure 5.1.3-7	Micrograph of Tensile Specimen 1-15 Showing Completely Recrystallized Structure. 50X.....	71

Page

Figure 5.1.3-8	Detailed Micrograph of Tensile Specimen 1-15 Showing Entrapped Inclusions Between Layers. 100X.....	71
Figure 5.2-1	Microsection of Weld Sample 3. 50X....	75
Figure 5.2-2	Microsection of Weld Sample 4. 50X....	75
Figure 5.2-3	Detailed Micrograph of Weld Sample 3 at the Ti/Re Interface. 250X.....	76
Figure 5.2-4	Detailed Micrograph of Weld Sample 4 at the Ti/Re Interface. 250X.....	76
Figure 5.2-5	Thrust Chamber Joints	77

LIST OF TABLES

		Page
Table 3-1	SSRT Fuel Element Performance Summary ..	5
Table 3-2	TDK Performance Summary	6
Table 4-1	Fuel Element Summary	16
Table 4-2	Test Instrumentation Requirements (HA2A)	26
Table 4-3	Option 1 Performance Testing Summary ...	28
Table 4-4	Thermal Block and Film Cooling Adaptor Test Summary	35
Table 4-5	GO_2 Injection Tests Summary	45
Table 4-6	GHe Injection Test Summary	47
Table 4-7	Columbium Chamber Tests Summary	48
Table 4-8	No Splash Plate Test Summary	50
Table 5.1.2-1	Fracture Comparisons, CVD Rhenium Tensile Specimens	66
Table 5.2-1	Candidate Brazing Alloys for Cb to Re ..	73
Table 5.2-2	Simulated Braze Joint Tests	74

1.0 SUMMARY

The Space Storable Rocket Technology (SSRT) Option 1 Program was initiated in October 1991 after completion of the Basic Program (reported in CR 189131 - May 1992). The program was restructured in mid-July 1992 to incorporate a Rhenium Technology Task and reduce the scope of the LO_2-N_2H_4 engine development. The program was also extended to late February 1993 to allow for the Rhenium Technology Task completion.

The Option 1 Program was devoted to evaluation of two new injector elements, evaluation of two different methods of thermal protection of the injector, evaluation of high temperature material properties of rhenium and evaluation of methods of joining the rhenium thrust chamber to the columbium injector and nozzle extension. In addition, critical experiments were conducted (Funded by Option 2) to evaluate mechanisms to understand the effects of GO_2 injection into the chamber, helium injection into the main LO_2, effect of the splash plate and effect of decreasing the aspect ratio of the 120-slot (-13a) element. The performance and thermal models were used to further correlate the test results with analyses.

The results of the work accomplished can be summarized as follows:

- A total of 88 tests was conducted with maximum performance attained of c*=5903 ft/sec(1799 m/sec) which projects to Isp_∞ = 346 lbf-sec/lbm (3394 n-sec/kg)(ϵ = 204).
- The highest performing element continued to be the -11 hybrid although the highest performing basic element was the -12 (90 slots).
- Engine performance has been demonstrated to be strongly driven by LO_2 boiling conditions in the oxidizer injector snout at the final oxidizer orifice. Film boiling yielded the highest performance while nucleate or no boiling yielded lower performance.
- The thermal block adaptor tests indicated low performance due to low temperature snout approaching saturation temperature of LO_2. However, the engine ran 20-seconds with low dome temperatures.
- The film cooling adaptor generated similar results to the thermal block adaptor.

- The thermal block adaptor was modified and tested with GO_2 injection downstream of the main LO_2 flow. Performance improved significantly with 5% GO_2 flowrate with low dome temperatures and the snout temperature indicating saturation to low film boiling regimes (highest performance). However, performance was still 1.5% below maximum achieved.

- The thermal block adaptor was tested with GHe injection into the main LO_2. The results indicated high performance (within 0.7% of maximum).

- The thermal block without the splash plate was evaluated. This configuration indicated thermal protection of the injector but performance was marginal due to either film boiling of the snout or nucleate boiling depending on the conditions.

- The final series evaluated the -13a hybrid without a splash plate or thermal block indicating a maximum c* = 5798 ft/sec (1767 m/sec) which was 1.8% below the -11 hybrid. The -11 hybrid is the maximum performance element tested to date.

- Materials property testing of CVD rhenium provided ultimate strength and elongation over the temperature range of 70-3400F (21-1871C).

- Investigations were conducted to evaluate methods of attachment of the rhenium thrust chamber to the columbium injector and nozzle extension. Welding and brazing methods were evaluated. Welding yielded brittle interfaces. However, brazing produced an effective way of joining rhenium and columbium. The joint configuration utilized a mechanical attachment with the braze as a seal.

2.0 INTRODUCTION

The increasingly demanding spacecraft missions and their associated requirements for increased payloads over the last thirty years have been successfully achieved by the steadily improving capabilities of spacecraft propulsion systems. These systems have used earth storable propellants. The technology level of these propellants and their systems have been repeatedly improved as the mission demands have grown.

Space storable propellant usage offers the advantage of using higher performance propellants to achieve increased weight into orbit. NASA and TRW have concluded that liquid oxygen is the best oxidizer. The Space Storable Rocket Technology (SSRT) Program has as one objective to determine the best fuel to use with the LO_2. The SSRT Program consists of four phases - Basic, Option 1, Option 2 and Option 3. The Basic Program which is reported in NASA CR 189131 (dated 12 May 1992) consisted of three tasks:

- Applications Evaluation

  -The results of this evaluation concluded that the maximum mission potential usage is the placement of satellites into geosynchronous earth orbit (GEO). The greatest use of these satellites is communication, surveillance, tracking, earth observation and meteorological applications.

  -The evaluation also concluded that the best propellant combination is LO_2-N_2H_4. This propellant combination provides the maximum mission and system capability in that the maximum payload into GEO can be achieved with this propellant combination.

  -The nominal engine requirements resulting from the system analyses were:

Thrust(F_∞)	200 lbf (890 n)
Chamber Pressure(Pc)	200 psia (138 n/cm^2)
Specific Impulse(Isp_∞)	340 lbf-sec/lbm(3335n-s/kg)

- Preliminary Design

  This task included the design and analysis of the testbed engine. As part of this task, a performance model was developed indicating the performance goal could be achieved. A thermal model was also developed and anchored to the test data obtained. The testbed engine was designed as a flexible unit allowing shimming to

achieve variations in both oxidizer and fuel independently and replaceable fuel elements to assess the impact of fuel slot number and geometry on performance and thermal characteristics.

- Exploratory Tests

  This task included the fabrication, test and analysis of data. Two test series were conducted. Six configurations were evaluated in 76 tests. Performance of 95% combustion efficiency was attained which projects to a Isp_∞ of >340 lbf-sec/lbm(3335 n-s/kg) (ϵ=204) which is an 8% improvement over existing flight apogee engines.

The Option 1 Program consisted of continued development of the LO_2-N_2H_4 engine, including evaluation of performance and thermal characteristics of the injector dome and thrust chamber. In addition, the program was restructured to develop rhenium engine technology. This report will discuss the results of design, manufacturing and test of new injector elements, thermal block adaptor, film cooling adaptor and critical experiments to assess injector/dome interactions. In addition, the rhenium technology will be discussed including presentation of high temperature material properties.

3.0 ANALYSIS

3.1 Performance

Performance analysis of the SSRT engine during the Option 1 program included injector mixing/atomization analysis, one and two dimensional equilibrium and kinetic combustion models (ODE, ODK and TDK), and two zone chamber combustion models derived from hot fire performance and thermal test data.

3.1.1 Injector Mixing/Atomization Analysis

The coaxial pintle injector model developed by Dr. Richard Priem in the Basic Program was used to explore the effects of slot number and size on injector atomization. A trend of increasing performance with increasing number of slots was established in the Basic Program testing, so it was logical to continue to increase the number of slots.

The Priem FORTRAN computer program was used to evaluate the -12 fuel element (90 slots) and the -13 fuel element (120 slots) respectively. Table 3-1 summarizes the results of the analysis compared to the actual hot fire results for these elements (and all other configurations tests previously). These results are presented for the fuel elements tested with the standard pintle, not the hybrid pintle. The Priem model predicted that performance increases as the slot size decreases, mainly due to the smaller fuel drop size, and therefore greater fuel vaporization. The test data indicated this effect is real up to a certain point, except that the performance for the 120 slot element was lower than for the 90 slot element. The difference may be due to the higher slot aspect ratio of the -13, which has been shown to reduce performance (compare the -9 to the -10 element).

TABLE 3-1

SSRT FUEL ELEMENT PERFORMANCE SUMMARY

FUEL EXTENSION	# SLOTS	ASPECT RATIO (H/W)	η C* ANALYSIS (%)	η C* TEST (Max %)	PROJECTED ISP LBF-SEC/LBM (Cf=1.885)
-3	30	0.64	87-90	87.0	312
-8	36	0.67	92-93	83.3	301
-7	40	2.23	90-93	91.7	331
-9	48	2.68	91-94	91.7	331
-10	48	4.82	92-94	91.2	329
-11	60	3.35	93-95	93.3	337
-12	90	4.37	95-96	94.1	339
-13	120	5.85	95-97	93.2	335

3.1.2 TDK Performance Model

Using the test data from the Option 1 test series, a two zone model of the chamber combustion process was constructed. The chamber was divided into two concentric zones, a fuel rich outer zone adjacent to the chamber wall that allows operation of the chamber within its thermal limits, and the core zone which contains most of the mass flow and operates closer to stoiciometric conditions. The mixture ratio of the outer zone was determined by thermal data from the copper chamber thermocouples (see section 3.2.2). The core zone mixture ratio and mass flow split were determined from the C* performance and the overall mixture ratio. The desired conditions are operation with the wall zone mass flow rate as small as practical while maintaining acceptable and stable chamber temperatures, and maintain the core zone at peak performance conditions.

TRW experience with engines operating on storable hypergolic propellants indicated that a wall zone mass flow of 20% of the total flow is reasonable. Using this as a baseline, two zone TDK models with wall zone gas temperatures compatible with both a columbuim and a rhenium chamber were developed. The results of this analysis is presented in Table 3-2. These results indicated that an Isp performance of 352 seconds can be obtained with columbium, and 360 seconds with rhenium. In both cases the core zone mixture ratio (O/F) was 0.875, which gave peak Isp performance in the zone. For the columbium case, a wall zone mixture ratio of 0.26 was used, which resulted in a maximum chamber temperature of 2600° F at the inside wall of the chamber just upstream of the throat. For a rhenium chamber, a wall zone of 0.50 was used, resulting in a peak inner wall temperature of 3870°F.

Table 3-2 TDK Performance Summary

	Columbium Chamber	Rhenium Chamber
Wall Zone O/F	0.24	0.50
Core Zone O/F	0.88	0.88
Wall Zone Tg (°F)	3000	4500
Wall Zone Mass Flow	20%	20%
Maximum Chamber Temp. (°F)	2600	3870
C* TDK (ft/sec)	5990	6110
Isp Vacuum (sec)	352	360
Cf Vacuum	1.891	1.894

The results above are ideal cases, and show the reasonable upper limit of performance for the SSRT engine. The difficult part was to find an injector configuration that can approach the conditions used in the two zone analysis. A two

zone model of the combustion conditions for test HA2A-4099 (Isp = 346 seconds) was developed by anchoring the data from this test. The resulting zone split was 29% mass flow in the wall zone at a mixture ratio of 0.26, and 71% mass flow in the core at a mixture ratio of 0.90. If the mass flow fraction to the wall zone could be reduced to 20%, and the core O/F remained the same, the performance would increase to 349 seconds. Of course, the performance could be increased further still if a rhenium chamber is used, allowing a higher mixture ratio wall zone to be used.

3.2 Thermal Analysis

3.2.1 Injector Thermal Analysis

Because LO_2 is generally a poor liquid coolant, cooling of the SSRT injector has been a prime design concern on this program. The approach was to evaluate two different methods of protecting the injector from overheating. The first method was a simple "thermal block" approach in which a thin metallic barrier would cover the injector face to prevent direct convective heat transfer to the injector. The heat conducted to the injector from the chamber would be controlled by material selection and dome geometry to a level compatible with the LO_2 main flow. The second approach was to provide film cooling of the injector face with LO_2. This method would reduce the face recirculation gas temperature and also provide active cooling of the injector in the internal film cooling passages and manifolds.

For the thermal block analysis, a SINDA model with variable geometry and material selection was developed. This model showed that by using low conductivity materials with high temperature capability for the injector body, the conductive heat load to the LO_2 passage could be removed by the LO_2 in subcooled forced convection. Material candidates included superalloys of nickel and cobalt. The main concerns were overheating of the thermal block piece since it would operate close to the gas temperature and high operating temperatures at the injector to chamber interface joint. Although the current injector did not have the proper dome geometry and material to operate under steady state conditions with the thermal block adaptor, it was decided to test the current injector with the thermal block to evaluate the effectiveness of the thermal block concept, and also provide information on gas recirculation temperatures in the injector area.

The 300 node SINDA model of the current injector that was developed in the basic Program was further improved and modified to analyze film cooling approaches to protect the injector from overheating. Figure 3-1 shows the nodal layout for this model. Specific modifications to the SINDA model for Option 1 included alteration of the dome area nodes to account for the film cooling passage.

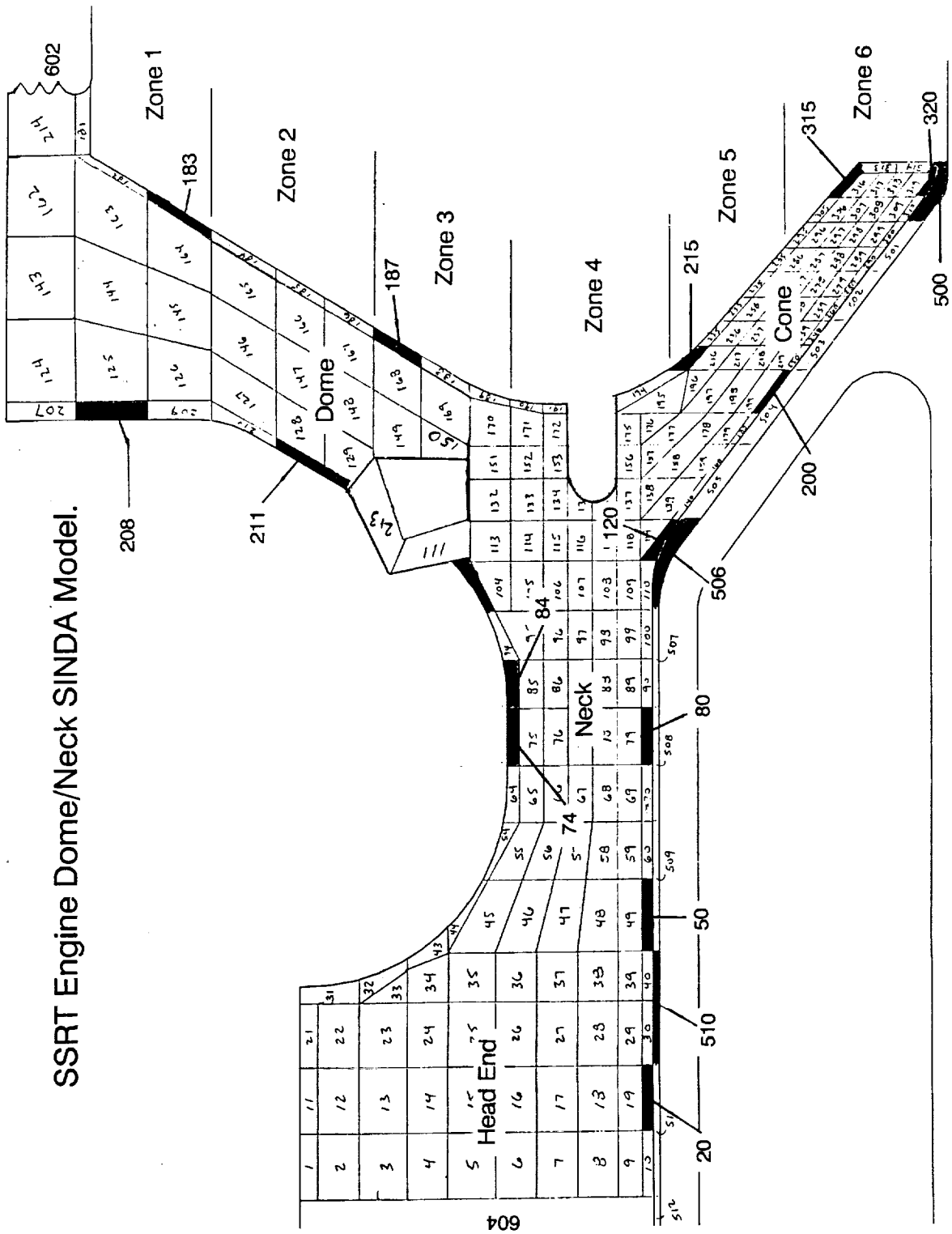

Figure 3-1 Injector Thermal Model Nodes

In establishing the film cooling flow rate desired, the method of Zucrow and Sellers was used, with an assumed film cooling efficiency of 25% and dome gas temperature of 2500°F. From this analysis, a film cooling flow rate of 4% of the main flow was calculated to maintain a liquid film over the injector face. The thermal model showed that if the average gas temperature at the face of the injector was 500°F or less, the injector would be thermally stable.

The injector was well instrumented with thermocouples during hot fire testing to obtain data to support analysis of new designs. Additional test diagnostics were added to the injector for this testing in order to measure the boundary conditions more accurately. These included a thermocouple probe inserted into an EDM'd hole into the injector snout to measure the snout temperature near the oxidizer injection point, and a platinum-rhodium sheathed thermocouple probe inserted through the PC port in order to measure the injector face recirculation gas temperature directly. Figure 3-2 shows the locations of these two probes.

The snout temperature (TIS) and PC port (TPC) probes helped anchor the SINDA model by providing thermal data not available in previous test series. Previously, it was not known if the snout was operating in the nucleate or film boiling regimes, because the long aspect ratio of the conical snout walls thermally isolate it from the injector dome. The direct measurement of the injector face gas with TPC eliminated it as a variable in the thermal model, allowing determination of the convective heat transfer coefficient to the injector face.

Thermocouple data from the snout probe (TIS) indicated that if the snout was not shielded from the combustion gas, the snout operated in the 100°F to 200°F temperature range, ie, well into film boiling for LO_2. The PC port probe (TPC) measured a gas temperature of 300°F to 2000°F, but usually read around 800°F to 1200°F under nominal test conditions.

The injector thermal model was used to anchor test data from test HA2A-4099, a high performance test that achieved 95% C* performance. The TPC and TIS probe temperatures from this test were 1000°F and 150°F respectively. Figure 3-3 shows the measured vs predicted temperatures for this test. The results indicated that in order for the snout temperature to remain at 150°F to 200°F during the test, either the heating effect to the snout had to decrease greatly part way through the test, or the heat transfer in the film boiling regime had to be much higher than predicted. Figure 3-4 shows the Q/A verses wall temperature curve for LO_2 used in the SINDA model. Note that the snout operated near the minimum point of this curve. This was an unstable thermal condition, and therefore an unlikely operation point. It was postulated

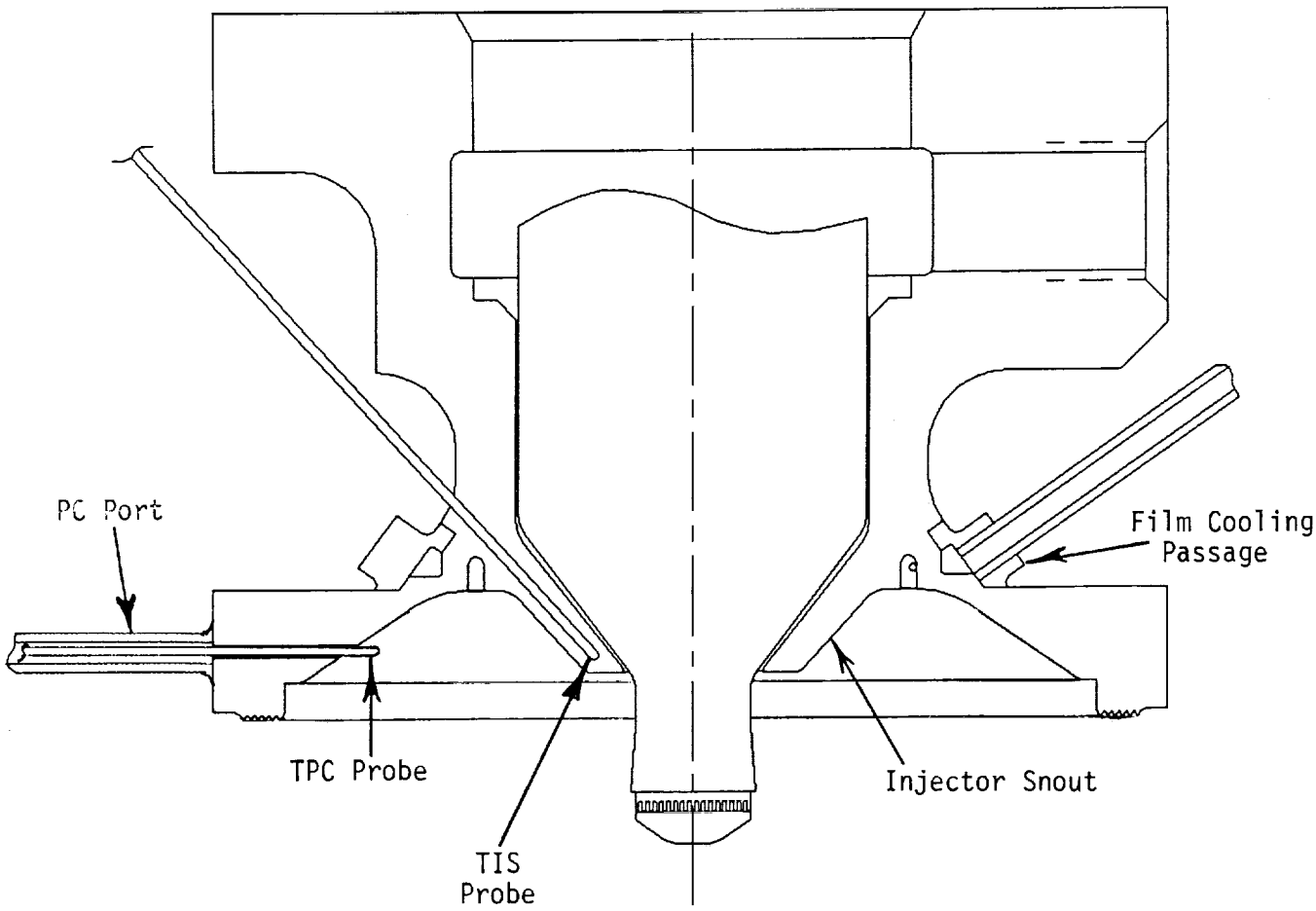

Figure 3-2. Location of Injector TC Probes.

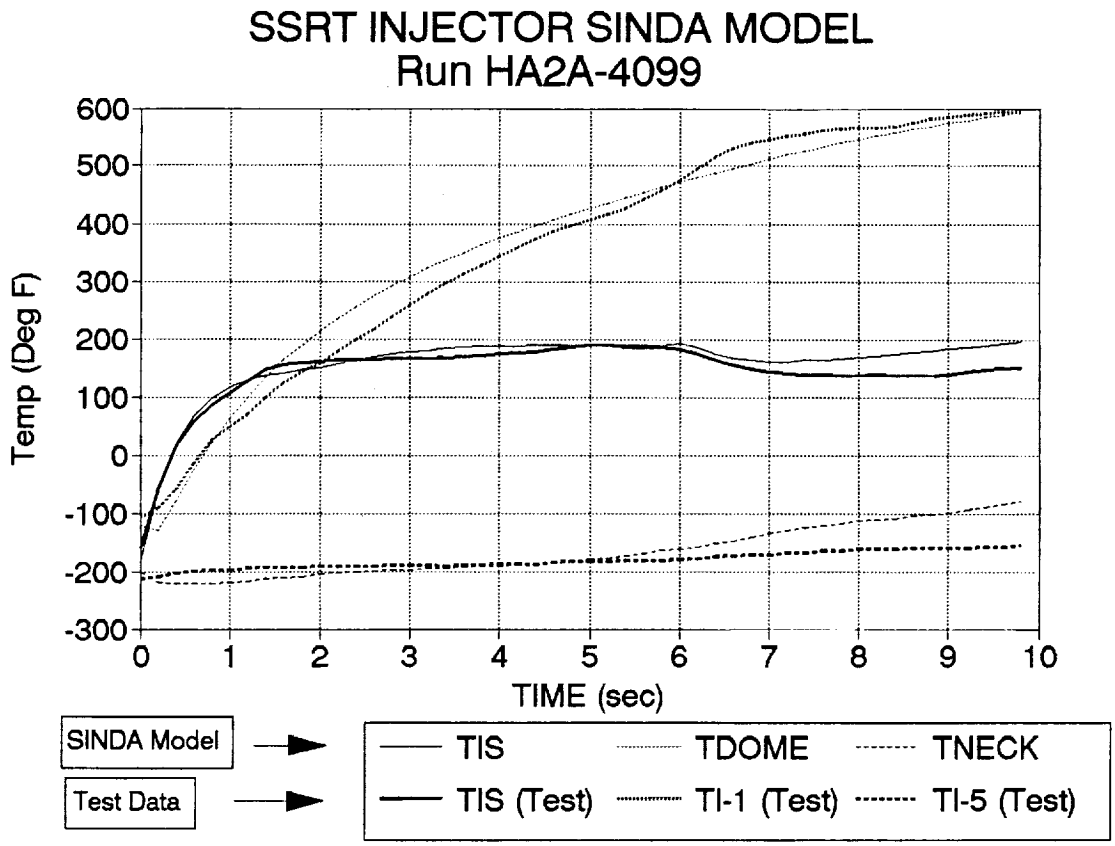

Figure 3-3. SINDA Model Results for Test HA2A-4099

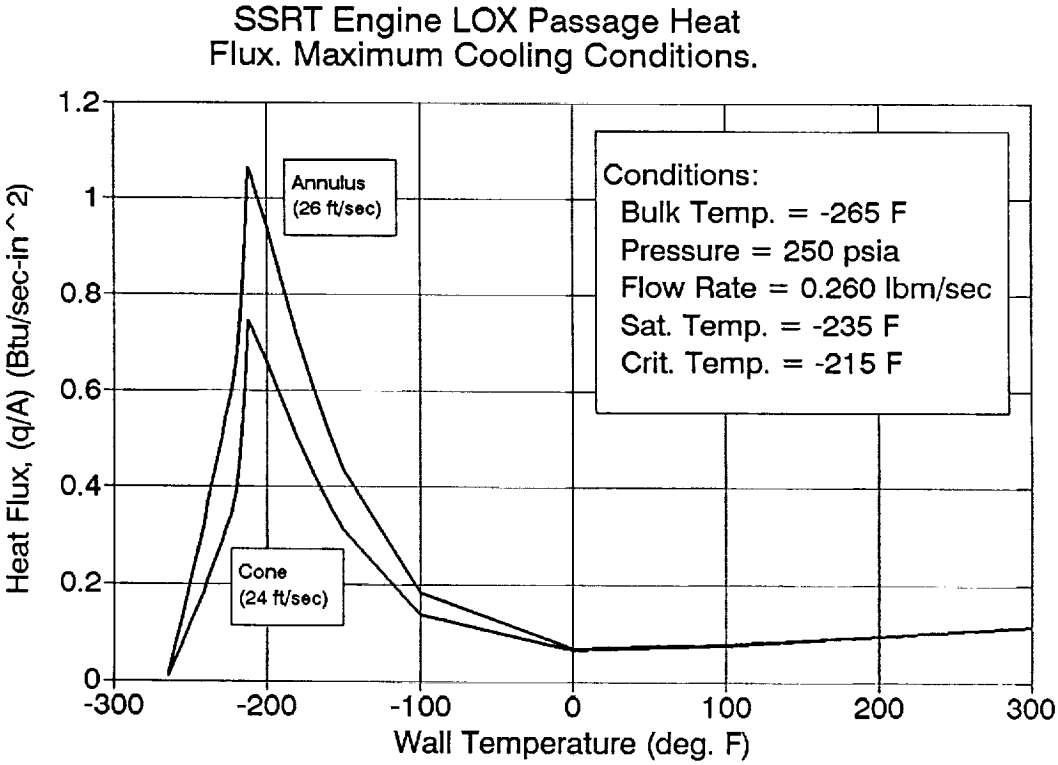

Figure 3-4. Q/A verses Twall for LO_2 in Injector

that because of the thin annular passages involved with the oxidizer circuit (annular gaps on the order of 0.010 inch), a stable film couldn't form, so the film boiling heat transfer was increased. Tests to characterize film boiling of liquid oxygen flow in a test article that closely simulates the oxidizer geometry are planned for the Option 2 program.

3.2.2 Thrust Chamber Thermal Analysis

For the Option 1 hot fire test series, a new copper chamber was designed and fabricated. The chamber walls were twice as thick as the previous design, allowing much longer test durations, and also included a 10:1 area ratio divergent nozzle to smooth the thermal response at the throat. A 250 node finite difference thermal model of the copper chamber was constructed to determine its thermal response during operation. Figure 3-5 shows the predicted transient temperature profiles at the throat node for various gas temperatures. This model indicated that about 20 seconds of operation could be obtained with the chamber for the current estimated wall gas temperatures in the 3000°F range.

Figure 3-6 shows the thermocouple data from test HA2A-4099 vs the predicted response at Row 2 (end of the barrel section) and the throat for a gas temperature of 3150° F. Figure 3-7 shows the predicted temperatures for a columbium chamber under the same heating conditions. Under these conditions, the maximum wall temperature was over 2700°F, which was too high for long life operation with a disilicide coating. However, if a more capable oxidation resistant coating is developed for columbium, then these temperatures are not excessive for a C103 alloy thrust chamber.

Figure 3-8 shows the resulting temperatures for operation at the above heating conditions in a rhenium thrust chamber. Here the maximum wall temperature was 2800°F because of the thinner wall section at the throat in a rhenium chamber. Iridium coated rhenium is capable of operation at temperatures well over 3000°F so there is no concerns with overheating at these conditions. More extreme thermal operating conditions that would allow increased performance are possible with a rhenium chamber.

4.0 HOT FIRE TEST RESULTS

4.1 Design Approach

The injector hardware used in the basic program was also utilized in Option 1 testing. This injector was designed to offer maximum flexibility in testing in order to evaluate the changes necessary to achieve high performance. A new copper

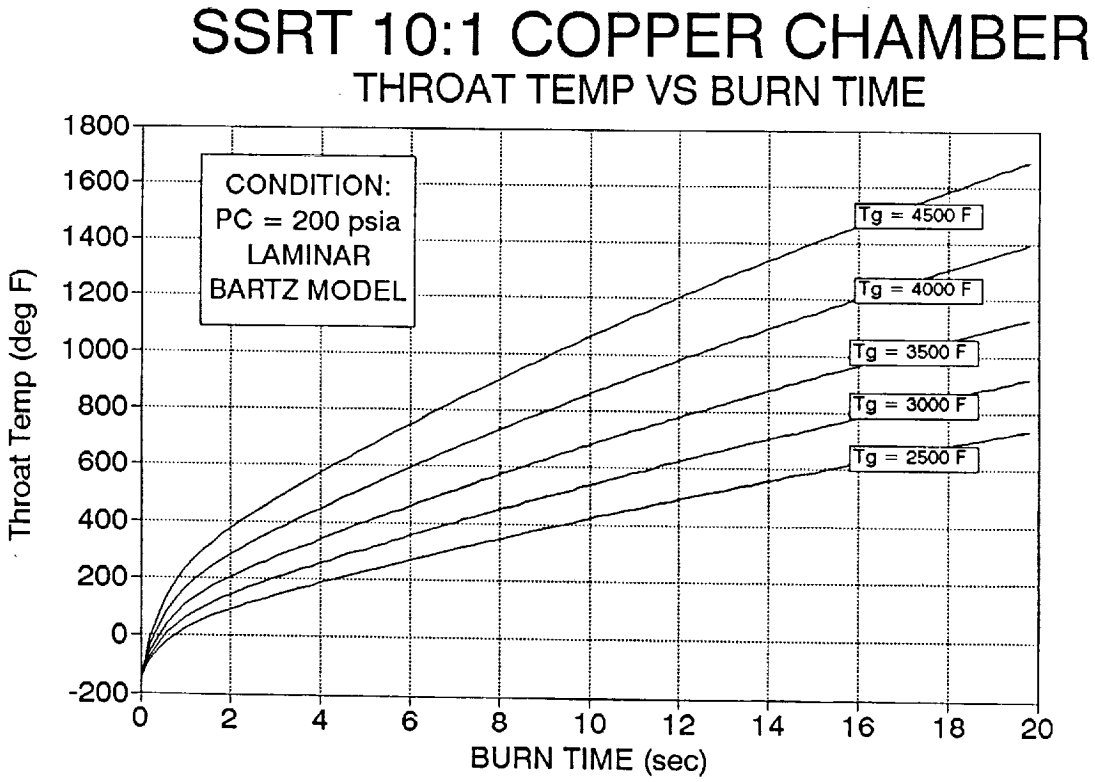

Figure 3-5. Copper Chamber Throat Temperatures

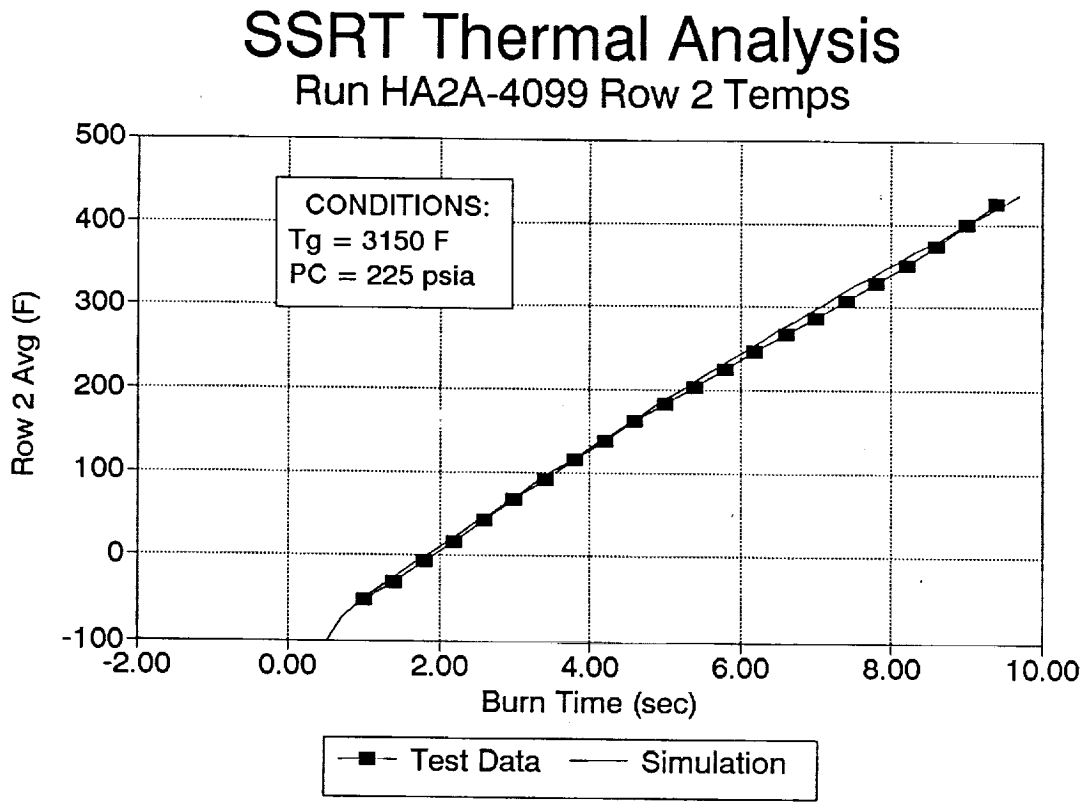

Figure 3-6. Copper Chamber Model Anchored to Test HA2A-4099 Data

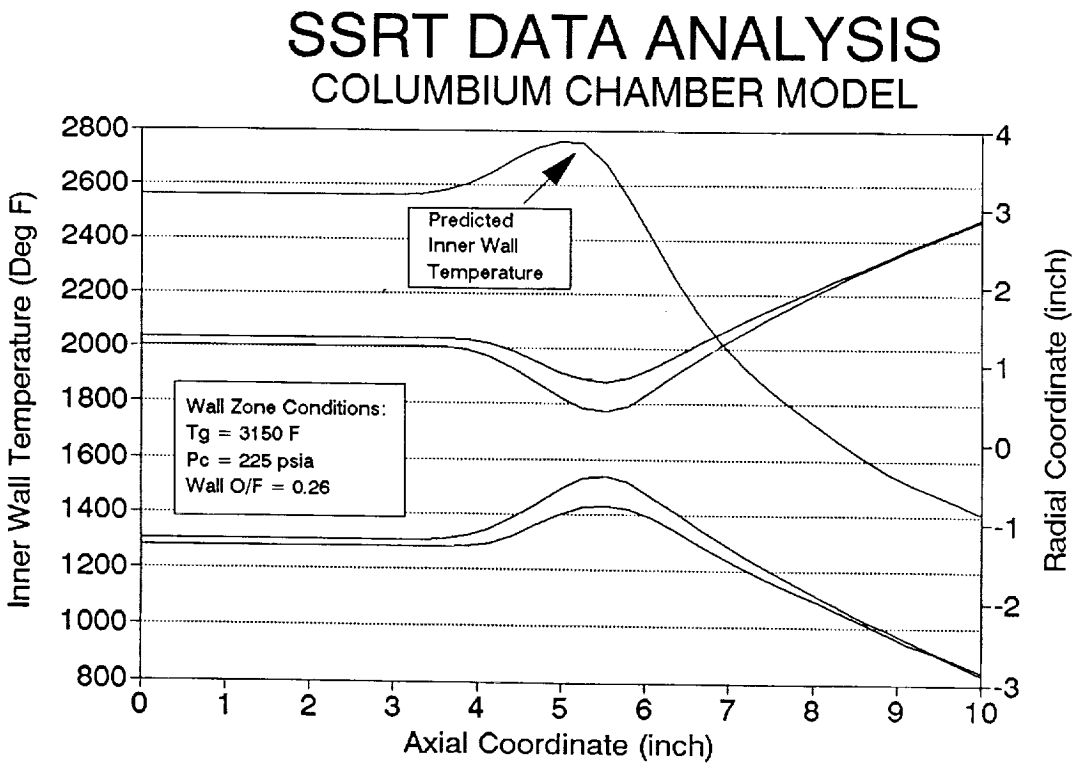

Figure 3-7. Predicted Steady State Columbium Chamber Wall Temperature

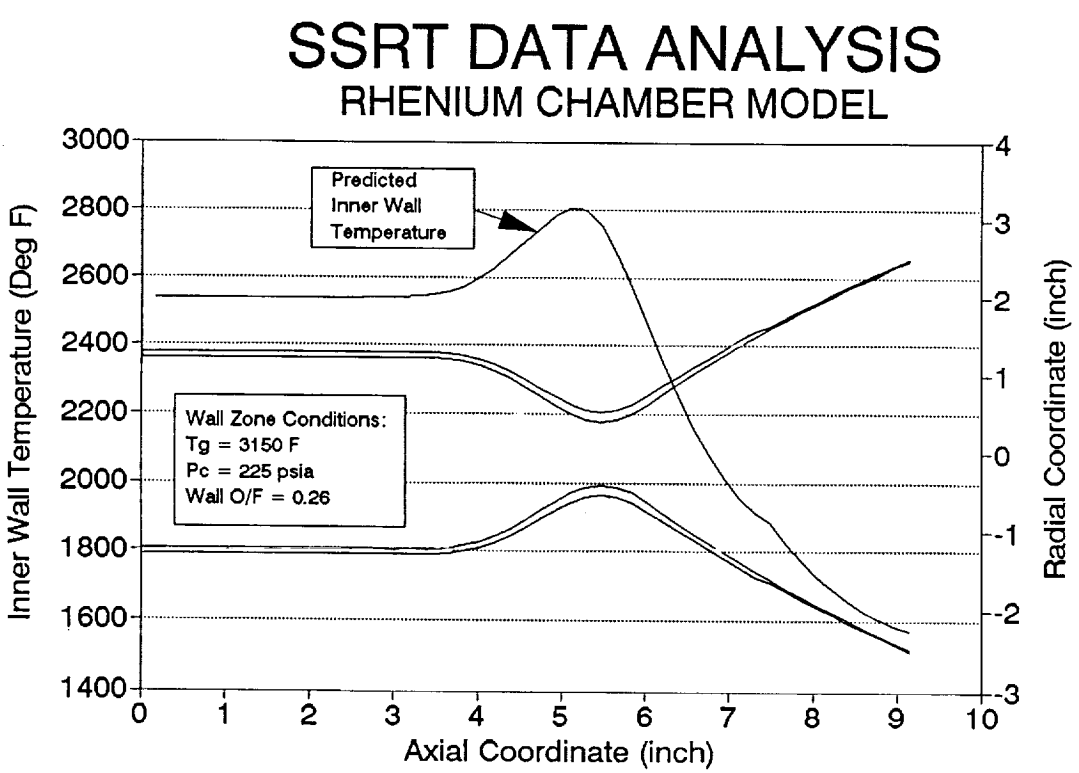

Figure 3-8. Predicted Steady State Rhenium Chamber Wall Temperature

chamber with thicker walls was constructed for Option 1 testing that would allow nearly twice the test duration as the previous chamber.

Two specific goals were established in conjunction with the Option 1 test series:

1) Further increase the engine performance with new injector element designs

2) Explore methods of controlling the head end temperatures during steady state operation.

In order to meet the first goal, two new fuel injector elements were designed based on the previous testing experience. The primary performance trend was slot number, primarily due to the finer drop size and enhanced vaporization rate generated by the smaller slots. Another parameter that appeared to affect performance was the aspect ratio of the slots (slot height to slot width). The -10 element had the same number of slots as the -9, yet had taller and narrower slots, and this element did not perform as well as the -9 element. In order to increase the slot number while maintaining the same slot area and blockage ratio, the aspect ratio must necessarily increase. Two new fuel elements were designed, the -12 with 90 slots, and the -13 with 120 slots. Table 4-1 summarizes the fuel elements tested to date.

Several methods were evaluated as possibilities for controlling the head end temperatures. These included film cooling, regenerative cooling, transpiration cooling and thermal blockage. After consideration of the pros and cons of these approaches, two concepts emerged as most promising, film cooling and thermal blockage.

Film cooling of the injector face involved injecting a small amount of LO_2 along the injector face in order to provide a layer of liquid and/or cold gas to protect the injector from convective heating. The cold layer and internal passages and manifolds would also provide some regenerative cooling effect to intercept heat conducted from the chamber to the injector.

The thermal blockage approach blocked the direct convective heating of the injector face with a thin metal shield. The metal operated near the gas temperature, so it was nearly adiabatic. The injector material and geometry would be designed such that the conducted heat load from the chamber could be carried by the LO_2 cooling in the main circuit. This technique was promising because of its simplicity and requires no modifications to the flow circuit. One potential drawback was that the recirculating gas in the injector region may be hotter than the material limit of the thermal block shield.

Table 4-1 Fuel Element Summary

FUEL EXTENSION	# SLOTS	SLOT ASPECT RATIO	OXIDIZER RAMP
-3	30	0.64	N
-4	30	1.38	N
-5	40	2.23	N
-6	30	1.38	Y
-7	40	2.23	Y
-8	36	0.67	Y
-9	48	2.68	Y
-10	48	4.82	Y
-11	60	3.35	Y
-12	90	4.37	Y
-13	120	5.85	Y

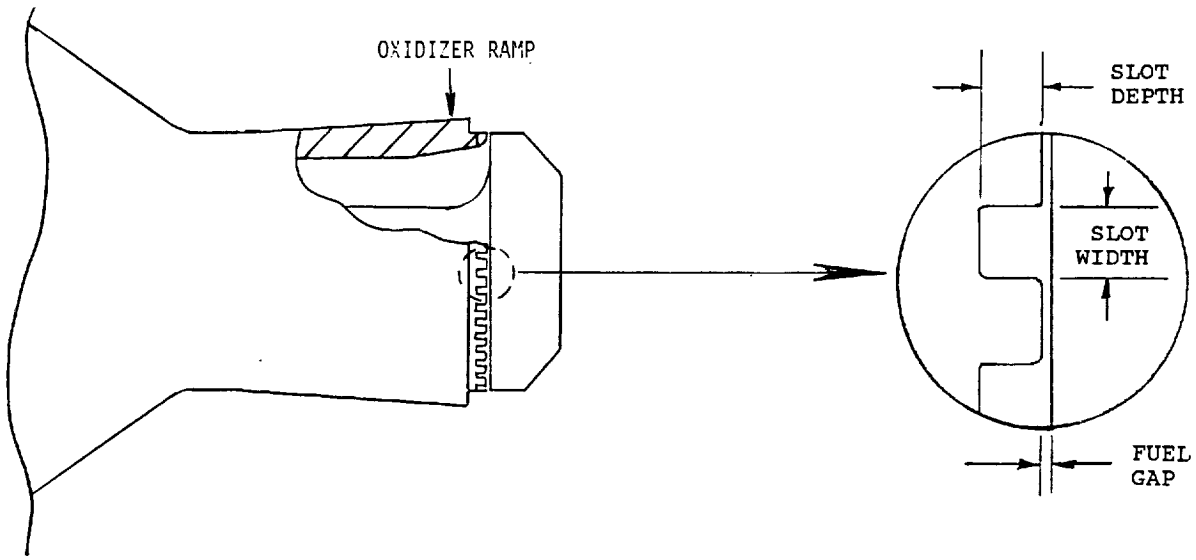

Testing of the film cooling and thermal block concepts was accomplished by modifications to the existing injector hardware. Although this hardware was not designed specifically for either of these concepts, useful information could be obtained on the effectiveness of the two cooling methods.

4.2 Hardware Design Description and Fabrication

The two new fuel injection elements were designed following the same general form as the previous four 200 lbf elements (-7,-9,-10 and -11). They all have an oxidizer ramp to uncouple the fuel delta P from oxidizer momentum. They all have the same total slot area, and all but the -10 element have the same blockage ratio (slot width per unit spacing). The sleeve extensions were designed to attach to the tip of the injector sleeve with a threaded connection sealed with a teflon O-ring.

The extensions were made from Nitronic 60 stainless steel because of its excellent gall resistance, a concern where the element threads onto the 15-5 PH sleeve. The slots were made by the EDM process. Due to the large aspect ratio of the -12 and -13 slots, they were formed using the wire EDM process, where in previous elements the slots were formed by ram EDM. The difference between the two methods was that the wire cut slots have a full radius at the bottom while the ram cut slots were squared off in the bottom with .003 inch corner radii.

Figure 4-1 shows the film cooled test article. The injector body was modified for film cooling by machining a manifold into the back side of the dome, and a distribution groove on face of the injector that was concentric with the manifold, separated by a thin wall. Four injection holes were EDMed through the outer manifold tangential with the inner groove. These holes swirled the LO_2 coolant inside the face groove, forming a thin, evenly distributed film. A closeout cover with a 1/8 inch feed tube was EB welded over the manifold groove on the backside of the injector.

A film cooling adaptor with a splash plate was fabricated from 15-5 PH stainless steel. The adaptor was made in two parts, the face plate and the splash ring, with a distribution manifold between them. The LO_2 coolant film flowed behind the face plate outward over the face of the injector, through 16 distribution holes into an outer manifold, and then was injected radially inward through 16 0.020 by 0.020 inch slots along the face of the adaptor. The 16 discreet film cooling jets spread to a thin film when they impinge on the injector snout, resulting in nearly 100% coverage of the snout. The LO_2 coolant flow to the injector

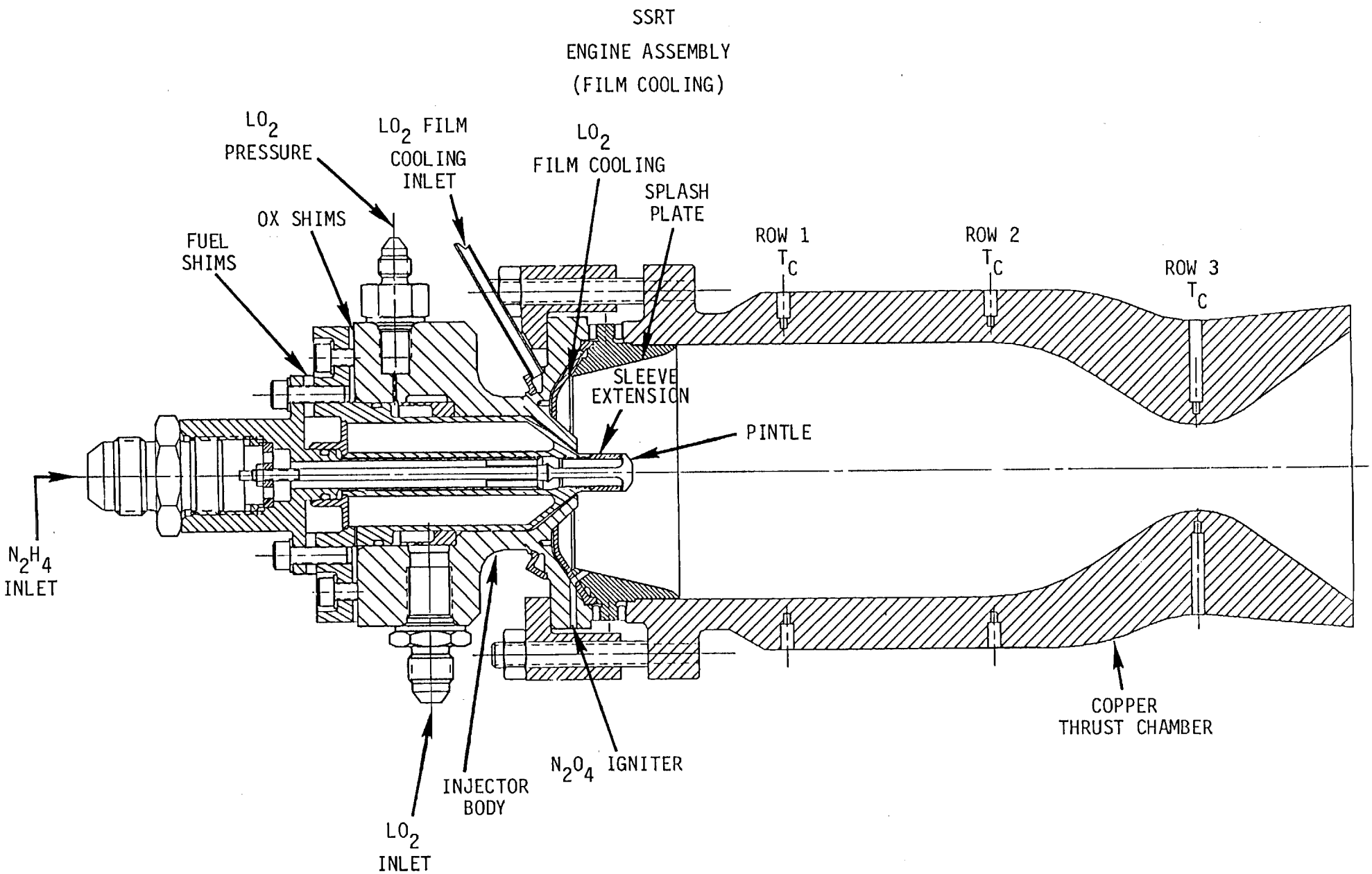
SSRT
ENGINE ASSEMBLY
(FILM COOLING)
LO_2 PRESSURE
LO_2 FILM COOLING INLET
LO_2 FILM COOLING
SPLASH PLATE
OX SHIMS
FUEL SHIMS
ROW 1 T_C
ROW 2 T_C
ROW 3 T_C
SLEEVE EXTENSION
PINTLE
N_2H_4 INLET
COPPER THRUST CHAMBER
N_2O_4 IGNITER
INJECTOR BODY
LO_2 INLET

FIGURE 4-1

was controlled by a cavitating venturi that was installed in a tee just ahead of the LO_2 main venturi. Three cavitating venturis were made to provide 10%, 12%, and 15% of the LO_2 flow for film cooling.

Figure 4-2 shows the thermal block engine assembly. The thermal block adaptor was similar in construction to the film cooling adaptor except that it was made in one piece and covered most of the snout in addition to the injector face. The thermal block was constructed of 15-5 PH stainless steel and was designed to clear the face of the injector by 0.020 inch. It contacted the snout on milled pads to center it on the injector. Type K thermocouple probes were attached to the back side of the face shield in four positions in order to determine the operating temperature of the adaptor face. Four TC probes were also brazed into the base of the splash plate.

A new copper chamber was also designed and fabricated in this option, as shown in Figure 4-3. The wall thickness was doubled (to 1/2 inch thick) and a 10:1 area ratio nozzle was incorporated. Type K thermocouple probes were brazed into the chamber wall located 0.10 inch from the inner wall. A PC port was also brazed in place at the start of the convergent section. This port was necessary since the head end PC port was utilized as an igniter port with the film cooled and thermal block adaptors.

Another modification to the injector was a change to the oxidizer injector geometry at the final injection point. Figure 4-4 shows the old configuration compared to the new configuration. Previously, a large (0.090 inch) radius at the oxidizer exit point created a smooth increase in injection area just down stream of the minimum oxidizer gap. This allowed the oxidizer to attach and diffuse to a lower velocity locally, creating a performance drop on some tests during the Basic Program hot fire testing. The problem was solved by machining a much smaller radius at the oxidizer exit point, allowing the flow to detach cleanly at the point of minimum area.

4.3 TEST SUMMARY

4.3.1 Test Plan

As part of the SSRT Option 1 program, hot fire tests were defined to provide performance and thermal input to the engine design. These tests were performed using the hardware that was tested in the Basic Program in 1991.

The exploratory tests performed in the Option 1 program were structured to evaluate further increases in performance over the 343 seconds Isp achieved in the basic program and to provide fundamental information on the effectiveness of the

SSRT

ENGINE ASSEMBLY

(THERMAL BLOCK)

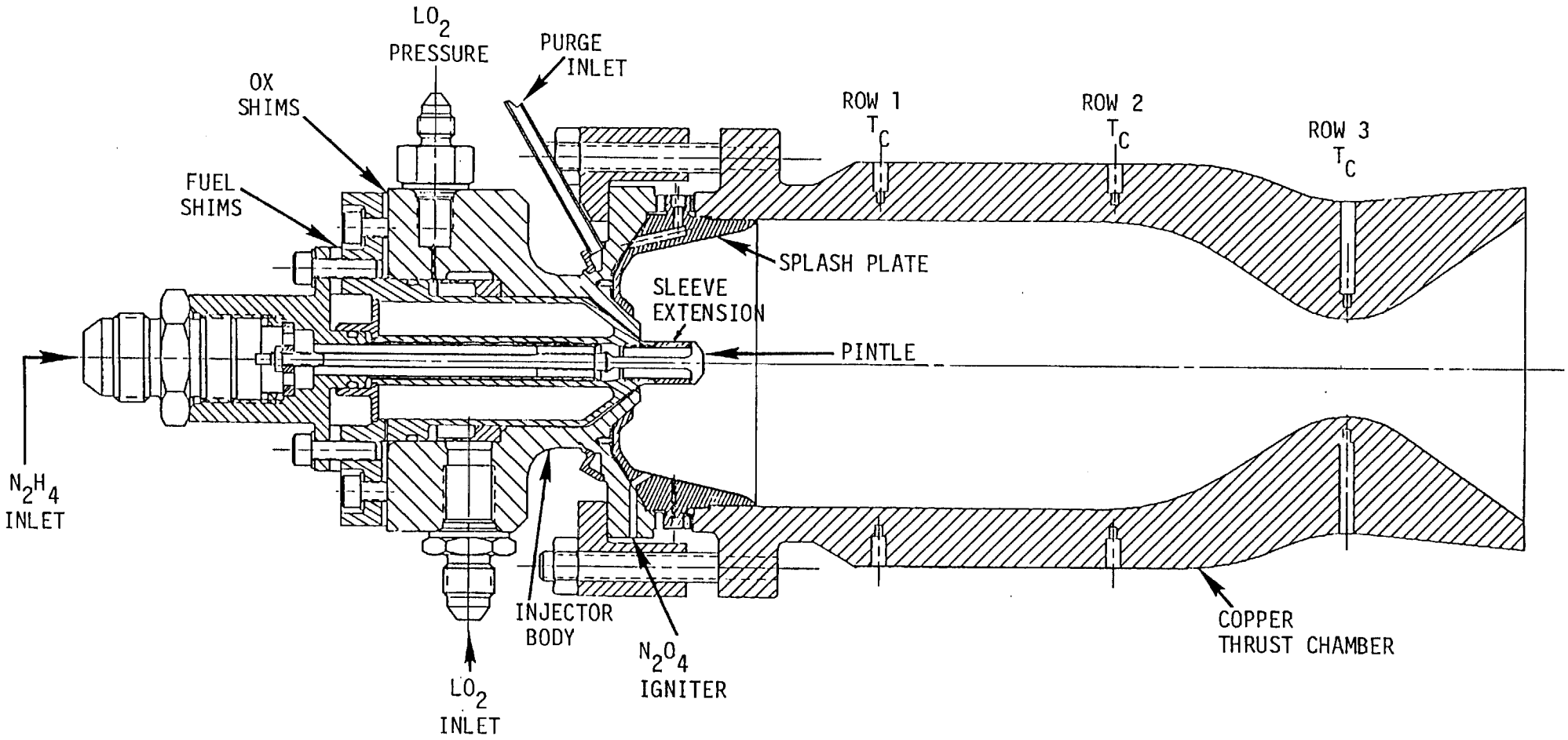

FIGURE 4-2

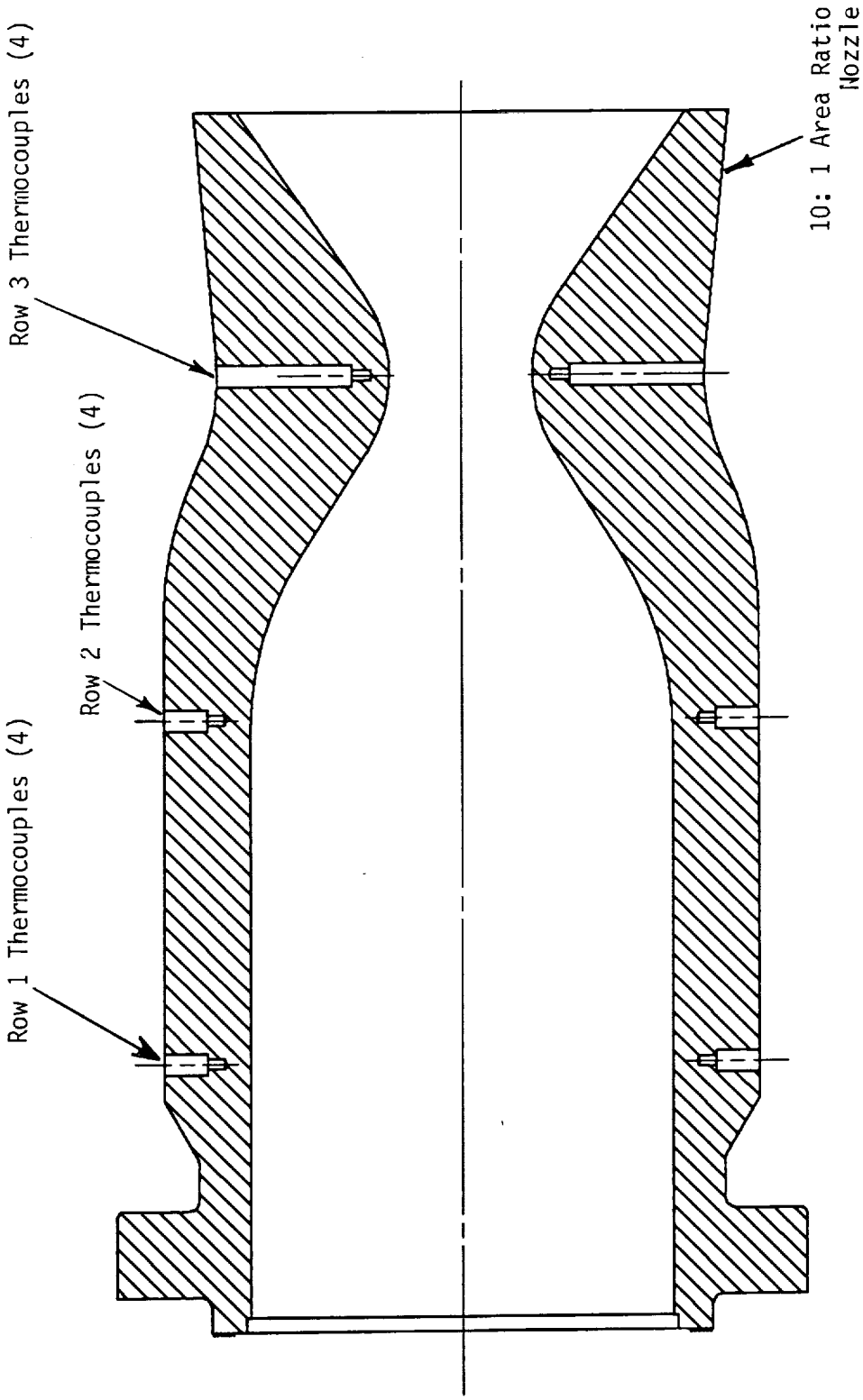

Figure 4-3. Heavy Wall Copper Chamber

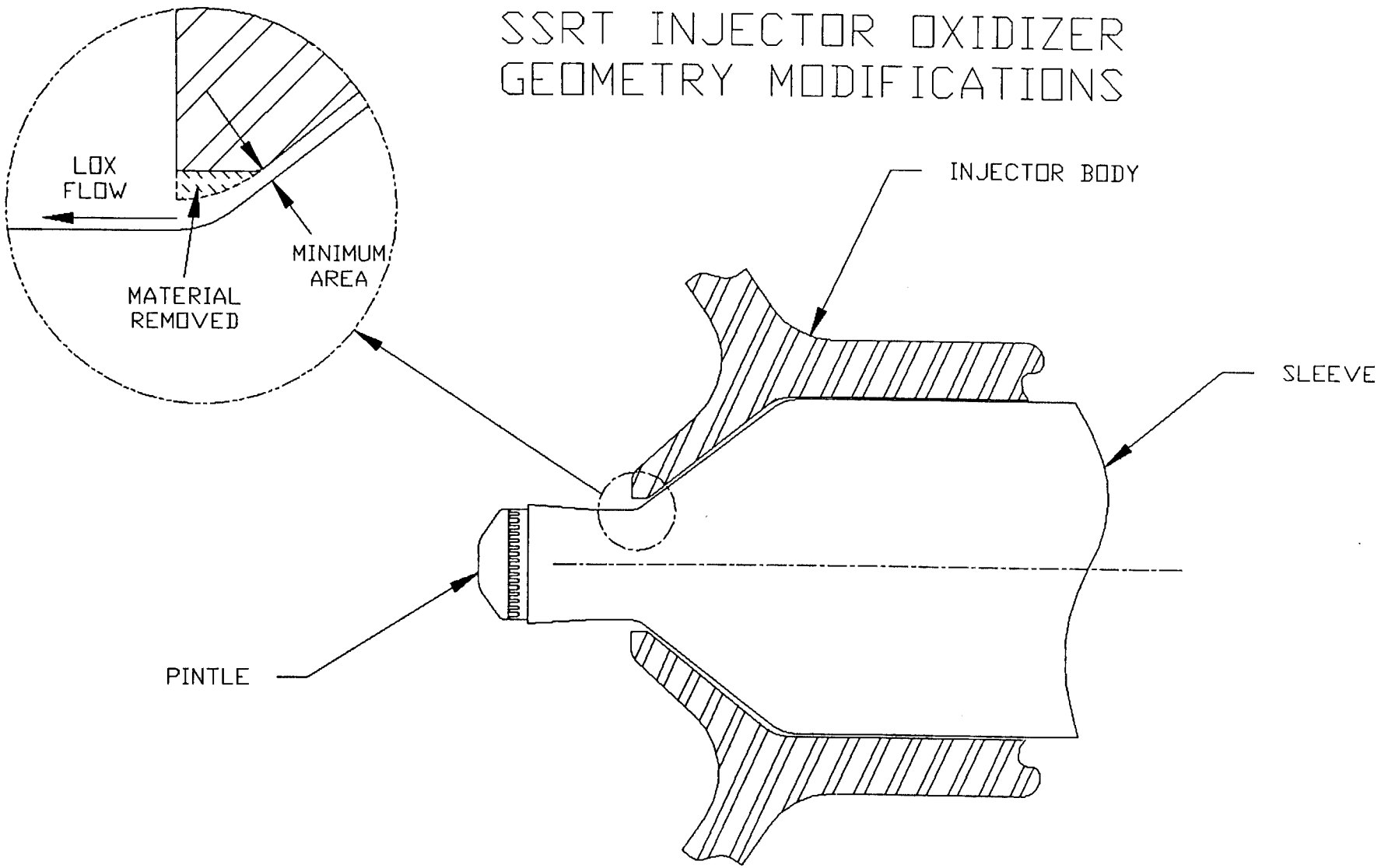
SSRT INJECTOR OXIDIZER
GEOMETRY MODIFICATIONS
LOX
FLOW
MINIMUM
AREA
MATERIAL
REMOVED
INJECTOR BODY
SLEEVE
PINTLE

FIGURE 4-4

film cooling and thermal block approaches to controlling the injector temperatures.

The Option 1 hot fire test series was divided into two parts, performance mapping of the two new elements, and injector cooling evaluations with film cooling and thermal block adaptors. Tests were shutdown when redline conditions on the chamber or injector thermocouples were met. These redline temperatures were:

Chamber TCs	1000°F
Injector TCs	600°F

Prior to the performance mapping of the two new fuel elements, a limited number of tests with the -11 element were conducted in order to ensure that the performance and thermal characteristics of the engine had not changed since the basic program testing in 1991.

4.3.1.1 Test Facility

All hot fire testing of the SSRT engine was performed at TRW's Capistrano Test Site (CTS) Facility in the HEPTS HA2A vacuum capsule. A facility schematic is shown in Figure 4-5. A mechanical pumping system maintained the test cell at less than 50 torr absolute pressure for all hot fire testing.

The fuel propellant tank was an 80 gallon hydrazine tank with an outer glycol jacket that allowed thermal conditioning of the propellant. Liquid oxygen propellant tankage included a 150 gallon run tank, fed from a 300 gallon LO_2 storage tank. Both LO_2 tanks were vacuum insulated. The LO_2 in the run tank was kept at its normal boiling point (-298F) by venting the tank to atmospheric pressure between tests. LO_2 propellant lines to the test capsule were insulated, and were chilled prior to a test by bleeding LO_2 from the run tank to the fire valve. The line downstream of the LO_2 fire valve and the injector were pre-chilled by liquid nitrogen prior to each test.

The igniter fluid was supplied by a small N2O4 tank and controlled by a cavitating venturi. Propellant line heaters were used on the fuel and igniter lines to prevent freezing of the propellants during engine start-up. All propellant lines were purged with GN_2 during the start up and shutdown transients. All valve timing was controlled by an IBM PC based timer that allowed millisecond timing resolution of the valve command signals.

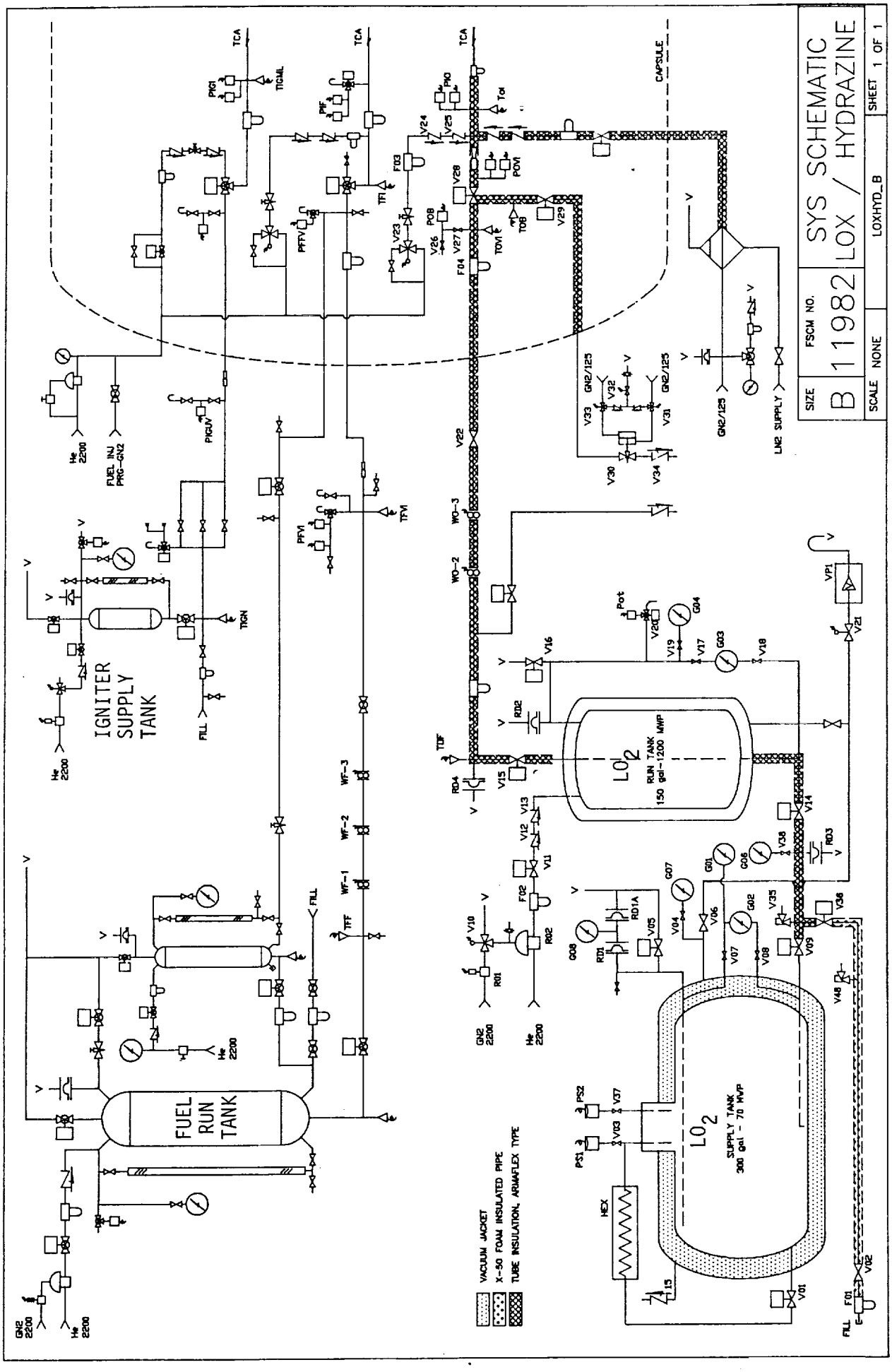

Figure4-5 . Test Facility Schematic.

4.3.1.2 Test Instrumentation and Date Recording

Performance evaluation of the SSRT engine was based on C* performance measurements. Redundant instrumentation was used on all performance related parameters, including propellant flow rates, chamber pressure transducers, and venturi inlet pressures. Cavitating venturis were used to control the flow rates to the engine. These venturis have been water flow calibrated. Three calibrated flowmeters in series were used to measure the fuel flow rate. The oxidizer flow rate was determined by use of a cavitating venturi, with flowmeter measurements as a backup. Chamber pressure was measured both at the head end and at the chamber pressure ports during performance mapping, and at the chamber port only during injector cooling tests.

Thermocouple instrumentation included 12 type K thermocouples brazed into the copper chamber. Also, 12 thermocouples were located at key locations on the injector to allow an assessment of the thermal characteristics of the injector head end. Other thermocouple instrumentation included propellant temperatures at the flowmeters, venturi inlets and engine inlets. An instrumentation list is presented in Table 4-2.

Critical temperature measurements such as chamber and injector dome temperatures were displayed on strip charts for real time monitoring during testing. Early shutdown of a test was determined by strip chart trends. Oscillograph recording of critical parameters was available for quick look and transient analysis of each test. All instrumentation was recorded on digital tape and printed in numeric format for data reduction analysis.

4.3.2 Performance Mapping Test Series

Option 1 performance of the SSRT engine was performed in May and June 1992. Table 4-3 summarizes the performance mapping tests of the -11, -12 and -13 fuel elements. In all, 35 tests were conducted in this series, accumulating 280 seconds of test duration. A peak C* of 5903 ft/sec was measured for the -11 hybrid element, representing a vacuum Isp of 346 seconds.

4.3.2.1 Verification Testing of -11 Fuel Element

In order to verify that the modifications to the injector body had not changed the performance and other characteristics of the engine, five tests were conducted with the -11 element (60 slots) installed in the injector. These tests were set up to be identical to five tests performed in the Basic Program in 1991 to allow a direct comparison of 1991 to 1992 results. The test conditions were to set a 0.0033 inch fuel gap and three different oxidizer gaps, 0.012 0.014 and 0.016 inches, to compare the oxidizer gap trend established in the basic program.

TABLE 4-2
TEST INSTRUMENTATION REQUIREMENTS (HA2A)

ID	RANGE	RECORD/DISPLAY METHOD			PARAMETER
		S/C	OSC	DVM	
PCN-1	0-300 PSIA	X	X		CHAMBER PRESSURE
PCN-2	0-300 PSIA				CHAMBER PRESSURE
PIO	0-1000 PSIA			X	OXID INLET PRESSURE
PID-1	0-750 PSIA	X	X		OXID DISTRIBUTION PRESSURE
PID-2	0-500 PSIA				OXID DISTRIBUTION PRESSURE
PIF-1	0-1000 PSIA	X	X	X	FUEL INLET PRESSURE
PIF-2	0-750 PSIA				FUEL INLET PRESSURE
POVI-1	0-1000 PSIA		X		OX VENTURI INLET PRESSURE
POVI-2	0-1000 PSIA				OX VENTURI INLET PRESSURE
PFVI-1	0-1000 PSIA				FU VENTURI INLET PRESSURE
PFVI-2	0-1000 PSIA				FU VENTURI INLET PRESSURE
PGOI	0-1000 PSIA		X		GASEOUS OXYGEN INLET PRES
PGOV	0-2000 PSIA			X	GO2 SONIC INLET PRESSURE
WO-2	0.15-0.35 LBM/S		X		OXID FLOWRATE
WO-3	0.15-0.35 LBM/S				OXID FLOWRATE
WF-1	0.30-0.45 LBM/S		X	X	FUEL FLOWRATE
WF-2	0.30-0.45 LBM/S				FUEL FLOWRATE
WF-3	0.30-0.45 LBM/S				FUEL FLOWRATE
PIGT	0-1000 PSIA			X	IGNITION TANK PRESSURE
PIGI	0-500 PSIA	X	X		IGNITION INLET PRESSURE
PA-1	0-50 TORR			X	CELL PRESSURE
PA-2	0-50 TORR				CELL PRESSURE
POT	0-1000 PSIA			X	OXID TANK PRESSURE
PFT	0-1000 PSIA			X	FUEL TANK PRESSURE
ACCEL	0-100 Gs		X		HEA ACCELERATION

TABLE 4-2 (Continued)
TEST INSTRUMENTATION REQUIREMENTS (HA2A)

ID	RANGE	RECORD/DISPLAY METHOD			PARAMETER
		S/C	OSC	DVM	
TOF	-350 to -200°F				OXID FEEDLINE TEMP
TFF	40 to 100°F				FUEL FEEDLINE TEMP
TFI	40 to 100°F			X	FUEL INLET TEMP
TOI	-350 to -200°F			X	OXID INLET TEMP
TOVI	-350 to 60°F				OXID VENTURI TEMPERATURE
TOGV	40 to 100°F				GO2 SONIC INLET TEMP
TIGML	40 to 300°F				IGNITER LINE TEMPERATURE
TFUML	40 to 300°F				FUEL LINE TEMPERATURE
TR-1	0 to 2000°F	X			CHAMBER/NOZZLE TEMPS
THRU	¦	¦			¦
TR-12	0 to 2000°F	X			CHAMBER/NOZZLE TEMPS
TI-1	-300 to 1000°F	X			INJECTOR DOME TEMPS
THRU	¦	¦			
TI-4	-300 to 1000°F	X			INJECTOR DOME TEMPS
TI-5	-300 to 1000°F				INJECTOR TEMPS
THRU	¦				
TI-10	-300 to 1000°F				INJECTOR TEMPS
TSP-1	-300 to 1000°F	X			SPLASH PLATE TEMPS
THRU	¦	¦			
TSP-4	-300 to 1000°F	X			SPLASH PLATE TEMPS
TIS	-300 to 1000°F	X			INJECTOR SNOUT PROBE
TPC	0 to 2500°F				PC PORT PROBE (TYPE R)

*ALL PARAMETERS TO BE RECORDED ON DIGITAL TAPE.

Table 4-3 Option 1 Performance Testing Summary

Fuel Element	Run No	Time Slice	Fuel Gap	OX Gap	Wt lb/sec	MR O/F	PC psia	C* ft/sec	TIS F
-11	4068	4.5	0.0033	0.0160	0.589	0.821	190.9	5560	143
-11	4069	7.0	0.0033	0.0160	0.590	0.804	193.8	5649	58
-11	4070	8.7	0.0033	0.0140	0.590	0.820	184.8	5390	418
-11	4071	7.4	0.0033	0.0140	0.590	0.802	195.3	5706	54
-11	4072	7.2	0.0033	0.0116	0.584	0.776	194.0	5731	218
-12	4073	6.4	0.0033	0.0140	0.592	0.798	191.8	5574	127
-12	4074	6.4	0.0033	0.0140	0.591	0.796	197.9	5763	189
-12	4075	8.6	0.0025	0.0140	0.594	0.803	197.4	5738	120
-12	4076	7.6	0.0016	0.0140	0.591	0.795	196.1	5724	116
-12	4077	7.4	0.0033	0.0116	0.588	0.787	197.4	5788	209
-12	4078	6.0	0.0033	0.0098	0.593	0.804	198.6	5772	199
-12	4079	8.2	0.0033	0.0116	0.584	0.693	191.5	5653	174
-12	4080	7.2	0.0033	0.0116	0.588	0.892	194.4	5704	191
-12	4081	7.6	0.0042	0.0140	0.593	0.808	194.9	5667	149
-13	4082	9.8	0.0033	0.0140	0.587	0.792	191.2	5618	68
-13	4083	9.8	0.0033	0.0116	0.589	0.800	194.8	5720	110
-13	4084	6.0	0.0033	0.0098	0.593	0.805	193.0	5599	193
-13	4085	9.2	0.0024	0.0116	0.593	0.801	196.5	5724	117
-13	4086	9.8	0.0015	0.0116	0.587	0.788	193.3	5683	129
-12 Hyb	4087	9.8	0.0031	0.0140	0.591	0.797	192.2	5617	82
-12 Hyb	4088	6.4	0.0031	0.0140	0.627	0.737	205.5	5649	153
-12 Hyb	4089	9.8	0.0031	0.0140	0.640	0.711	210.9	5699	199
-12 Hyb	4090	9.8	0.0020	0.0140	0.623	0.729	206.3	5731	151
-12 Hyb	4091	9.8	0.0020	0.0140	0.639	0.687	213.4	5777	106
-12 Hyb	4092	8.2	0.0020	0.0140	0.640	0.697	209.7	5656	179
-12 Hyb	4093	9.7	0.0011	0.0140	0.623	0.730	203.3	5642	53
-12 Hyb	4094	4.2	0.0020	0.0116	0.625	0.733	174.8	4796	681
-12 Hyb	4095	6.0	0.0020	0.0116	0.626	0.731	188.0	5159	450
-12 Hyb	4096	9.8	0.0020	0.0160	0.628	0.735	207.8	5724	104
-11 Hyb	4097	7.4	0.0021	0.0140	0.640	0.692	214.5	5777	137
-11 Hyb	4098	9.4	0.0021	0.0140	0.656	0.681	220.8	5822	133
-11 Hyb	4099	9.6	0.0021	0.0140	0.666	0.658	226.8	5895	149
-11 Hyb	4100	6.4	0.0021	0.0140	0.680	0.642	226.9	5760	152
-11 Hyb	4101	9.6	0.0021	0.0140	0.591	0.655	196.4	5734	177
-11 Hyb	4102	8.5	0.0021	0.0140	0.699	0.645	238.3	5903	156

Figure 4-6 shows the results of the -11 testing for 1991 and 1992. Although it appears that the C* performance has dropped approximately 50 ft/sec from the 1991 results, this was accounted for by the fact that the copper chamber was much cooler at the end of the test than in the 1991 testing. Previous testing has shown that when the chamber wall temperatures exceed about 500°F, an increase in performance of approximately 50 ft/sec was observed. This increase was attributed to decomposition of liquid fuel on the chamber wall. With the new heavy wall copper chamber, the wall temperatures were below 500°F at shutdown when the injector temperature redline was exceeded. If 50 ft/sec was added to the 1992 data to account for fuel decomposition at the chamber wall, then the performance for two of the three points was nearly identical.

Another difference in the Option 1 data was the higher performance at the 0.0118 oxidizer gap. When this test was made during 1991, a severe drop in performance was observed; but for the Option 1 testing, performance was actually higher at the smaller oxidizer gap than the other points, and also indicated a more realistic data trend. The explanation for the low performance in the 1991 data was the oxidizer attachment problem discussed in section 4.2. From the Option 1 data, there are indications that the problem has been solved by the injector modification.

An important finding from the injector snout thermocouple probe was that the snout temperature operated in the 200°F range, well into film boiling for liquid oxygen. Before the TIS probe was installed, it had been assumed from thermal data that the LO_2 injection point operated in the nucleate boiling regime. Oxidizer pressure drop calculations show an increase of approximately 15% in the oxidizer pressure drop due to vapor generation. It was determined later, during the thermal block and film cooling testing, that boiling and vapor generation at the LO_2 injection point had a profound effect on performance of this engine.

4.3.2.2 Performance of the -12 Element

The -12 element (90 slot) was tested first with the standard pintle, starting with a .0033 inch fuel gap and .0140 inch oxidizer gap. Performance for this element was in the 91% to 94% C* efficiency range. The performance of the -12 element alone (without the hybrid pintle) was the highest of all fuel elements tested on the SSRT program.

Figure 4-7 shows the performance trend of the -12 element vs oxidizer gap, along with the data from the -11 and -13 elements. The trend indicated was very similar to the -11 trend, except the -12 performance was approximately 1% higher. Figure 4-8 presents the performance trend of the -12

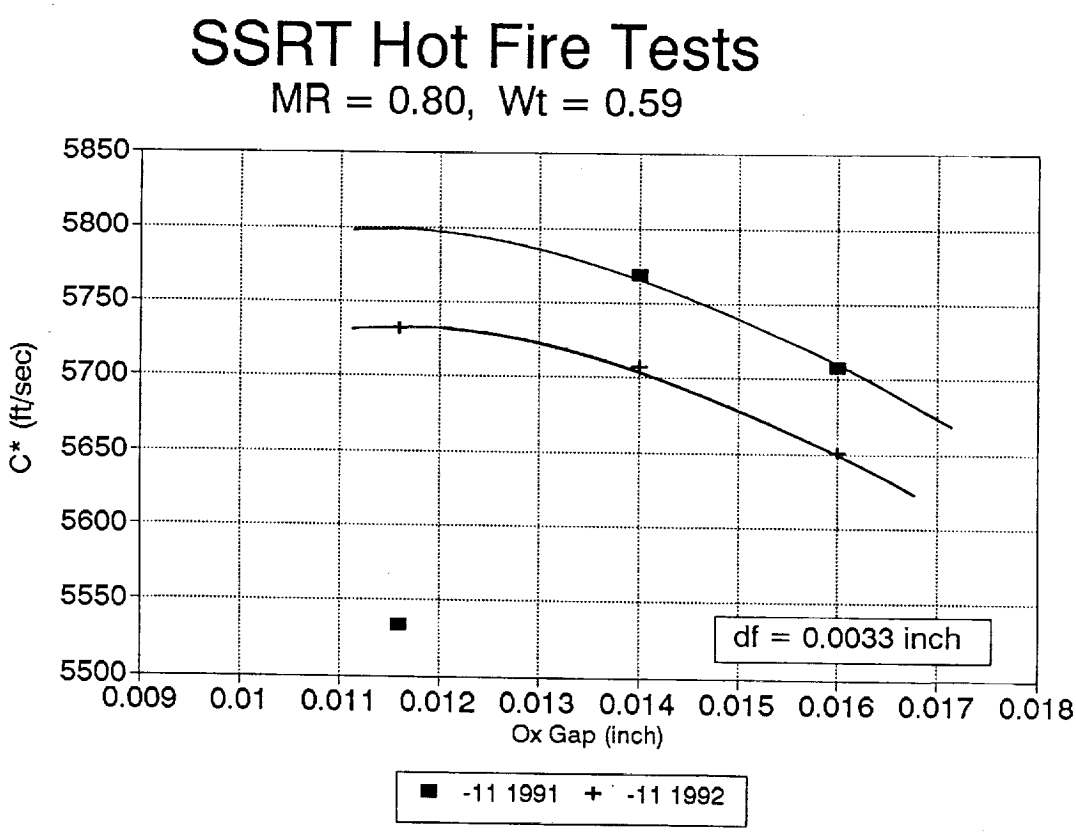

Figure 4-6. -11 Element Testing, 1992 vs 1991 Results

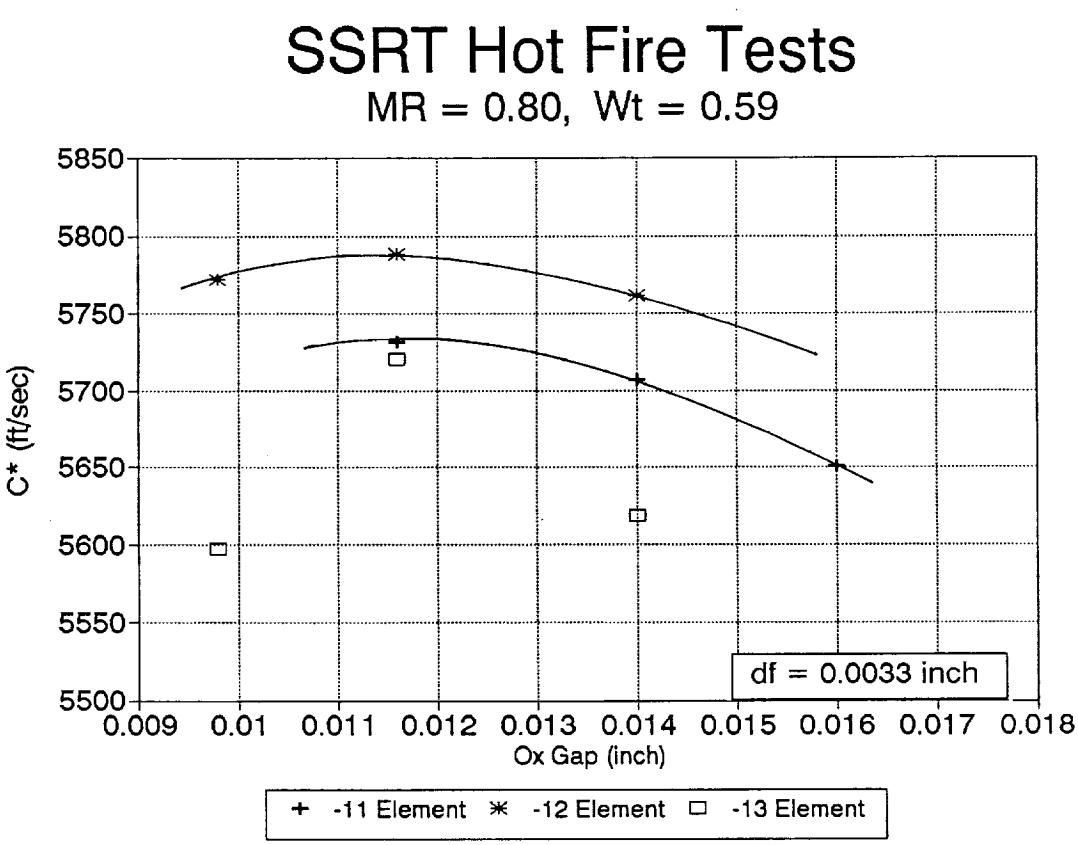

Figure 4-7. -11, -12 and -13 Performance vs Ox Gap

element vs fuel gap at a 0.014 oxidizer gap. The data at the 0.0033 fuel gap and smaller gaps indicated that the trend favored even larger fuel gaps, but when a 0.0042 fuel gap was tested the performance dropped off significantly.

Testing of the -12 element with the hybrid pintle showed no improvement in performance as it did with the -11 element, in fact the performance was in general lower and showed more scatter than the -12 element alone did. Figure 4-9 compares the -12 hybrid to the -11 hybrid element performance vs momentum ratio. For the same momentum ratio, the -12 hybrid element showed less performance than the -11 hybrid, but there appears to be a trend of increasing performance with lower momentum ratio that was not further explored.

Testing of the -12 hybrid at the smallest oxidizer gap (do = 0.0116 inch) resulted in low C* performance, with extremely high injector heating rates. In the two tests at this oxidizer gap (HA2A-4094 and 4095) the injector gas temperature as measured by TPC was 1800°F to 2000°F and TIS was over 500°F and climbing at shutdown. Performance was on the order of 78% to 84% C* efficiency, indicating large changes in the combustion characteristics at these operating conditions.

4.3.2.3 Performance of the -13 Fuel Element

The -13 element testing produced a maximum performance of 93% C* efficiency, which was below both the -11 and -12 performance. The performance trend of the -13 element was similar to the -11 and -12 elements, as seen in Figure 4-7, except that the trend peaks much more prominently at the 0.0118 oxidizer gap. This was mostly attributed to data scatter due to the fact that the chamber temperatures for these tests were in the range where the fuel would start to decompose on the chamber wall (300°F to 500°F), resulting in the performance increase as described above.

The performance trend for the -13 vs fuel gap is shown in Figure 4-8. Apparently, the high aspect ratio of the slots for this element resulted in lower performance than the other elements. Since the performance of the -12 hybrid was lower than the -12 alone, the -13 element was not tested with the hybrid pintle in this series.

4.3.2.4 Performance Mapping of the -11 Hybrid Fuel Element

After the performance mapping of the -12 and -13 elements were complete, the result was that the highest performance achieved to date was the -11 hybrid element tested in the basic program. At this point the decision was made to install the -11 hybrid element and try to improve the

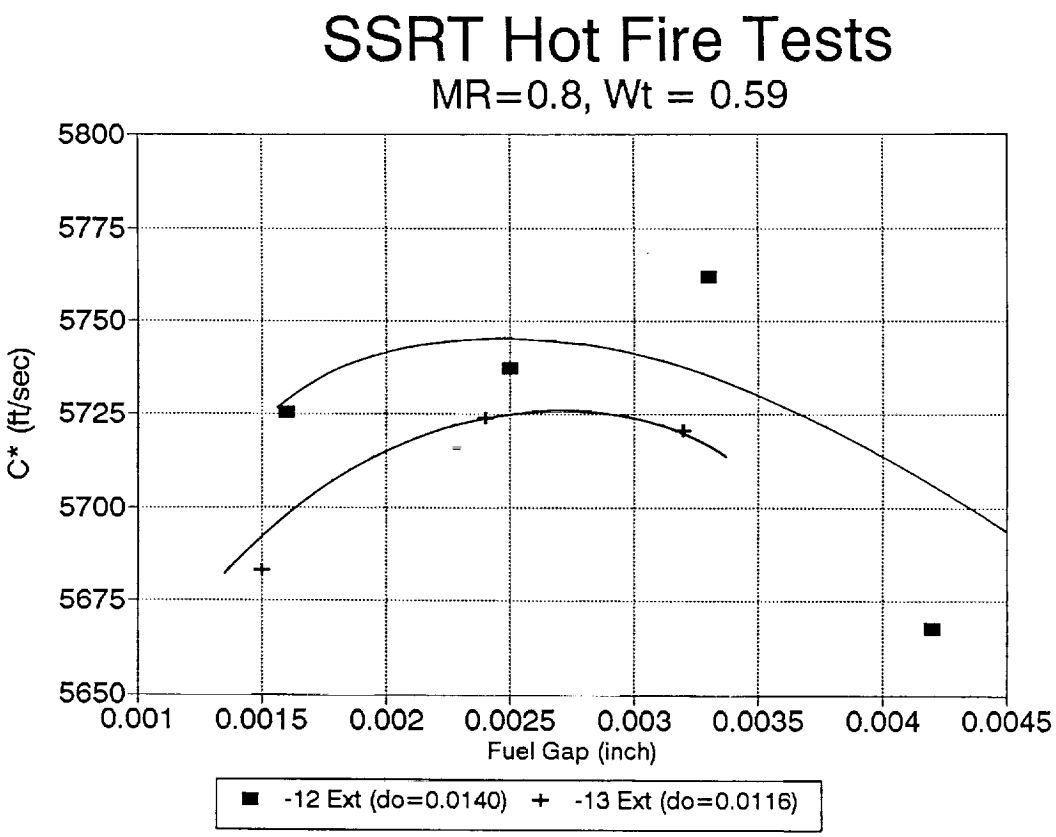

Figure 4-8. -12 and -13 Performance vs. Fuel Gap

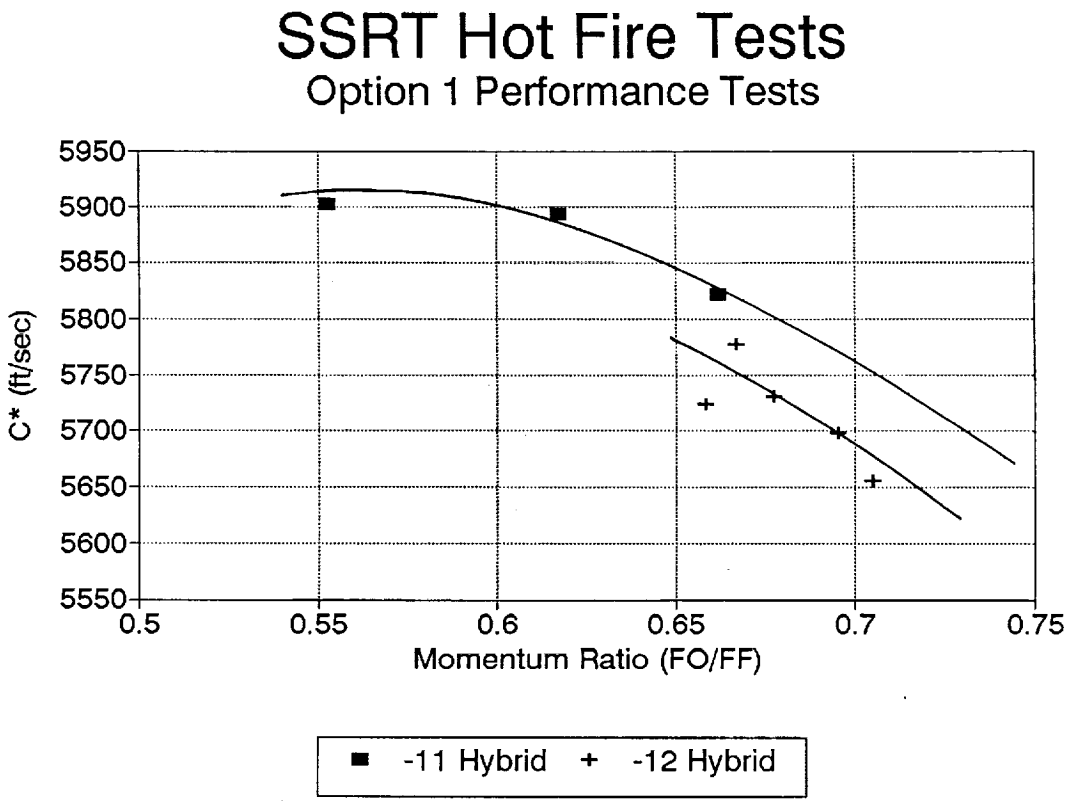

Figure 4-9. -11 Hybrid and -12 Hybrid Performance vs Momentum Ratio

performance by increasing the fuel flow rate, thus lowering the mixture ratio. When this was attempted in the 1991 test series, oxidizer attachment problems at the oxidizer injection point caused the performance to drop off significantly. The points that did not have this problem, indicated that the performance could be increased if the mixture ratio was decreased, as shown in Figure 4-10. This graph shows the 1991 test data which reached 5860 ft/sec at a mixture ratio of 0.69, and the data from the current series, which peaked at over 5900 ft/sec C* at 0.65 mixture ratio. The high performance was achieved by increasing the fuel flow rate while leaving the LO_2 flow rate at the nominal 0.26 lb/sec. This also resulted in an increase in total flow. In order to explore the total flow effect, a test was made at the nominal flow rates, but at the same mixture ratio as the high flow rate cases. The result was that the lower flow rate case had nearly 3% lower performance than the high flow cases, as shown in figure 4-11. At higher mixture ratios in the 1991 testing, the performance did not generally increase with total flow, thus it appears that high performance was a product of both high flow rates and low mixture ratio.

LO_2 injector temperatures as measured at TIS were typically in the 100°F to 200°F range, well into film boiling. Although film boiling is usually associated with thermal runaway and burnout, in this case the temperatures seemed to be well controlled. In fact, on a typical test, TIS may exceed 200°F early in the test, then drop down under 150°F towards the end of the test. As discussed in section 3.2.1, the film boiling heat transfer may be enhanced due to the narrow annular oxidizer passages in the injector.

TPC indicated injector gas recirculation temperatures in the 800°F to 1000°F range for most of the -11 hybrid testing. These temperatures were low enough to indicate that the thermal block concept was feasible.

4.3.3 Injector Cooling Evaluation Testing

After the performance mapping of the -11, -12 and -13 elements was completed, the injector cooling adaptor tests were initiated. The -11 hybrid element was used to evaluate the thermal block and film cooling adaptors since it had demonstrated the best performance.

Table 4-4 summarizes the thermal block and film cooled adaptor tests. All tests ran the full 20 second timed duration, but the performance was as much as 6% lower than for the same injector conditions with no injector cooling.

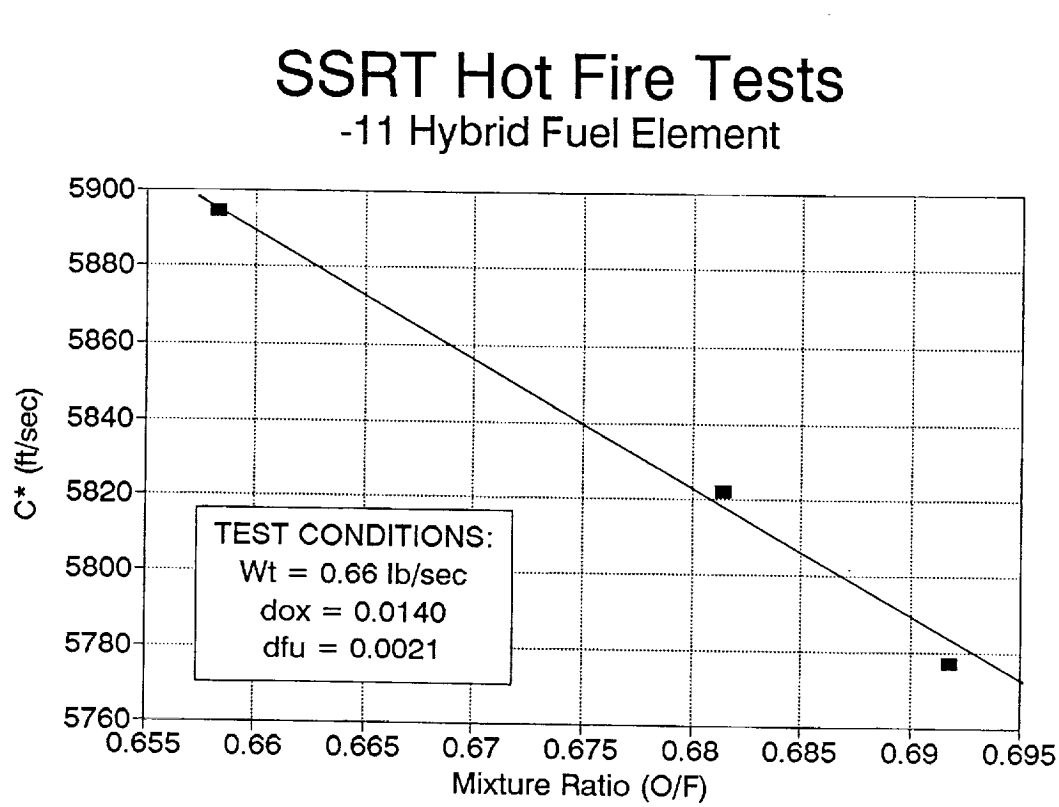

Figure 4-10. -11 Hybrid Element Performance vs Mixture Ratio

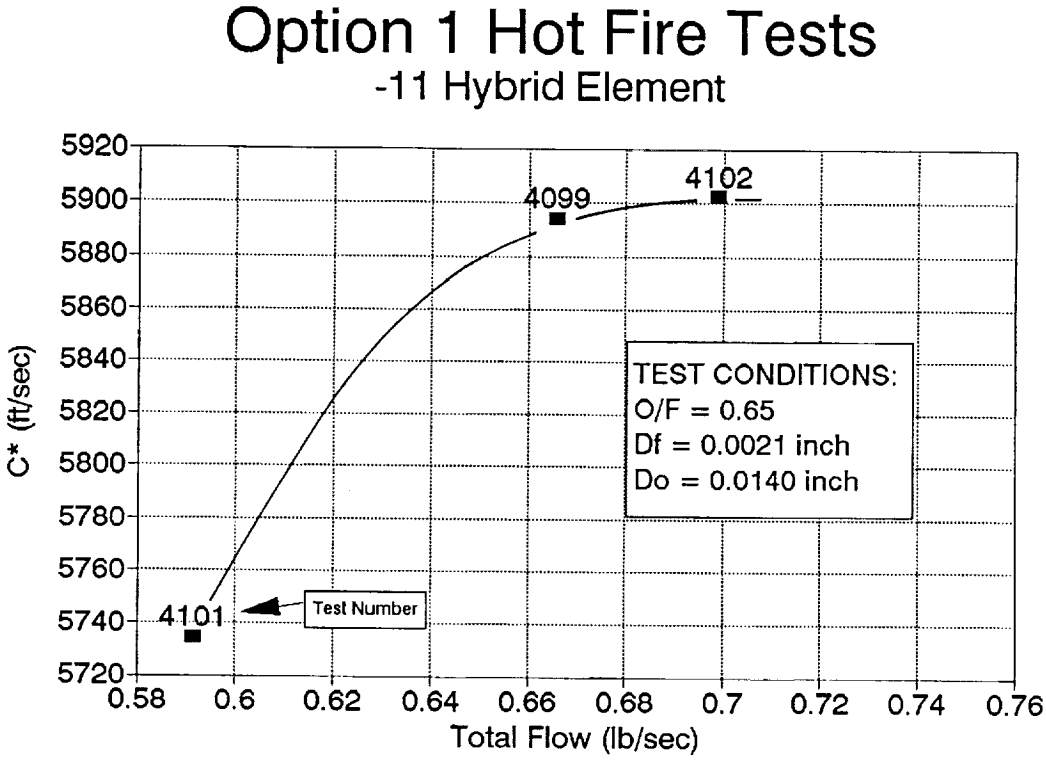

Figure 4-11. Performance vs Total Flow for -11 Hybrid Element

Table 4-4 Thermal Block and Film Cooling Adaptor Test Summary

THERMAL BLOCK ADAPTOR

Fuel Element	Run No	Time Slice	Fuel Gap	OX Gap	Wt lb/sec	MR O/F	PC psia	C* ft/sec	TIS °F
-11 Hyb	4105	19.8	0.0021	0.0140	0.6621	0.655	211.1	5545	-260
-11 Hyb	4106	19.8	0.0021	0.0140	0.6626	0.654	211.5	5553	-262
-11 Hyb	4107	19.8	0.0021	0.0140	0.6631	0.711	206.1	5393	-247
-11 Hyb	4108	19.8	0.0021	0.0140	0.6680	0.611	212.6	5539	-264
-11 Hyb	4109	19.9	0.0021	0.0116	0.6675	0.668	210.4	5482	-258
-12	4110	19.8	0.0033	0.0098	0.5900	0.796	179.2	5259	-217
-12	4111	19.8	0.0033	0.0098	0.6678	0.799	192.6	5013	-247
-12	4112	19.8	0.0033	0.0098	0.6632	0.662	203.2	5324	-219

FILM COOLING ADAPTOR

Fuel Element	Run No	Time Slice	Fuel Gap	OX Gap	% Film Cooling	Wt lb/sec	MR O/F	PC psia	C* ft/sec	TIS °F
-11 Hyb	4113	19.8	0.0021	0.0140	3.47	0.6862	0.713	217.3	5510	-62
-11 Hyb	4114	19.8	0.0021	0.0140	6.19	0.6872	0.716	226.4	5748	-257
-11 Hyb	4115	19.8	0.0021	0.0140	1.06	0.6617	0.657	211.7	5573	-237
-11 Hyb	4116	19.8	0.0021	0.0140	8.30	0.6814	0.745	228.5	5846	-254
-11 Hyb	4117	19.8	0.0021	0.0140	5.24	0.6891	0.605	222.2	5621	-242
-11 Hyb	4118	19.8	0.0021	0.0140	0.00	0.7015	0.732	223.1	5548	-198
-11 Hyb	4119	19.8	0.0021	0.0140	0.00	0.7007	0.802	215.2	5362	-188
-11 Hyb	4120	19.8	0.0021	0.0140	0.00	0.7094	0.650	227.0	5588	-220

4.3.3.1 Thermal Block Adaptor Tests

As mentioned above, the TPC measurements indicated that the gas recirculation temperatures at the injector were in the 1000°F range, which should be low enough to allow steady state operation with the thermal block adaptor. This was true, as witnessed by the fact that all of the thermal block and film cooling tests were run the full 20 second test duration, limited only by chamber temperatures. The snout temperatures were typically around -250°F, well below the nucleate boiling regime.

The -11 hybrid was tested under the same conditions as test 4099, where a performance of 95% C* was achieved. With the cooled injector, TIS was nearly 400°F cooler than the uncooled case, and the performance was 6% to 8% lower. The fact that the injector conditions had changed considerably was also evident in the thermal block surface temperature measurements, most of which were measuring temperatures below zero degrees F. These measurements were taken close to the area where the TPC probe was measuring gas temperatures around 1000°F for the uncooled testing. Clearly the thermal block adaptor was shutting off the injector gas heating, and also the engine performance.

Although the injector performance was much lower with the thermal block adaptor, the performance trend for momentum ratio was much the same, as shown in Figure 4-12. Performance for the -11 hybrid element peaks at a momentum ratio of around 0.5 as in the uncooled injector tests (Figure 4-9).

In an attempt to increase the injector recirculation gas temperature, the -12 element was installed with a small oxidizer gap (do = 0.0098 inch). For this element the injector temperatures were increased but the performance was lower. TIS indicated operation in the nucleate boiling regime, and the thermal block face TCs were reading a few hundred degrees F. Figure 4-13 shows the trend of injector face temperature vs momentum ratio for the thermal block adaptor.

Post test inspection of the thermal block and film cooling adaptor showed very little heat stains and no distortion or erosion of the surfaces. As expected, the tip of the splash plates showed the most heat discoloration.

4.3.3.2 Film Cooling Adaptor Tests

The film cooling adaptor was installed in the engine along with the -11 hybrid fuel element. Difficulties in getting the proper LO_2 film cooling flow were encountered due to "vapor lock" at the tangential injection holes. For most of the film cooling tests, the back pressure was high enough that the film cooling venturi was out of cavitation.

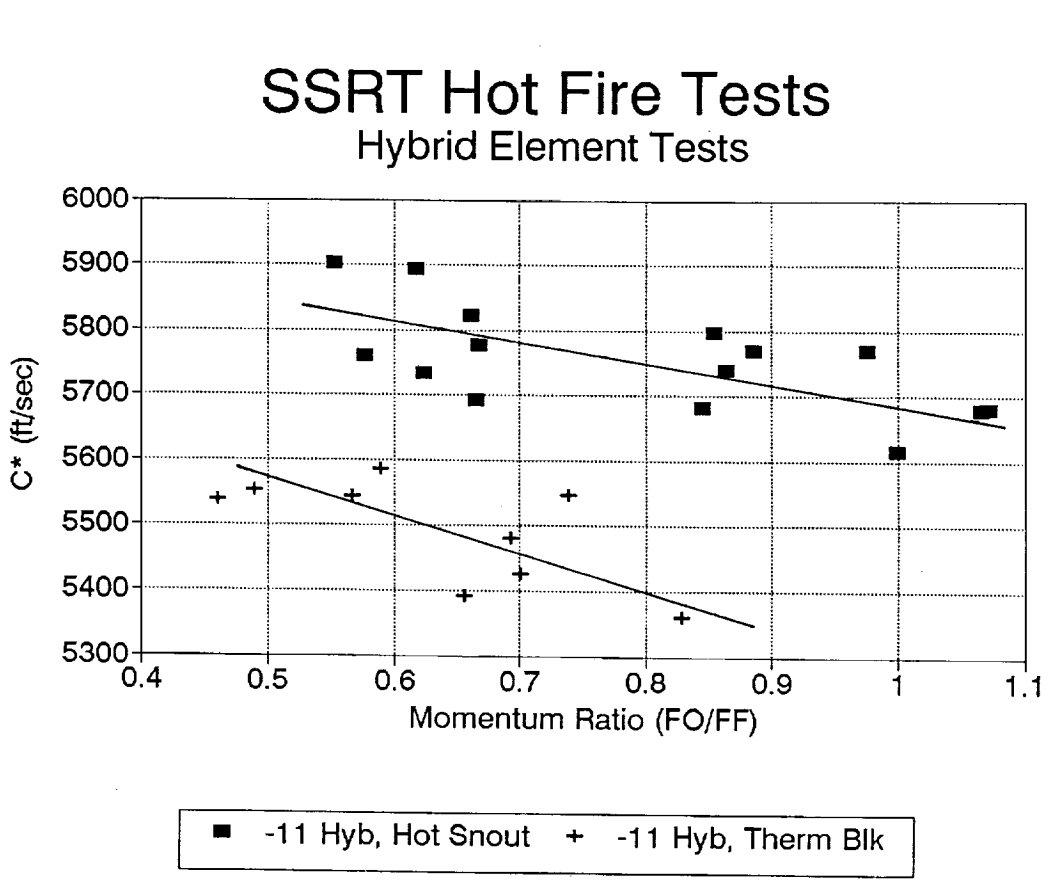

Figure 4-12. Performance Trends, Cooled vs Uncooled

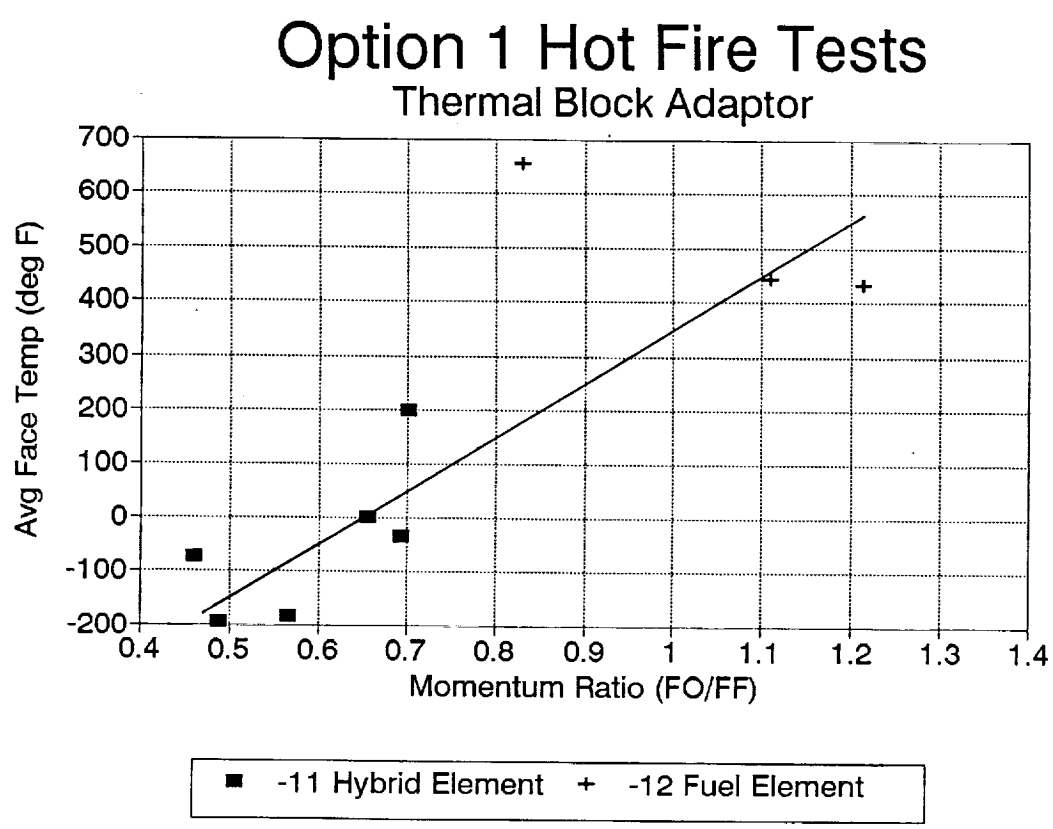

Figure 4-13. Injector Face Temperature vs Momentum Ratio

Performance and injector temperatures with the film cooling were similar to the thermal block results. TIS was near the LO_2 bulk temperature, and the performance was only about 50 ft/sec higher at best. The film cooling results did indicate a performance increase as the film cooling flow was increased, as shown in Figure 4-14.

The last three tests of this series were conducted without film cooling to compare to the tests with film cooling. Even thought the snout was completely exposed with the film cooling adaptor, TIS was still in the -200°F range, and performance was low. These results indicate that the splash plate portion of the film cooling adaptor probably has an effect of lowering the gas recirculation temperature in the injector region.

4.3.4 Summary of Results of Option 1 Testing

The results of the Option 1 testing culminated in 35 tests accumulating 280 seconds of hot fire duration. Three major categories of testing were accomplished.

4.3.4.1 Performance Evaluation

High performance (Isp = 346 lbf-sec/lbm) was achieved using the -11 hybrid fuel element, which is the highest performing element tested to date. The -12 basic fuel element (without the hybrid pintle) was the highest performing basic fuel element achieving an Isp of 340 lbf-sec/lbm. The -13 element had lower performance (Isp = 335 lbf-sec/lbm) than expected due to the high aspect ratio of the slots. All tests were terminated in ten seconds or less due to injector dome temperature redlines. Therefore, the injector must be cooled by some auxiliary means.

4.3.4.2 Thermal Block Evaluation

A thermal block adaptor was evaluated to determine its ability to protect the injector from high temperatures. The thermal block allowed full duration operation in the copper thrust chamber (20 seconds) with low dome temperatures° (<100F). The performance was about 5% lower than with no thermal block and the injector snout operated cold (-250°F).

4.3.4.3 Film Cooling Adaptor Evaluation

A film cooling adaptor was evaluated to evaluate the ability of LO_2 film cooling to protect the injector from high temperatures and assess its performance. The results were similar to the thermal block adaptor - low performance and low injector temperatures.

4.3.4.4 Overall Assessments

As a result of the Option 1 hot fire results, a set of critical experiments were defined to acquire a better understanding of the mechanisms relating to the injector operation.

4.4 Option 2 Critical Experiment Tests

Based on the thermal block and film cooling test results, a set of critical experiments were devised to try to acquire a better understanding of the mechanisms which relate injector temperatures at the LO_2 injection point to engine performance. Although these experiments were funded on the Option 2 program, the results were included here because the information gained is instrumental in understanding the results of the Option 1 testing, and in feeding the design of the next engine.

4.4.1 Test Approach and Hardware Modifications

Two major results of the Option 1 test series were:

1) The profound effect of injector snout temperature on performance

2) The apparent effect of the splash plate on injector recirculation gas temperature

A set of critical experiments was designed to provide more information in regards to the above results. In particular, it was desired to see if the vapor generation at the oxidizer injection point during film boiling could be simulated, and also to investigate a thermal block design with no splash plate. An additional test was to inject helium into the upstream LO_2 line to investigate the effect of bubble interaction on the LO_2 injection stream, and its relation to performance.

The prevailing theory for the increase of performance due to high snout temperatures was the formation of oxygen vapor at the injection point. Gaseous oxygen (GO_2) is much more reactive than LO_2, so it was postulated that the GO_2 formed at the injection point was accelerating the combustion of the fuel at the impingement point of the LO2. The added heat release from the GO_2 reaction would vaporize more of the fuel, allowing it to burn more completely before it impinged with the chamber wall. Thus, in effect, a small amount of oxygen vapor (15% by volume) in the main LO2 injection stream would "bootstrap" the main impingement reaction, thereby producing high performance. In the case where the injector snout was cooled, no vapor was generated, and the liquid-

Option 1 Hot Fire Tests

-11 Hybrid, Film Cooling Adaptor

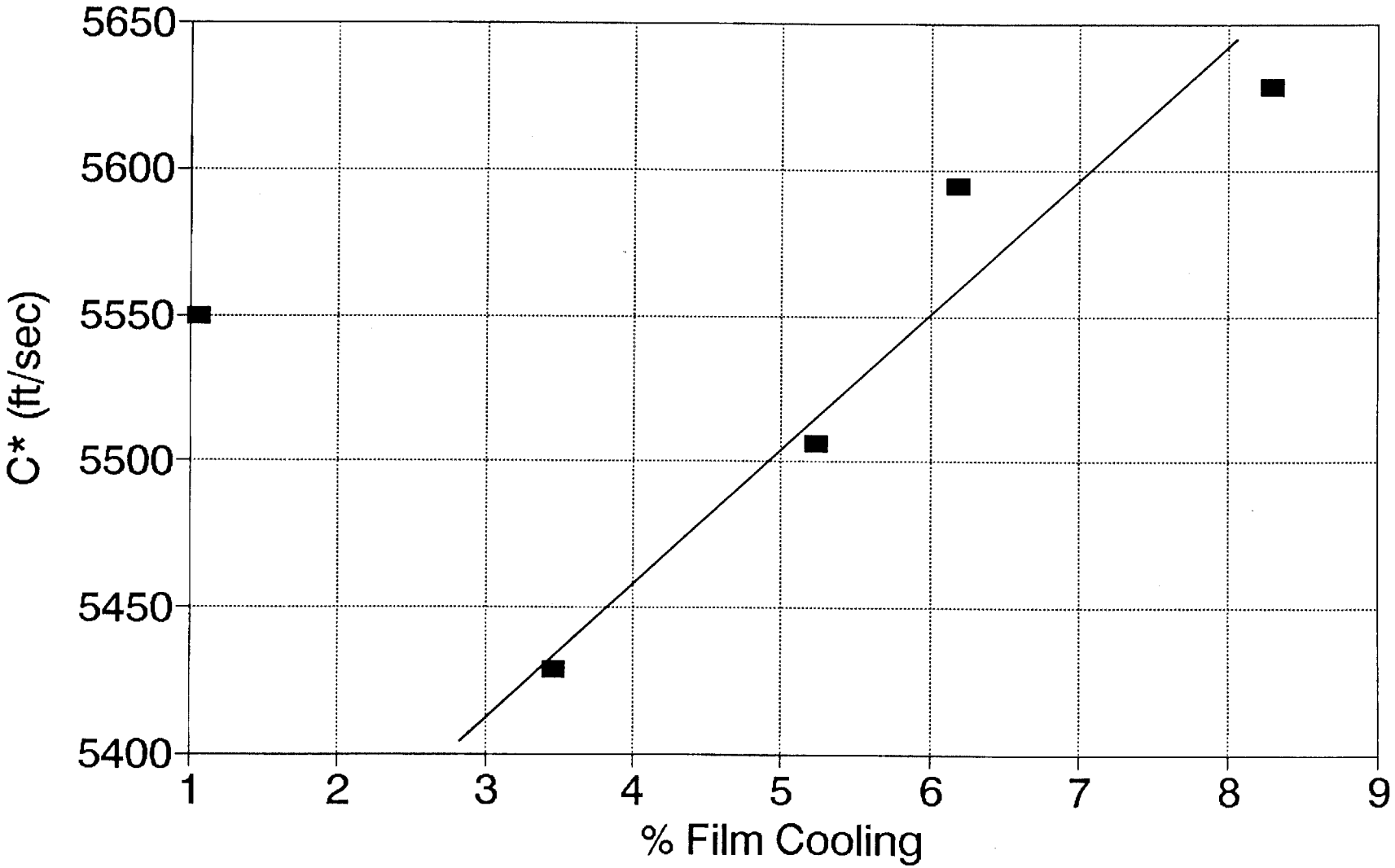

Figure 4-14. Performance verses % Film Cooling

at the injection point was accelerating the combustion of the fuel at the impingement point of the LO2. The added heat release from the GO_2 reaction would vaporize more of the fuel, allowing it to burn more completely before it impinged with the chamber wall. Thus, in effect, a small amount of oxygen vapor (15% by volume) in the main LO2 injection stream would "bootstrap" the main impingement reaction, thereby producing high performance. In the case where the injector snout was cooled, no vapor was generated, and the liquid-liquid impingement of the LO_2 and hydrazine results in the LO_2 chilling the fuel, thereby delaying the vaporization and combustion reactions. Evidence of the positive effect of oxygen vapors on performance was seen with the film cooling test, where an increase in performance was related to the amount of film cooling flow. The film cooling flow was partly GO_2 at injection, and probably all GO_2 by the time the film reached the impingement point. It is possible that this added GO_2 content to the injection area helped the combustion reaction as discussed above.

In order to more closely simulate vapor generation at the oxidizer injection point, it was necessary to directly inject GO_2 in the immediate vicinity of the LO_2 stream. The method of achieving this condition was to modify the thermal block adaptor used in the Option 1 testing to inject GO_2 at the snout tip, concentric with the LO_2 main flow. Figure 4-15 shows the injector assembly with the thermal block adaptor for GO_2 injection. The tip of the GO_2 injector had a deflector that would direct the GO_2 to impinge on the main LO_2 flow. This deflector could also be cut off to see the effect of having the GO_2 flow parallel to the main LO_2 flow if the test data warranted.

Cold flow testing of the GO_2 adaptor was performed with water to simulate the LO_2 and GN_2 to simulate the GO_2. The results showed that GN_2 flow rates above an equivalent of 5% by weight gas flow would break up the water stream into droplets, surround by a fine mist. The fine mist generated by this GN_2 "airblast" was determined to be approximately 13% of the total water flow.

In order to simulate the effect of GHe injection into the LO_2 feed line, water flows of the oxidizer circuit were also made with GN_2 injected into the LO_2 inlet line. At an equivalent flow of 1% by weight GN_2 injection, the water flow pressure drop of the oxidizer circuit was more than doubled. The stream appearance was a bushy even spray of droplets. Less fine mist was visible compared to the GO_2 adaptor, but the pattern was more controlled and evenly distributed.

Figure 4-16 shows the new face thermal block adaptor that was fabricated. This adaptor had nearly the same injector side contour as the previous adaptor, except no splash plate. Instead, it blended into the chamber wall just down stream of

FIGURE 4-15

SSRT Engine Assembly
GO_2 Injection - Thermal Block

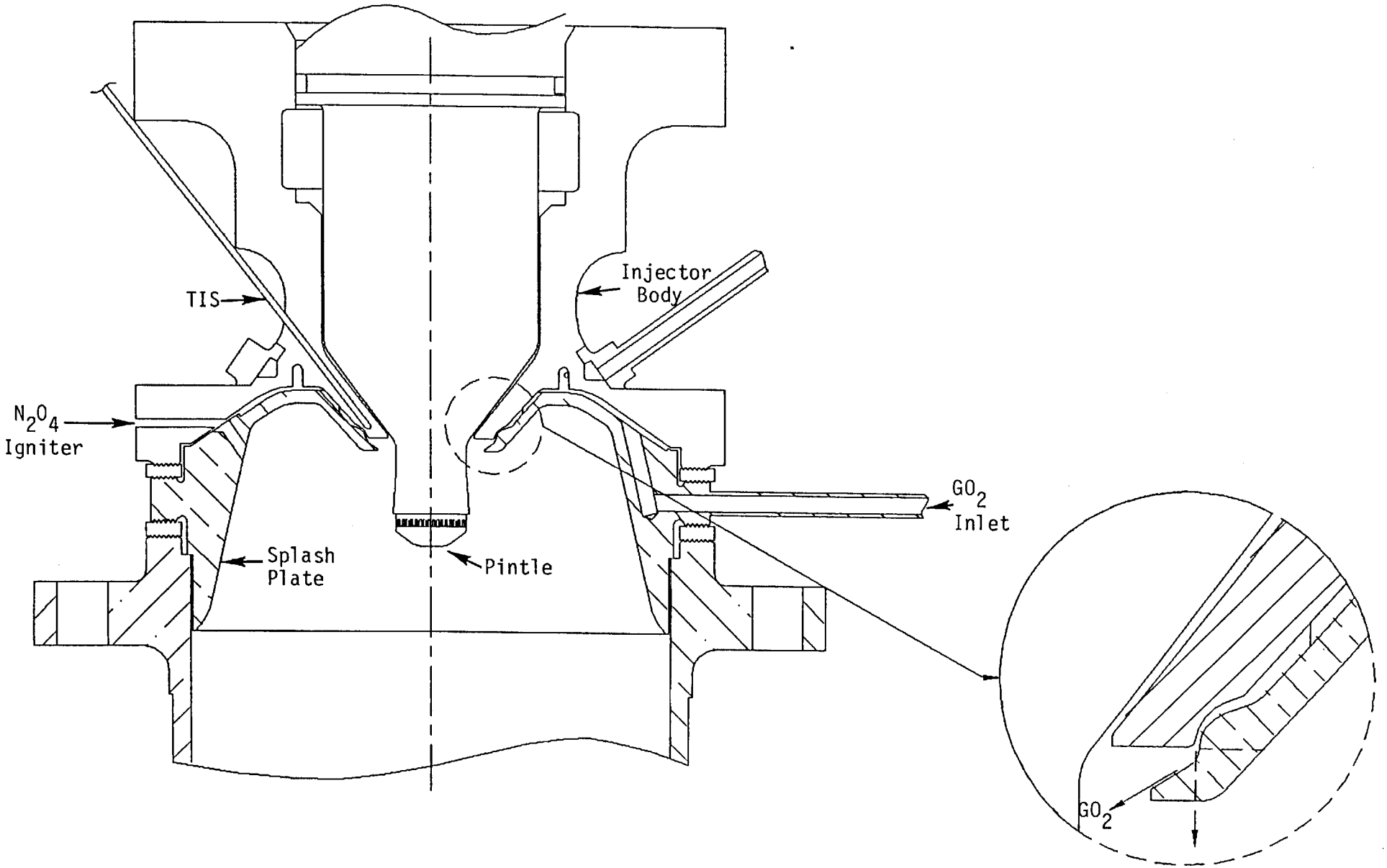

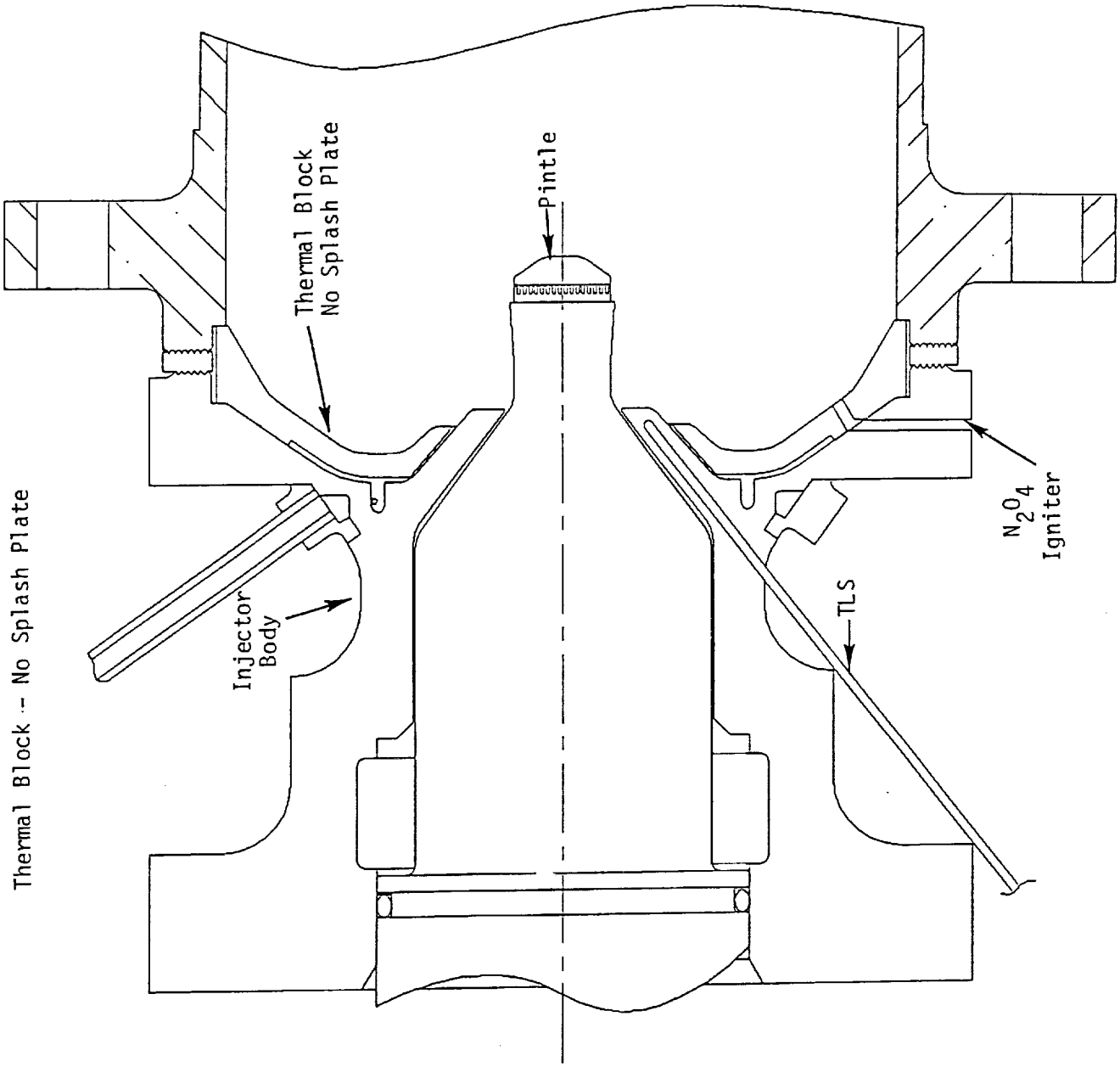

Figure 4-16
SSRT Engine Assembly
Thermal Block - No Splash Plate

13 were shortened by machining off the tops in order to reduce the aspect ratio of the element. The new element, called the -13a, had a slot aspect ratio (height/width) of 4.15 compared to an aspect ratio of 5.85 before the modification. The modification also reduced the slot area by 30%, resulting in a higher fuel delta P and injection velocity for the same fuel gap.

4.4.2 Critical Experiment Hot Fire Tests

The Option 2 critical experiment hot fire testing was performed in September and October of 1992 at the CTS HA2A test facility. In all, 38 tests were made, accumulating 520 seconds of firing duration.

The tests demonstrated that both GO_2 and GHe injection increased the engine performance, but neither of them resulted in the performance increase that film boiling at the oxidizer final orifice produced. Testing with the thermal block adaptor with no splash plate indicated a performance increase of 350 ft/sec resulted when comparing the oxidizer injection in film boiling compared to no film boiling. Testing with the splash plate only showed that low performance was achieved even if the oxidizer injector was in film boiling.

4.4.2.1 GO_2 Injection Hot Fire Results

The GO_2 injection adaptor was installed for the first series of critical experiment tests. Table 4-5 summarizes the GO_2 injection tests. GO_2 injection flow rates of 1% to 10% equivalent LO_2 mass flow rate were made. GO_2 flow was supplied from standard K bottles, controlled by a sonic orifice. Testing was made with both the -11 hybrid and the -13a hybrid fuel elements. Liquid propellant flow conditions were the same as test 4099.

Figure 4-18 shows the results of C* performance vs $\%GO_2$ flow for both the -11 hybrid and the -13a hybrid fuel elements. Performance was highest at the 5% GO_2 flow rate, remaining nearly the same or dropping slightly at higher flow rates. This may be due to the fact that at GO_2 flows above 5%, the "airblast" effect on the oxidizer stream was excessive, resulting in a broken up spray pattern and reduced performance. A peak performance of 5826 ft/sec was achieved with the -13a hybrid element at 5% GO_2 flow rate.

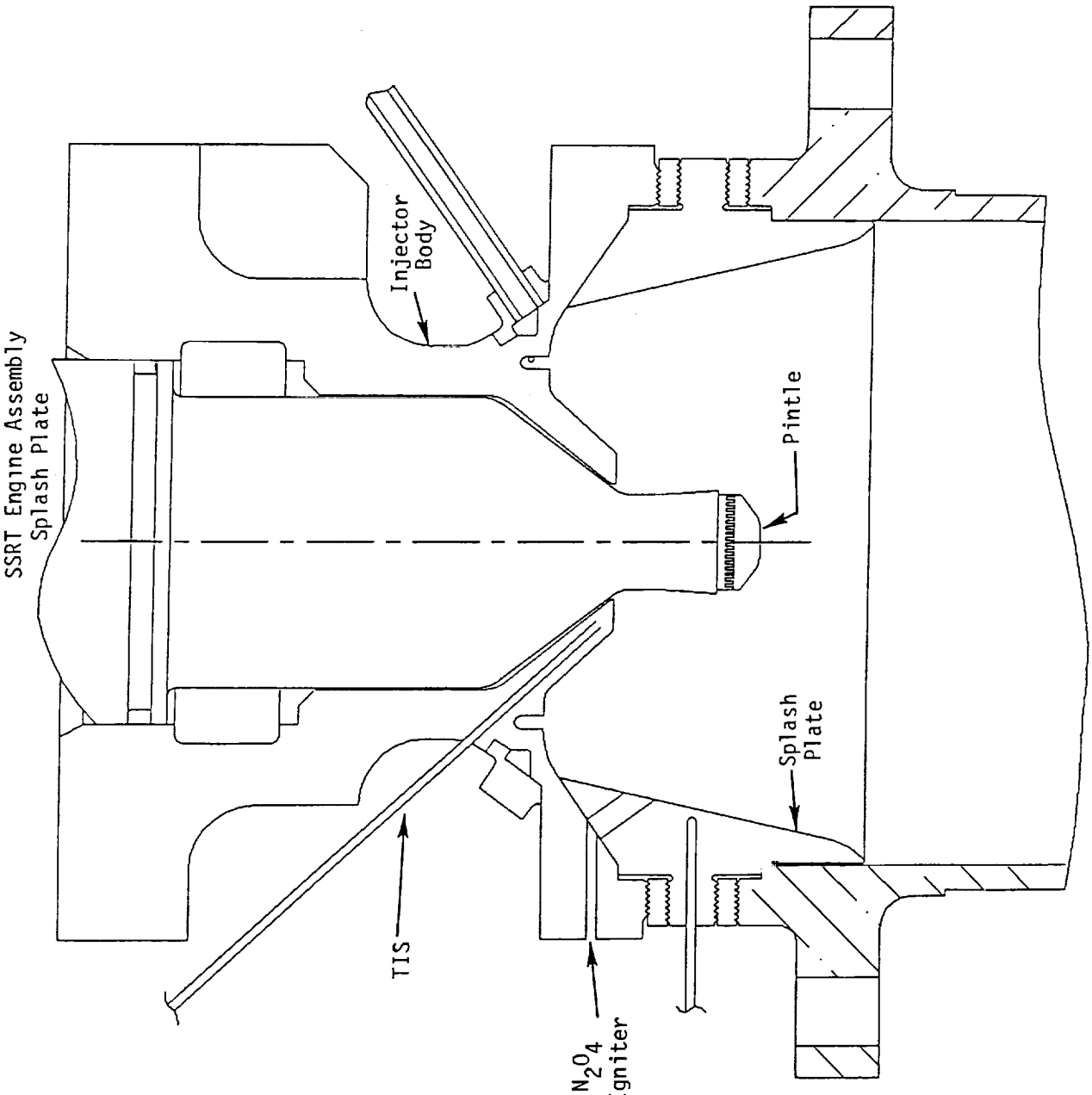

Figure 4-17
SSRT Engine Assembly
Splash Plate

Table 4-5. GO2 Injection Tests Summary

Run No	Time Slice	Fuel Gap	OX Gap	% GO2 of Wox	Wt lb/sec	MR O/F	PC psia	C* ft/sec	TIS F
-11 Hybrid Fuel Element									
4121	4.8	0.0021	0.0141	1.85	0.6666	0.676	211.7	5430	-215
4122	19.1	0.0021	0.0141	3.03	0.6644	0.665	212.5	5539	-221
4123	17.9	0.0021	0.0141	5.02	0.6703	0.678	219.4	5685	-131
4124	19.7	0.0021	0.0141	7.54	0.6785	0.695	221.0	5656	-145
4125	19.1	0.0021	0.0141	10.19	0.6833	0.709	224.0	5699	-101
4126	19.7	0.0021	0.0141	11.05	0.6607	0.655	212.8	5584	-152
4127	19.7	0.0021	0.0131	11.17	0.6581	0.649	213.3	5629	-117
4128	19.7	0.0021	0.0131	10.11	0.6823	0.711	224.7	5730	-114
4129	18.9	0.0021	0.0118	10.50	0.6845	0.710	224.4	5696	-145
4130	17.1	0.0021	0.0131	9.45	0.7106	0.776	235.7	5772	-132
4132	17.1	0.0021	0.0131	10.25	0.7170	0.690	235.3	5710	-104
4133	19.9	0.0021	0.0131	0.00	0.6575	0.648	214.4	5661	-215
-13a Hybrid Fuel Element									
4134	19.5	0.0019	0.0131	1.97	0.6657	0.664	213.0	5556	-183
4135	16.7	0.0019	0.0131	4.63	0.6735	0.684	225.2	5826	-125
4136	16.9	0.0019	0.0131	10.28	0.6888	0.724	227.9	5759	-124
4137	17.9	0.0019	0.0131	7.62	0.6786	0.698	224.3	5751	-134
4138	15.7	0.0019	0.0131	4.41	0.6983	0.749	227.4	5662	-127
4139	15.7	0.0019	0.0131	4.39	0.7408	0.686	239.1	5617	-173
4140	10.9	0.0019	0.0131	0.00	0.6611	0.653	213.5	5577	-180

Snout temperatures (TIS) during the GO_2 tests were in the nucleate and low film boiling regime (-215 to -100°F) due to the effect of the GO_2 flow heating the oxidizer snout. Test durations were 11 to 20 seconds, limited by chamber throat temperature redlines.

4.4.2.2 GHe Injection Tests

The next series of tests would determine the effect of bubbles in the LO_2 flow by injecting helium gas into the LO2 run line. Helium gas was supplied by the site bulk supply and was controlled by a sonic venturi in the helium line. The gas was injected into the 1/2 inch LO_2 line approximately 12 to 15 inches upstream of the injector. The tests were started without the helium injection, then the helium gas was turned on 10 seconds into the test. This would allow assessment of the effect of the helium gas on a particular test without inducing scatter due to test to test repeatability.

Table 4-6 presents the GHe injection test summary. A data point with the helium on and off are presented for each test. The helium injection was performed with the -13a fuel element since this element had demonstrated the best performance in the GO_2 tests. The GO_2 adaptor was left in place to act as a thermal block, allowing longer test durations.

Figure 4-19 shows the effect of helium on performance. Each test had two data points, one taken at about 9 seconds into

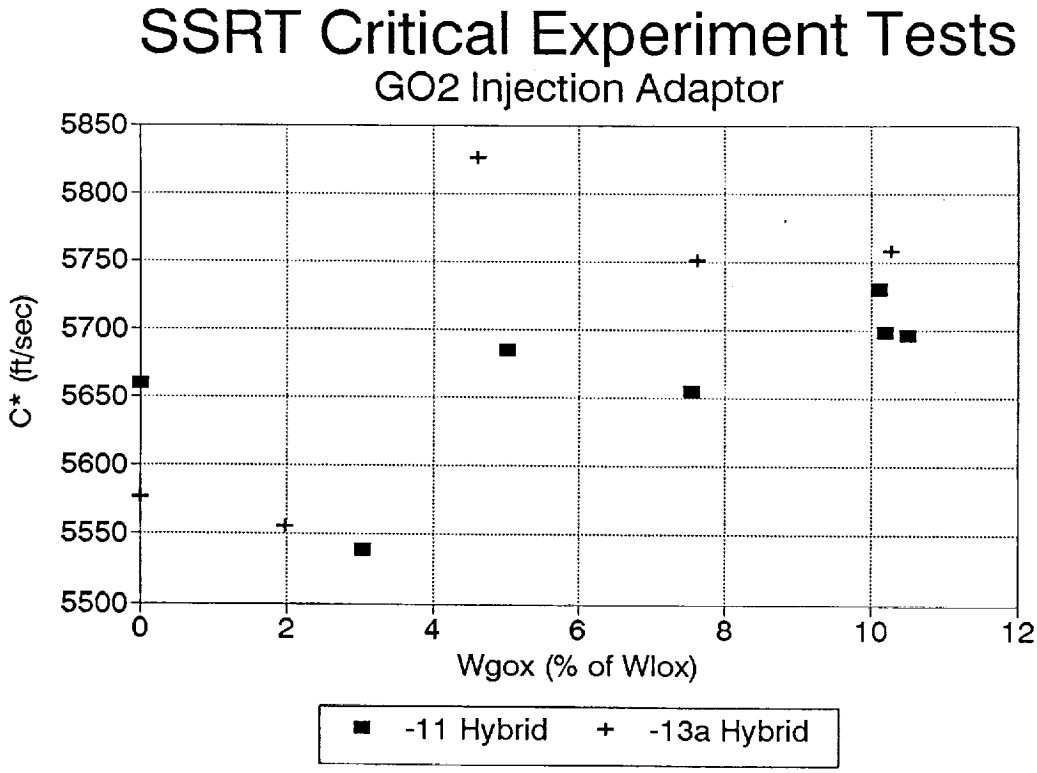

Figure 4-18. Performance verses GO_2 Flow Rate

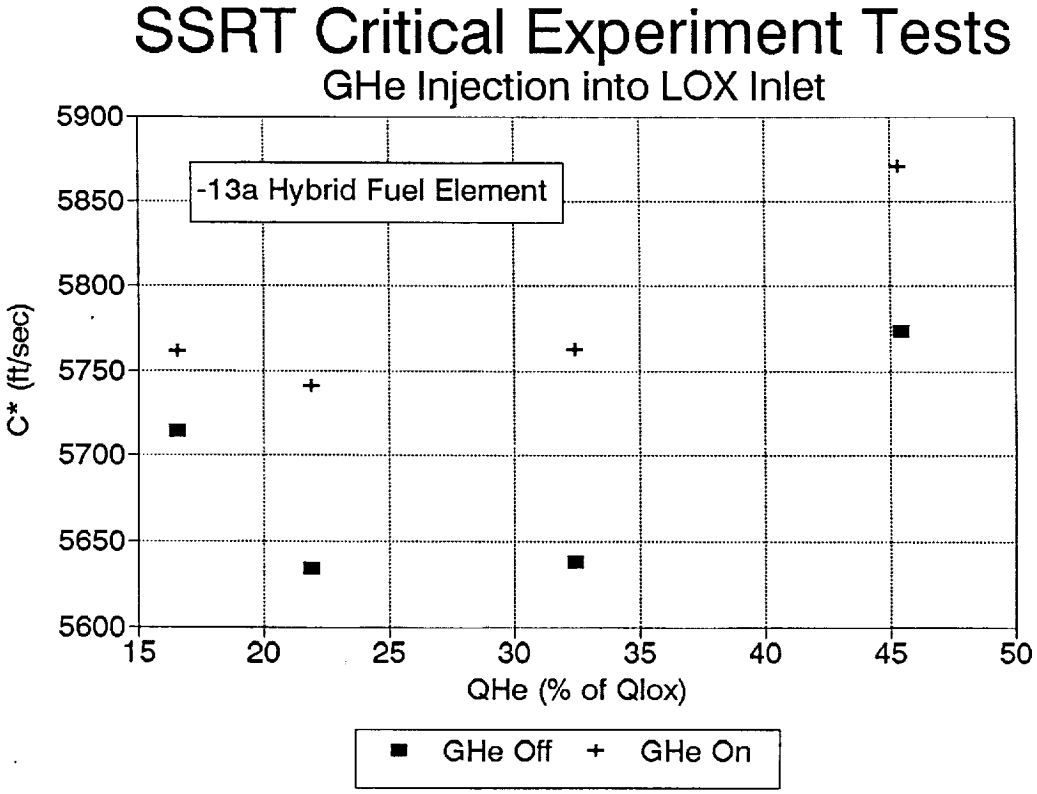

Figure 4-19. C* Increase Due to GHe Injection

the test, before the helium was turned on, and one data point taken 1.6 seconds later after the helium flow was on. Notice the performance increased when the helium was on, and that the performance increase was generally related to the volume percent of helium injected into the LO_2. These results indicated that the helium bubbles have an immediate and strong effect on performance. Figure 4-20 shows TIS data taken at the same two time slices for each test. These results indicated that the helium injection reduced the cooling capability of the LO_2, resulting in a rapid increase in the snout temperature. This effect was put to use in later testing to artificially increase the snout temperature.

Table 4-6. GHe Injection Test Summary

Run No	Time Slice	Fuel Gap	OX Gap	PC psia	He Vol % of LO2	Wt lb/sec	MR O/F	C* ft/sec	TIS F
-13a Hybrid Element									
4141	9.5	0.0019	0.0131	214.6	0.0	0.6560	0.642	5634	-207
4141	10.9	0.0019	0.0131	217.9	21.9	0.6553	0.640	5737	-189
4142	9.5	0.0019	0.0131	213.8	0.0	0.6554	0.640	5634	-187
4142	10.9	0.0019	0.0131	218.1	32.4	0.6554	0.640	5757	-151
4143	9.1	0.0019	0.0131	218.6	0.0	0.6619	0.657	5712	-169
4143	10.5	0.0019	0.0131	220.1	16.6	0.6620	0.657	5759	-171
4144	9.1	0.0019	0.0131	220.0	0.0	0.6611	0.658	5767	-181
4144	10.5	0.0019	0.0131	223.3	45.3	0.6611	0.658	5864	-107

Table 4-7. Columbium Chamber Tests Summary

Run No	Time Slice	Fuel Gap	OX Gap	Wt lb/sec	MR O/F	PC psia	C* ft/sec	TIS F
4145	4.9	0.0019	0.0131	0.6610	0.654	217.3	5624	-75
4146	9.9	0.0019	0.0131	0.6619	0.657	213.7	5572	-156
4147	14.1	0.0019	0.0131	0.5661	0.714	183.1	5593	224

4.4.2.3 Columbium Chamber Hot Fire Testing

After completion of the GHe injection tests, the decision was made to install the columbium chamber and test the engine for longer durations than the copper chamber would allow. Red line temperatures of 2400°F were established as the shutdown criteria. The -13a Hybrid element was used, along with the splash plate adaptor. Table 4-7 summarizes the columbium chamber tests.

The first test was a checkout test of five second run duration. The second test was run for 10 seconds, and resulted in a maximum chamber temperature of 2100°F at the end of the chamber barrel section. The performance on these two runs was low (averaging around 5600 ft/second C*). The snout temperature probe read -75 to -150°F, very low considering that the snout was unprotected from the combustion gases. Inspection of the chamber revealed a streak at the throat, between the TR-11 and TR-12 thermocouple probes.

On the third test with the columbium chamber, a burn through at the throat occurred at 14.1 seconds into the test. The strip chart recorders indicated a maximum temperature of about 2300°F, but it was soon discovered that the strip chart was set up incorrectly and the temperature was actually over 2500°F in the vicinity of the burn through. On the opposite side of the chamber from the burn through, the temperatures were reading only about 1900°F, indicating very uneven heating at the throat.

TIS was approximately 200°F for the test, but the C* was still only 5600 ft/sec. The conclusion was that the splash plate may have prevented high performance, and may also have contributed to the uneven temperature distribution.

4.4.2.4 Thermal Block with No Splash Plate Results

Table 4-8 presents the results of the testing with the thermal block adaptor with no splash plate. The copper chamber was reinstalled on the engine along with the thermal block adaptor without a splash plate. The -11 hybrid fuel element was installed, and the propellant flow conditions of test 4099 were set. The first test with this adaptor

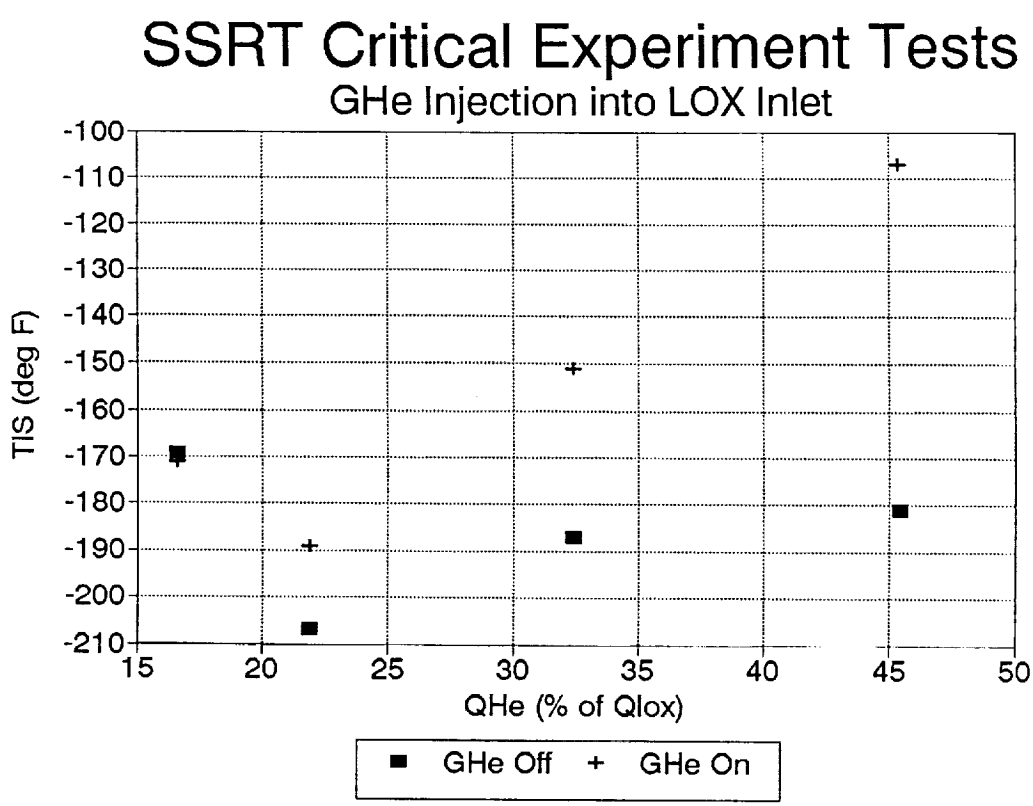

Figure 4-20. TIS Temperature Increase due to GHe Injection

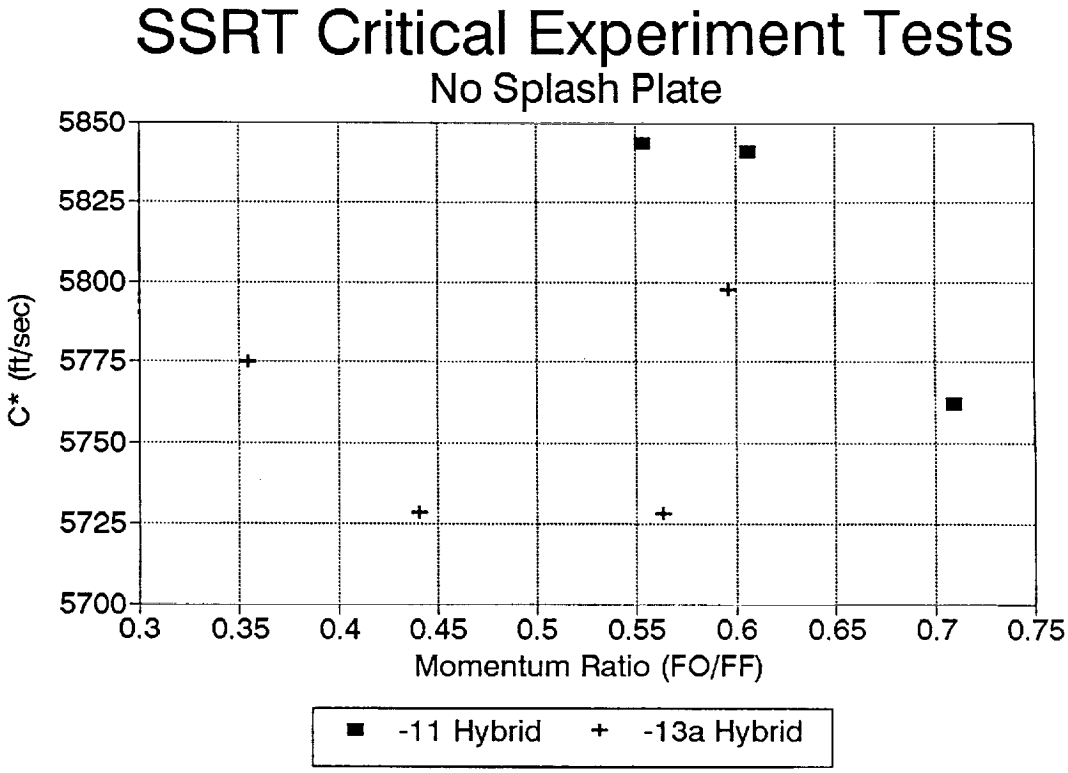

Figure 4-21. C* vs Momentum Ratio for -13a Hybrid Element

Table 4-8. No Splash Plate Test Summary

Run No	Time Slice	Fuel Gap	OX Gap	Wt lb/sec	MR O/F	PC psia	C* ft/sec	TIS °F
-11 Hybrid, Thermal Block, No Splash Plate								
4148	12.7	0.0022	0.0141	0.6628	0.655	223.8	5841	108
4149	19.9	0.0022	0.0141	0.6924	0.632	221.1	5543	-191
4150	11.1	0.0022	0.0141	0.6921	0.638	233.4	5844	152
4151	12.3	0.0022	0.0118	0.6933	0.638	230.7	5762	225
-13a Hybrid, No Splash Plate, No Thermal Block								
4152	7.7	0.0021	0.0141	0.6225	0.725	209.4	5798	170
4153	6.5	0.0021	0.0141	0.6242	0.717	207.7	5728	174
4154	9.3	0.0021	0.0141	0.7065	0.593	235.9	5775	174
4155	5.7	0.0021	0.0141	0.6586	0.666	218.9	5728	179

achieved 5841 ft/sec C* with a 108 degree snout temperature (TIS). The fuel flow rate was increased by 5% for the next test, test HA2A-4149. The C* for this test (HA2A - 4149) was 5540 ft/sec and TIS was -191°F. Apparently the thermal blockage of this adaptor was marginal, so it could yield either nucleate boiling or film boiling at the oxidizer injector, depending on the test conditions. For test 4150, the previous test conditions were repeated, but this time the helium injection was turned on for the first five seconds of the test in order to allow the snout to get hot (the helium injection circuit had never been disconnected). This ploy worked, as the TIS reading was now 150° and the C* performance was 5840 ft/sec, an increase of 300 ft/sec over the previous test. These two runs clearly demonstrated that the snout temperature has a profound effect on the performance of the SSRT engine.

On test 4151, the test conditions of 4149 were repeated, except a 0.0118 oxidizer gap was set in order to simulate the increase in oxidizer velocity due to film boiling as in test 4150. The higher oxidizer velocity caused increased injector heating, and TIS reached 225 during the test without the use of helium injection. Performance was 5762 ft/sec for this test, 1.4% lower than for the 0.0141 inch oxidizer gap.

Inspection of the hardware after the test revealed that a hole had been burned through the thermal block adaptor on the side of the injector that coincided with the burn through on the columbium chamber. Only the thermal block adaptor was damaged; no damage was done to the injector or chamber. Apparently the -13a element had a very hot local zone on one side of the injector. Post test water flows of the oxidizer circuit revealed a streak in the oxidizer sheet in line with the hot spot. The cause of the streak was determined to originate from a small indentation in the oxidizer injection bore caused by contact with the ramp on the fuel extensions during assembly. It is concluded that this disturbance in the LO_2 flow caused the local hot zone in the combustion field, and may have been detrimental to performance.

4.4.2.5 No Splash Plate, No Thermal Blockage Results
For the final test sequence in this series the injector was tested as a basic injector, without any adaptors installed, as it had been for the performance testing in the Option 1 series. The -13a hybrid element was installed to allow a direct comparison of its performance to the -11 hybrid element tests from Option 1. Figure 4-21 shows the C* performance of the -13a hybrid and -11 hybrid vs momentum ratio. The -13a element showed no discernable trend, and operated at a lower performance level than the -11 hybrid element. Injector heating was uneven with the -13a element, as was the chamber circumferential thermal distribution. The -13a element appeared to be very sensitive to oxidizer maldistributions, resulting in large thermal variations in the injector and chamber combustion zones.

As a result of these tests all the objectives of the critical experiments were met.

4.4.2.6 Summary of the Results of the Critical Experiments

The results of the critical experiments gave a better understanding of the mechanisms relating to injector operation. The results are summarized as follows:

- GO_2 injection downstream of the main LO_2 injection point improved the performance of the engine, even with a cold injector snout, but performance was still 1.5% below maximum performance.

- GHe injection into the LO_2 feed line improved the performance to within 0.7% of maximum performance, demonstrating the role of gas generation in the LO_2 stream on improving performance.

- The thermal block adaptor with no splash plate demonstrated thermal stability with marginal performance.

- Reducing the aspect ratio of the -13 element indicated improved performance, but still 1.8% below maximum with uneven thermal characteristics. Therefore, no further work will be done with the 120 slot element.

5.0 Rhenium Technology

The SSRT LO_2-N_2H_4 engine operates at high performance and attendant high wall temperatures exceeding the limits of existing silicide (R512E) coated columbium thrust chambers. Rhenium (iridium coated internally) thrust chambers provide a capability to 4000°F operating temperatures. However, material properties of the chemically vapor deposited (CVD) rhenium are unknown. Therefore, the rhenium technology task has been incorporated into the SSRT program to evaluate material properties of rhenium to temperatures of 3400°F and also develop joint designs for integration of the injector to the rhenium thrust chamber and rhenium thrust chamber to the columbium nozzle extension.

5.1 Material Property Definition

5.1.1 Materials Testing

Material samples of CVD rhenium were received from NASA-LeRC and machined to the configuration of Figure 5.1-1. Material tests were conducted over a range of temperatures from room temperature (~ 70°F) to 3400°F which was the maximum internal wall temperature based on thermal analyses which is presented in Figure 5.1-2. The nozzle joint area was thermally analyzed and the results are presented in Figure 5.1-3 which indicate the joint is below 2100°F. Material properties were obtained over the temperature range by testing thirteen samples over the temperature range. The data obtained, ultimate strength, elongation and reduction of area, are presented in Figures 5.1 - 4,5,6. Yield strength and modulus were also planned to be obtained but the holes in the samples elongated and these two parameters could not be obtained. However, four room temperature samples were tested at TRW for elastic modulus and the results indicated 56-60 x 10^6 psi. Yield strength on annealed CVD samples indicated 8-14 ksi at room temperature.

5.1.2 Microscopy Analysis of Tensile Specimens

Upon completion of the tensile testing, the samples were evaluated by microscopy using the scanning electron microscope (SEM). Figure 5.1.2-1 shows the fracture of a room temperature sample as CVD deposited and Figure 5.1.2-2 shows the comparison to an annealed sample. Figures 5.1.2-3 and 4 show other annealed samples tested at room temperature. The annealing appears to show the layering effects of the rhenium which is CVD in multiple layers, whereas this effect is not as pronounced in the as deposited sample. Figure 5.1.2-5 through 14 show views of samples tested at high temperatures (1500-3400°F). These samples also exhibit the layering effects. In fact, the 2800-3400°F tested samples appear to exhibit ductile and brittle behavior. A summary of the fracture comparisons are shown in Table 5.1.2-1.

Figure 5.1-1

RHENIUM TENSILE SPECIMEN

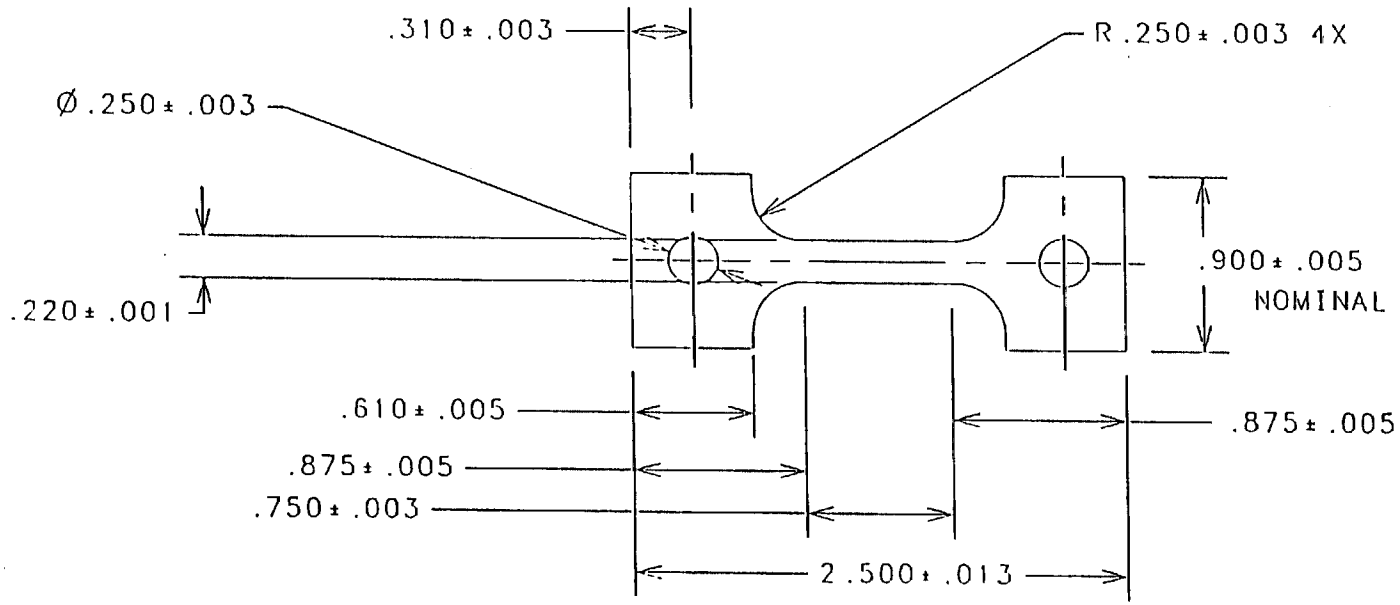

ALL DIMENSIONS IN INCHES

THICKNESS: .060 INCHES

Figure 5.1-2

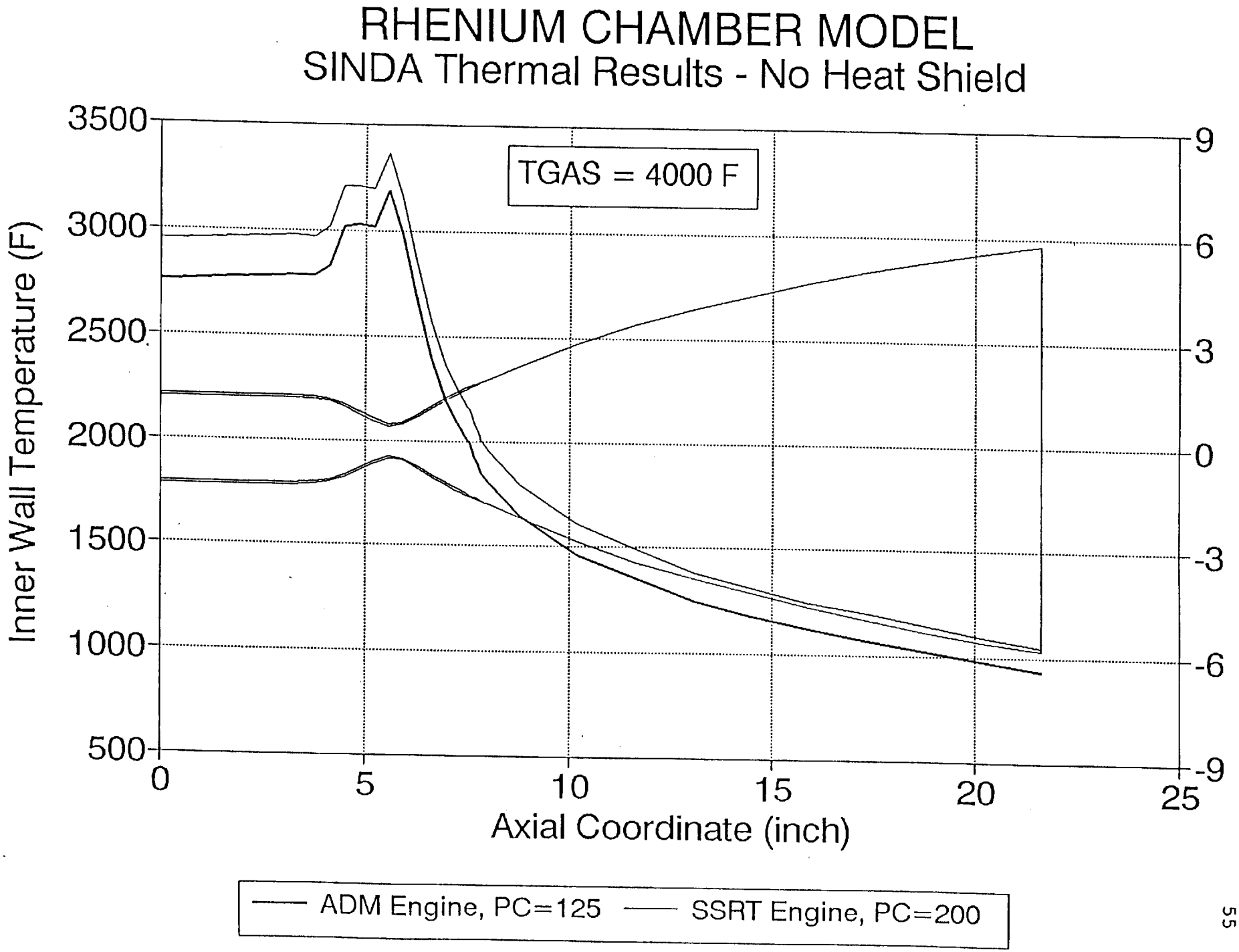
RHENIUM CHAMBER MODEL
SINDA Thermal Results - No Heat Shield
TGAS = 4000 F
Inner Wall Temperature (F)
3500
3000
2500
2000
1500
1000
500
9
6
3
0
-3
-6
-9
0
5
10
15
20
25
Axial Coordinate (inch)
ADM Engine, PC=125
SSRT Engine, PC=200

Figure 5.1-3

RHENIUM CHAMBER MODEL
Sinda Thermal Results - No Heat Shield

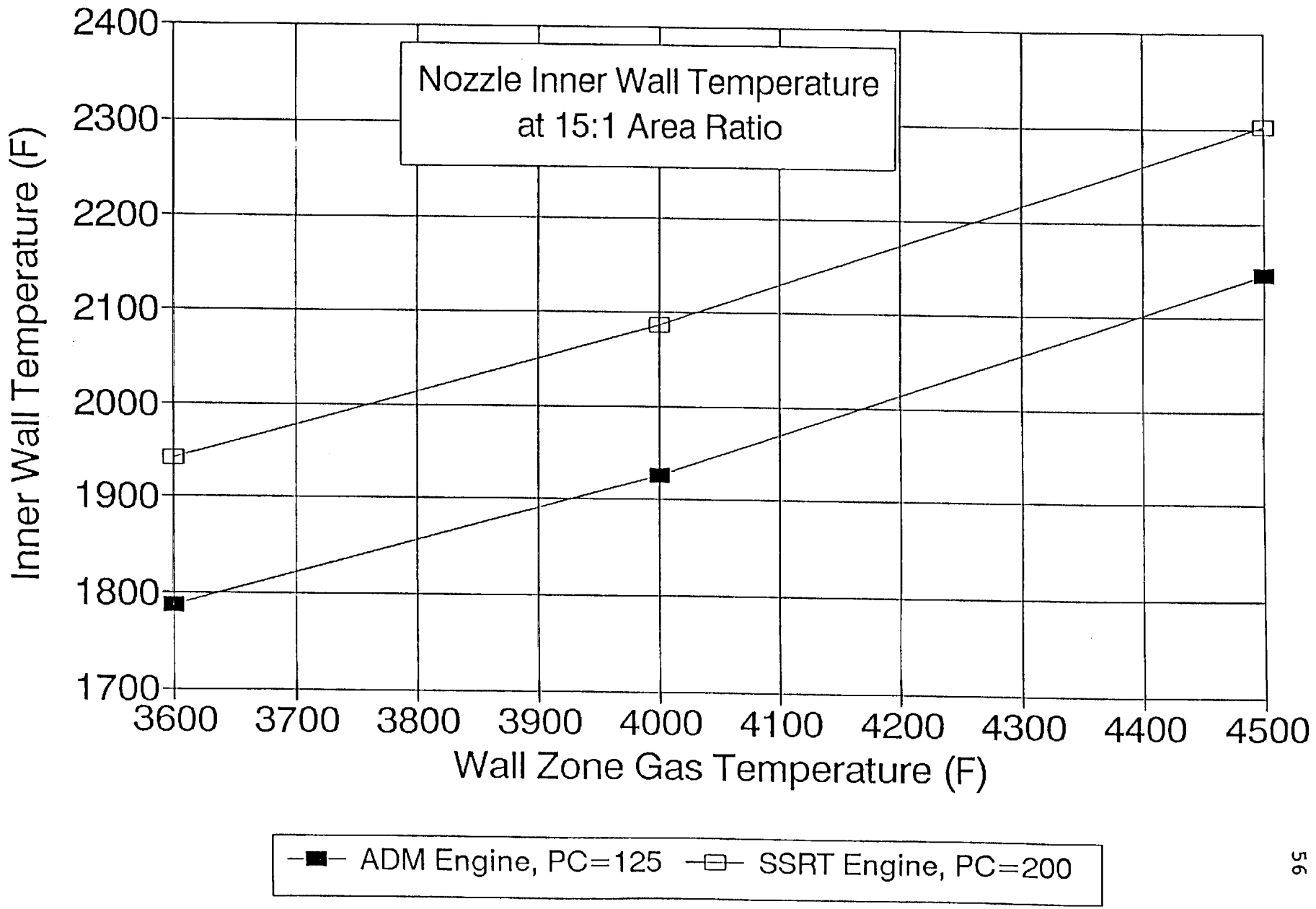

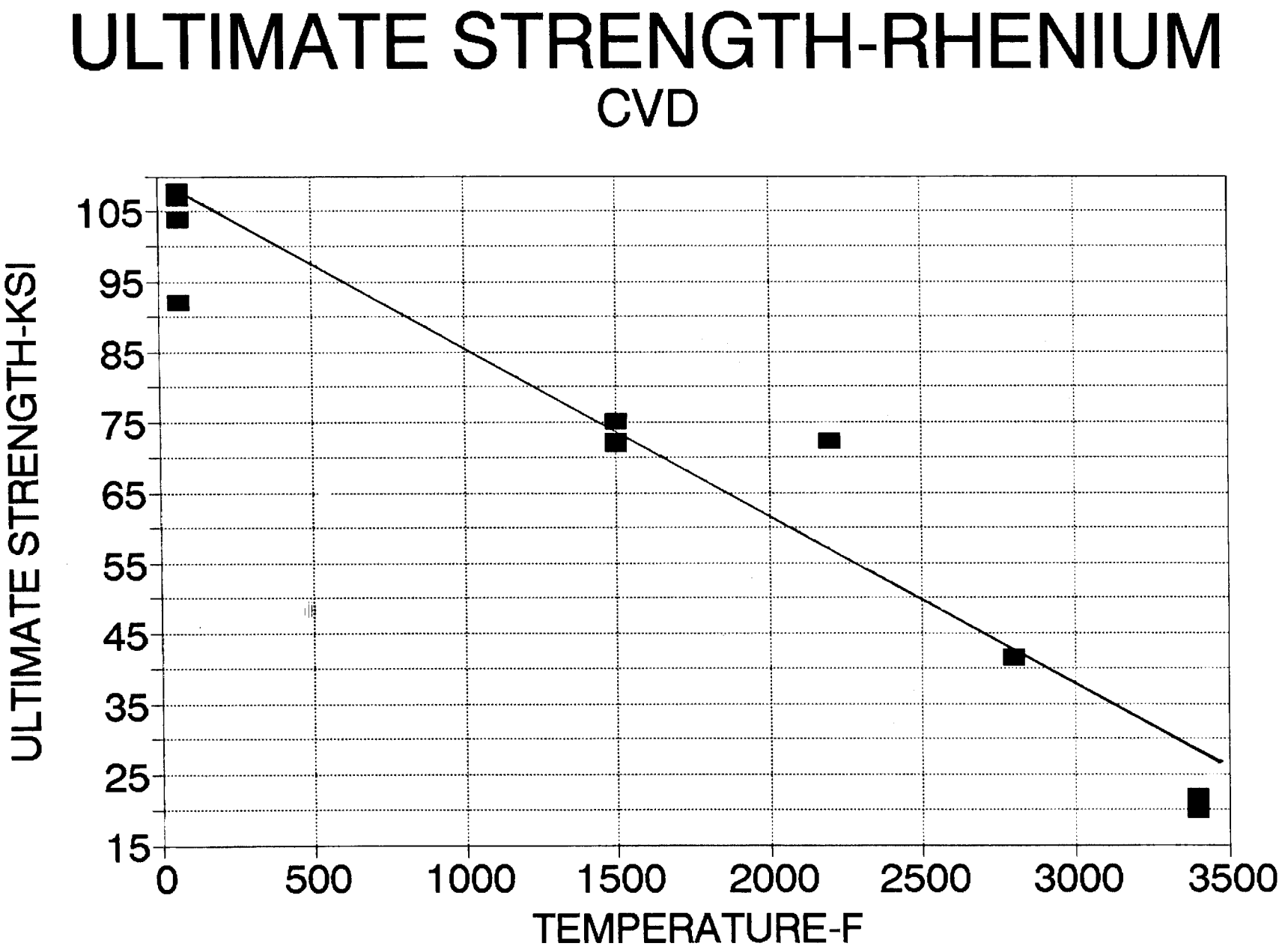
ULTIMATE STRENGTH-RHENIUM
CVD
ULTIMATE STRENGTH-KSI
105
95
85
75
65
55
45
35
25
15
0
500
1000
1500
2000
2500
3000
3500
TEMPERATURE-F

Figure 5.1-4.

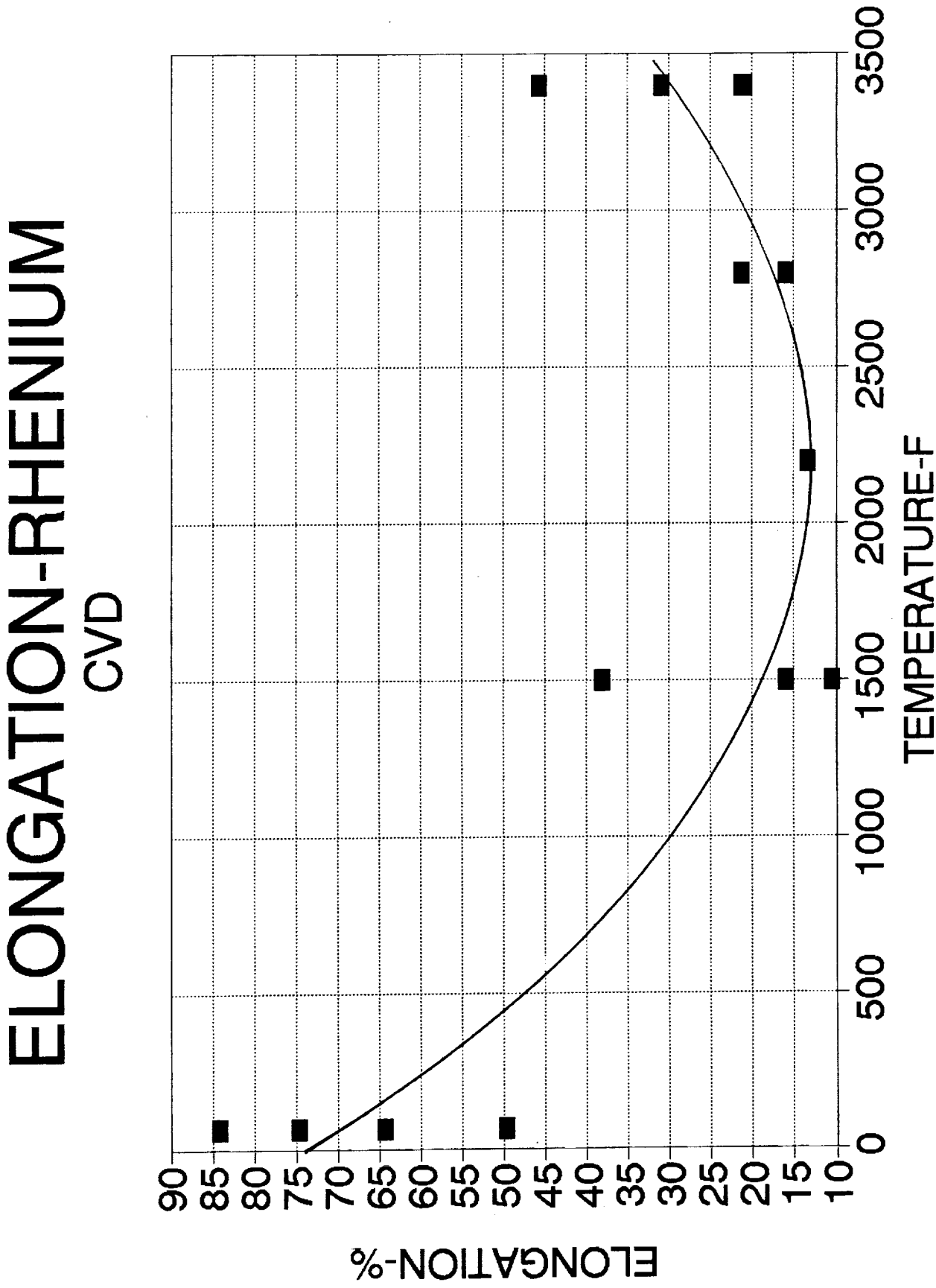
ELONGATION-RHENIUM
CVD
ELONGATION-%
TEMPERATURE-F
90
85
80
75
70
65
60
55
50
45
40
35
30
25
20
15
10
0
500
1000
1500
2000
2500
3000
3500

Figure 5.1-5.

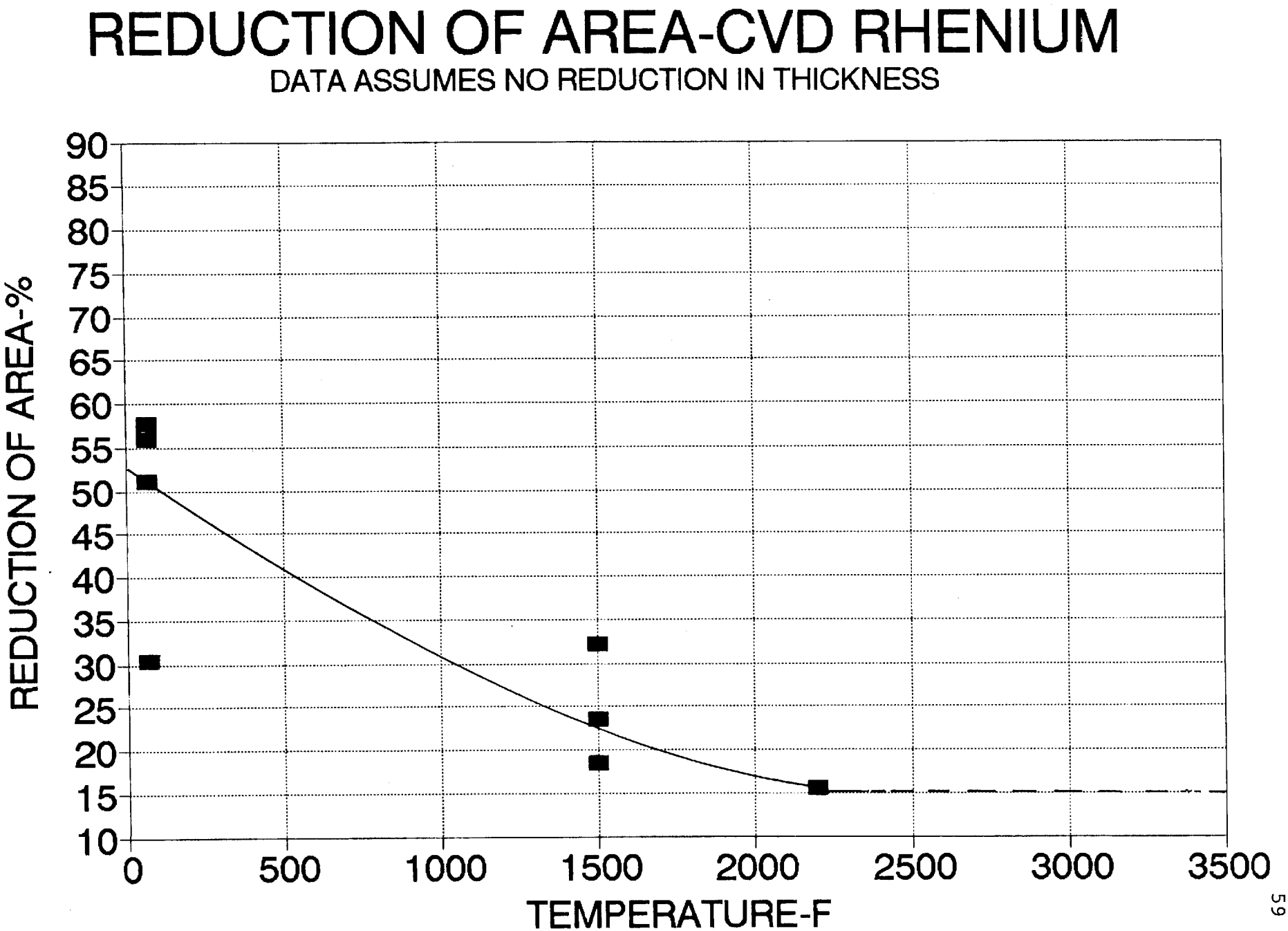
REDUCTION OF AREA-CVD RHENIUM
DATA ASSUMES NO REDUCTION IN THICKNESS
REDUCTION OF AREA-%
90
85
80
75
70
65
60
55
50
45
40
35
30
25
20
15
10
0
500
1000
1500
2000
2500
3000
3500
TEMPERATURE-F

Figure 5.1-6.

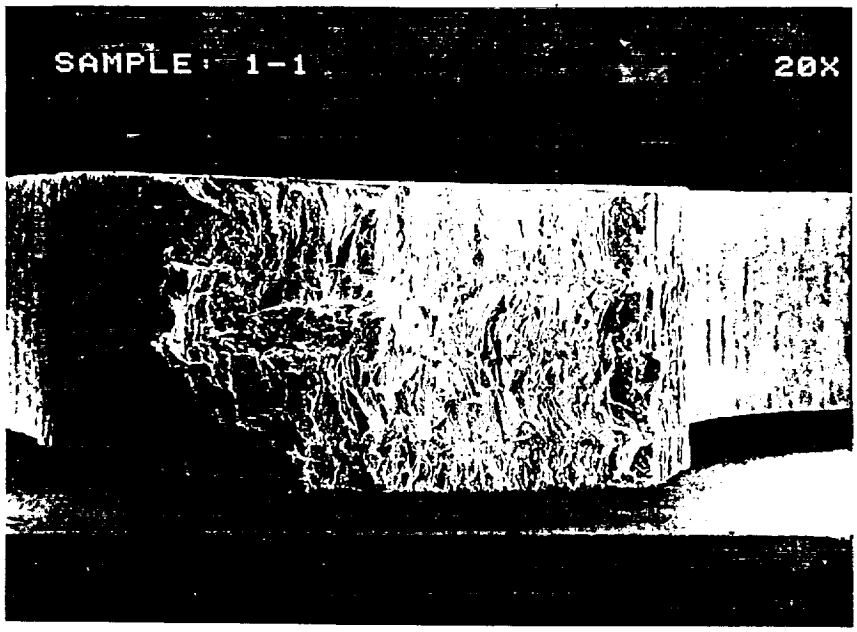

Figure 5.1.2-1. SEM view of fracture in tensile specimen 1-1, 75F, as deposited. 20X.

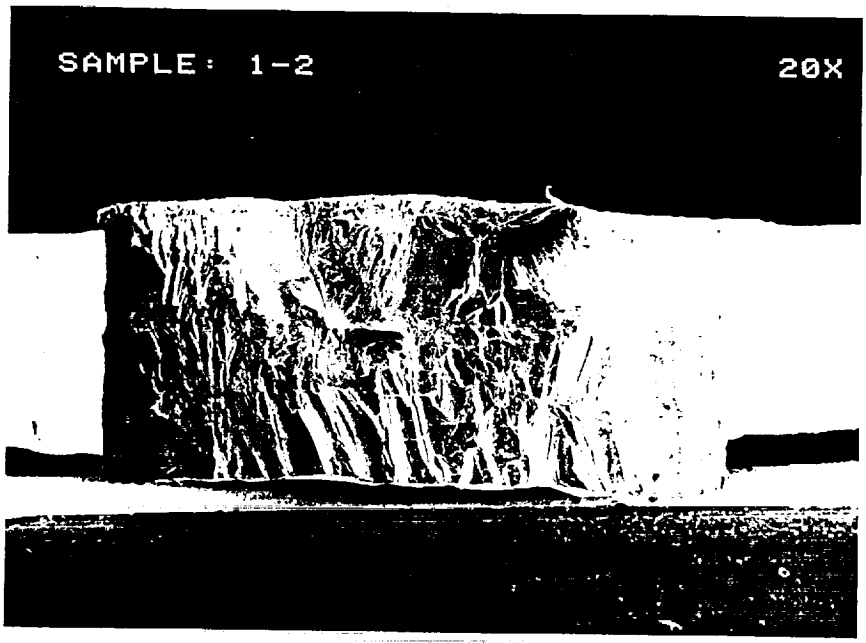

Figure 5.1.2-2. SEM view of fracture in tensile specimen 1-2, 75F, annealed. 20X.

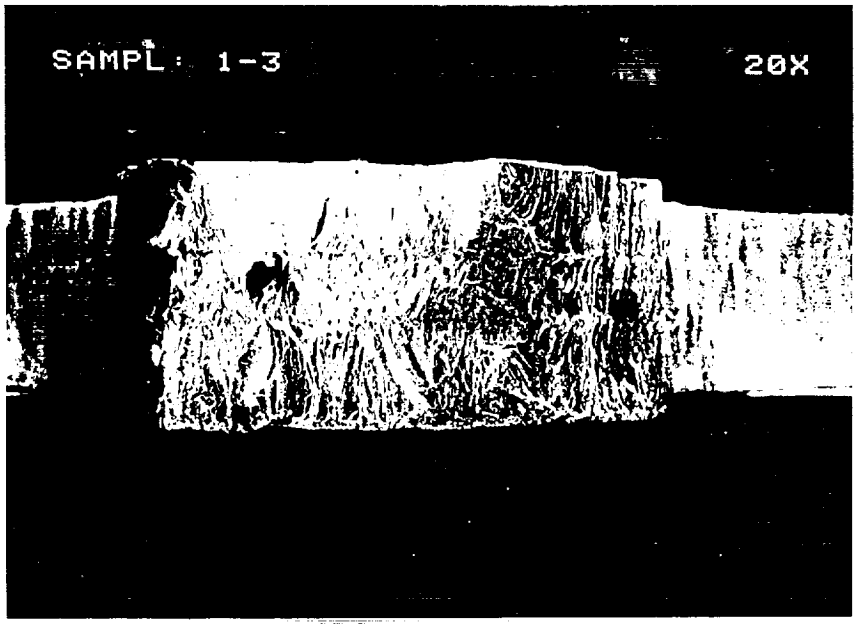

Figure 5.1.2-3. SEM view of fracture in tensile specimen 1-3, 75F, annealed. 20X.

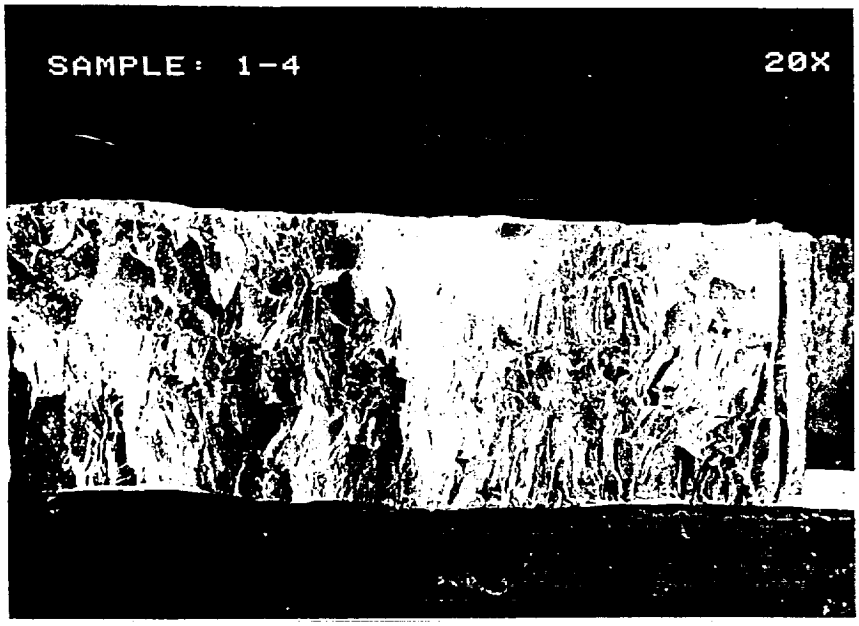

Figure 5.1.2-4. SEM view of fracture in tensile specimen 1-4, 75F, annealed. 20X.

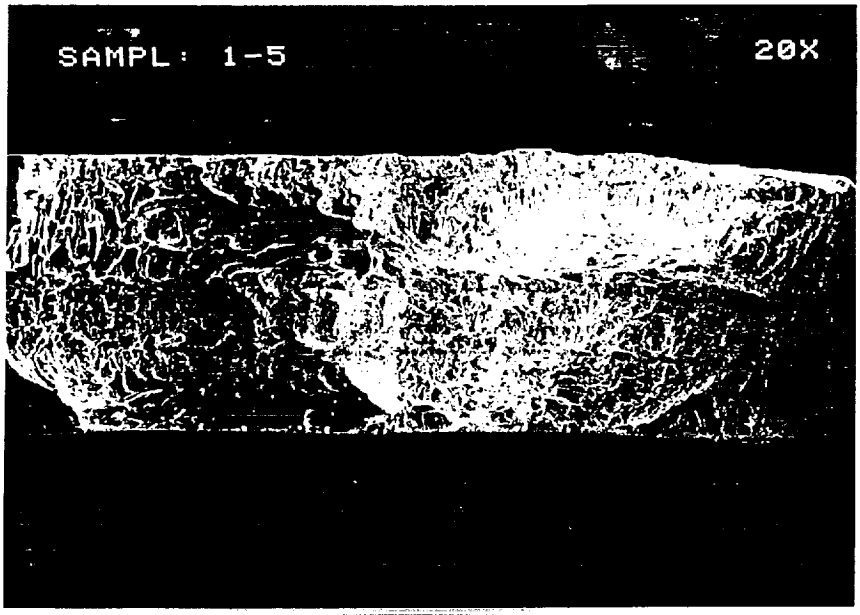

Figure 5.1.2-5. SEM view of fracture in tensile specimen 1-5, 1500F, as deposited. 20X.

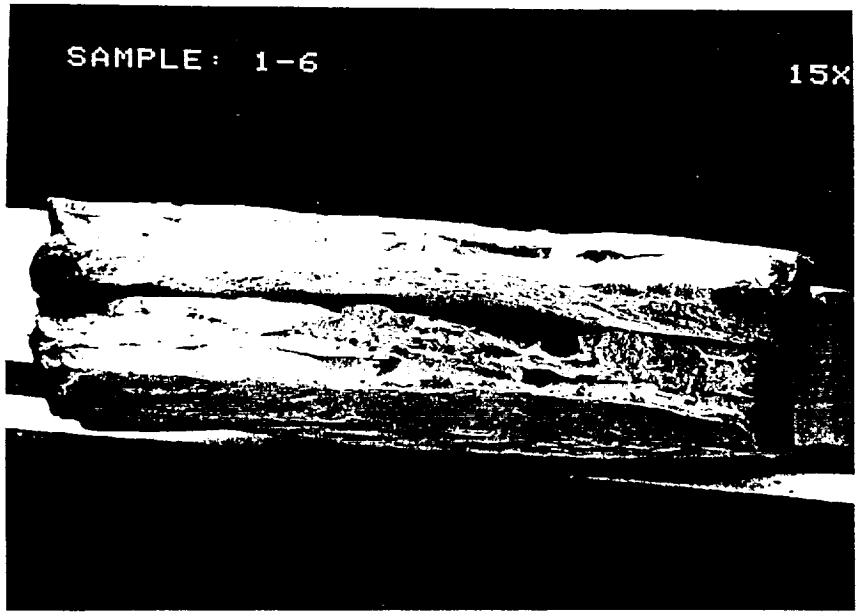

Figure 5.1.2-6. SEM view of fracture in tensile specimen 1-6, 3400F, annealed. 20X.

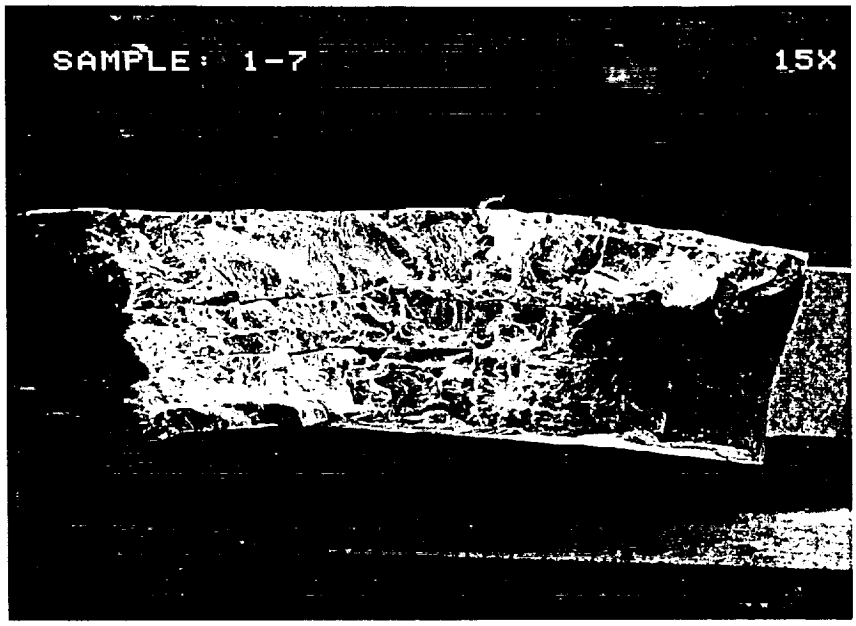

Figure 5.1.2-7. SEM view of fracture in tensile specimen 1-7, 1500F, annealed. 20X.

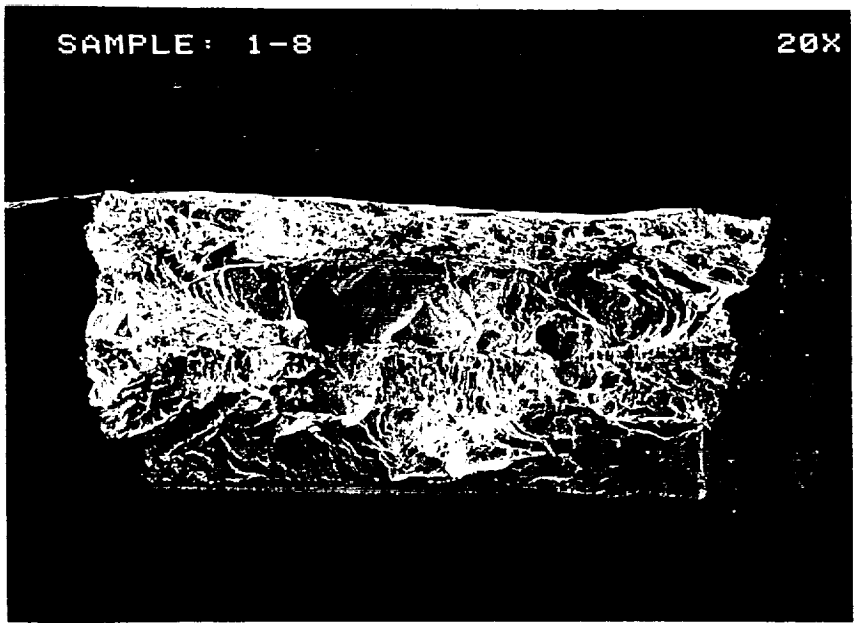

Figure 5.1.2-8. SEM view of fracture in tensile specimen 1-8, 1500F, annealed. 20X.

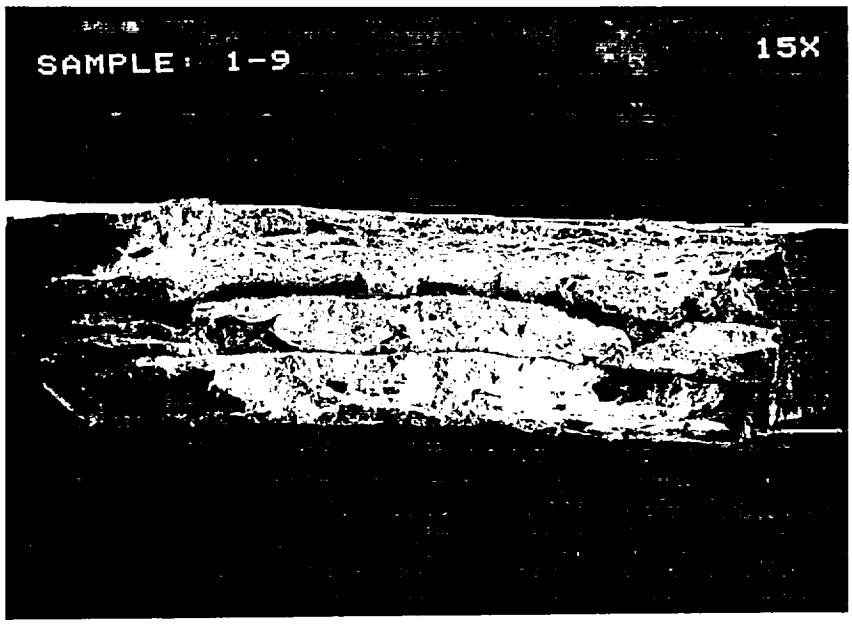

Figure 5.1.2-9. SEM view of fracture in tensile specimen 1-9, 2200F, annealed. 20X.

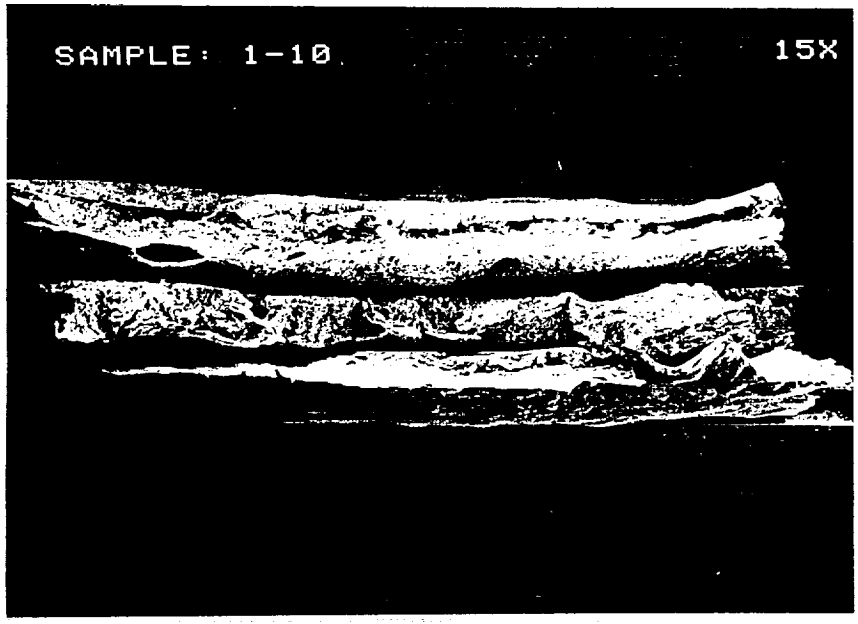

Figure 5.1.2-10. SEM view of fracture in tensile specimen 1-10, 3400F, annealed. 20X.

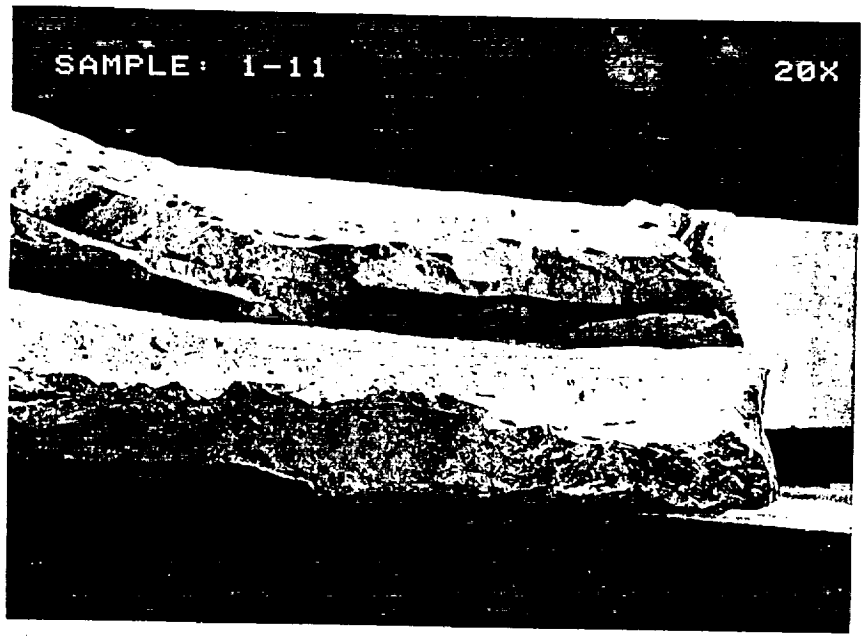

Figure 5.1.2-11. SEM view of fracture in tensile specimen 1-11, 2800F, annealed. 20X.

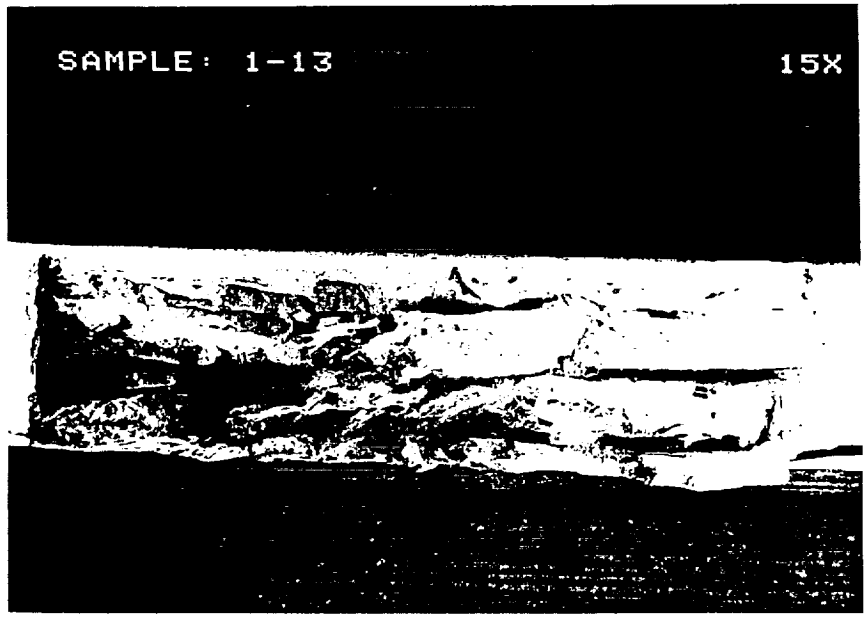

Figure 5.1.2-12. SEM view of fracture in tensile specimen 1-13, 2800F, annealed. 20X.

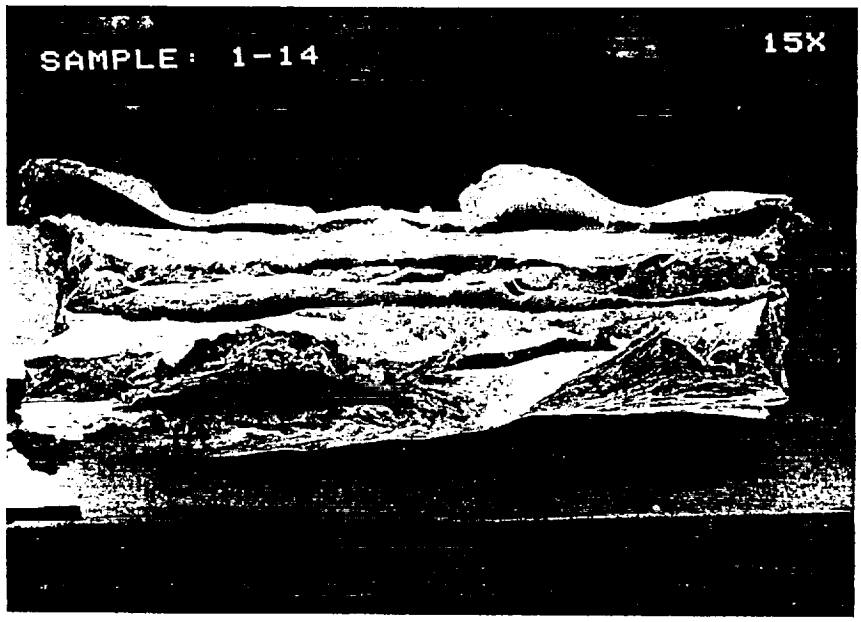

Figure 5.1.2-13. SEM view of fracture in tensile specimen 1-14, 3400F, annealed. 20X.

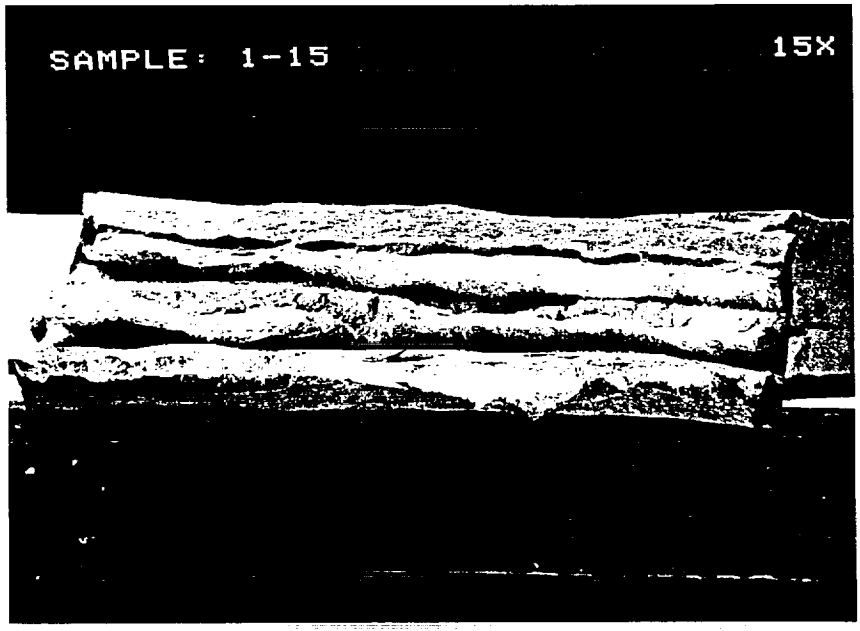

Figure 5.1.2-14. SEM view of fracture in tensile specimen 1-15, 3400F, annealed. 20X.

TABLE 5.1.2-1

FRACTURE COMPARISONS

CVD RHENIUM TENSILE SPECIMENS

Specimen ID	Condition	Temperature (F)	Layers Necked
1-1	Deposited	75	0/5
1-2	Annealed	75	0/5
1-3	Annealed	75	0/5
1-4	Annealed	75	0/5
1-5	Deposited	1500	0/5
1-6	Annealed	3400	2/5
1-7	Annealed	1500	0/5
1-8	Annealed	1500	0/5
1-9	Annealed	2200	0/5
1-10	Annealed	3400	3/5
1-11	Annealed	2800	0/5
1-13	Annealed	2800	0/5
1-14	Annealed	3400	5/5
1-15	Annealed	3400	5/5

5.1.3 Microscopy Analysis of Samples Prior to Materials Test

The samples were evaluated prior to and after annealing to determine the grain structure prior to initiation of high temperature materials testing. Figures 5.1.3-1 through 7 show these results. The results indicate that there are both columnar and recrystallized layers. In addition Figure 5.1.3-8 shows the interfaces between layers including entrapped inclusions/voids between layers.

5.2 Joint Design

5.2.1 Methods of Attachment

There are two prime highly reliable methods of attachment of the injector (columbium) to the rhenium chamber (Iridium coated) and rhenium chamber to the columbium (R512E silicide coated) nozzle extension. These are welding and brazing. Mechanical attachment was not considered as a primary reliable method due to the potential for hot gas leakage. Investigations were conducted to evaluate both welding and brazing.

5.2.1.1 Weld Investigations

Investigations were conducted to evaluate electron beam (EB) welding of columbium (C103) to rhenium. Direct electron beam welding of columbium to rhenium resulted in cracking in the weld due to a brittle phase. Consequently, shims of various materials were evaluated as fillers to the weld. These fillers evaluated were molybdenum, titanium and tantalum. The welds with molybdenum, titanium and tantalum all cracked and separated with failure occurring in the weld on the rhenium side for the samples using tantalum and titanium fillers. A titanium filler shim of 0.035 inch (twice the filler width of the others) was also evaluated and showed no cracking - titanium appeared brazed to the rhenium (no rhenium melting). This indicated an inter-molecular bond was formed between the titanium and rhenium. Figures 5.2-1 through 5.2-4 show microsections of these samples. As a result, this technique was further evaluated.

An investigation was conducted evaluating the EB titanium braze (inter-molecular bond). The mechanical properties were evaluated at room temperature. The results indicated:

Ultimate Strength	38.0 35.9 ksi
Yield Strength	26.1 22.5 ksi
Elongation	2% 2%

Figure 5.1.3-1. Micrograph of tensile specimen 1-2 after annealing showing combination of columnar and recrystallized layers. 40X.

Figure 5.1.3-2. Micrograph of tensile specimen 1-4 after annealing showing completely recrystallized structure. 40X.

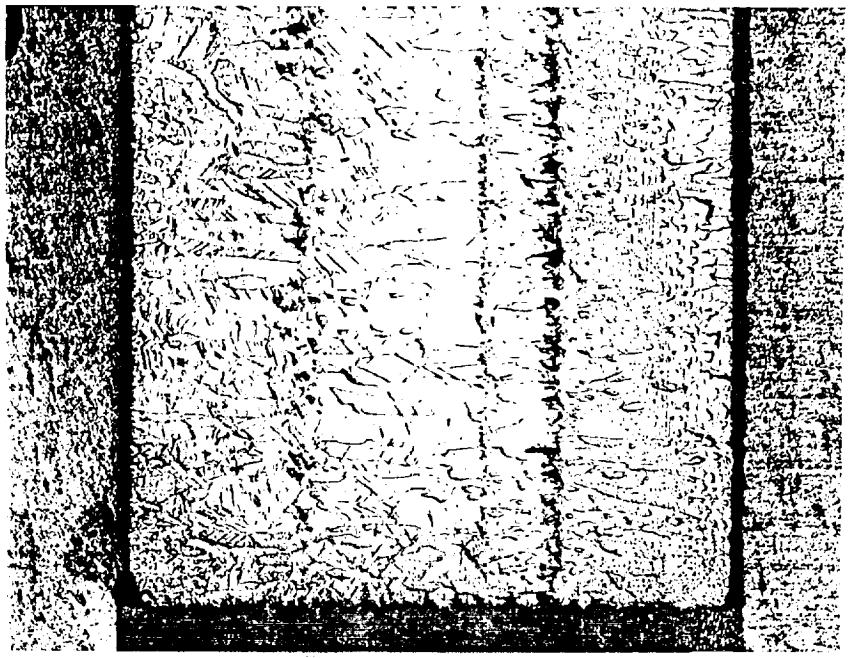

Figure 5.1.3-3. Micrograph of tensile specimen 1-6 before annealing showing columnar structure as deposited. 50X.

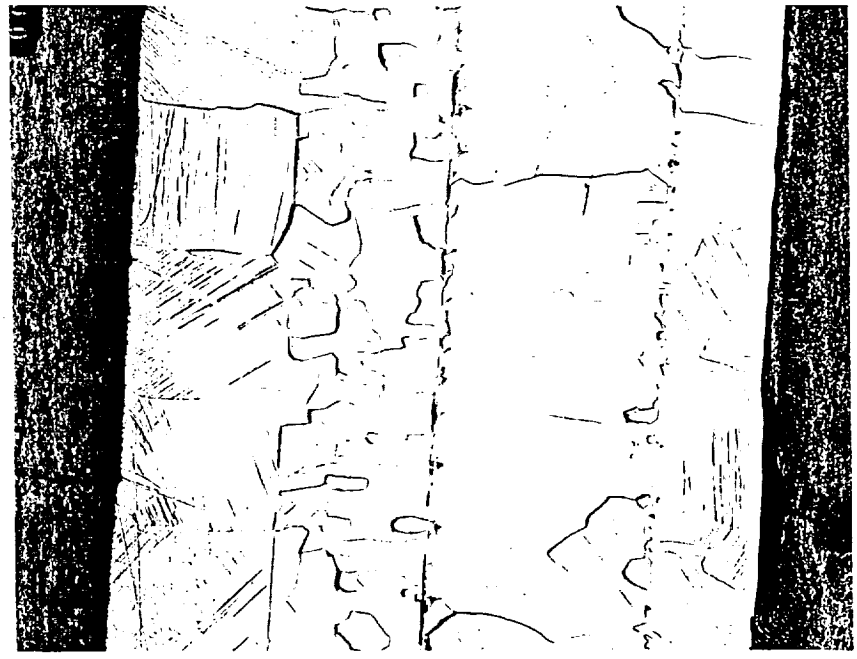

Figure 5.1.3-4. Micrograph of tensile specimen 1-8 after annealing showing combination of columnar and recrystallized layers. 50X.

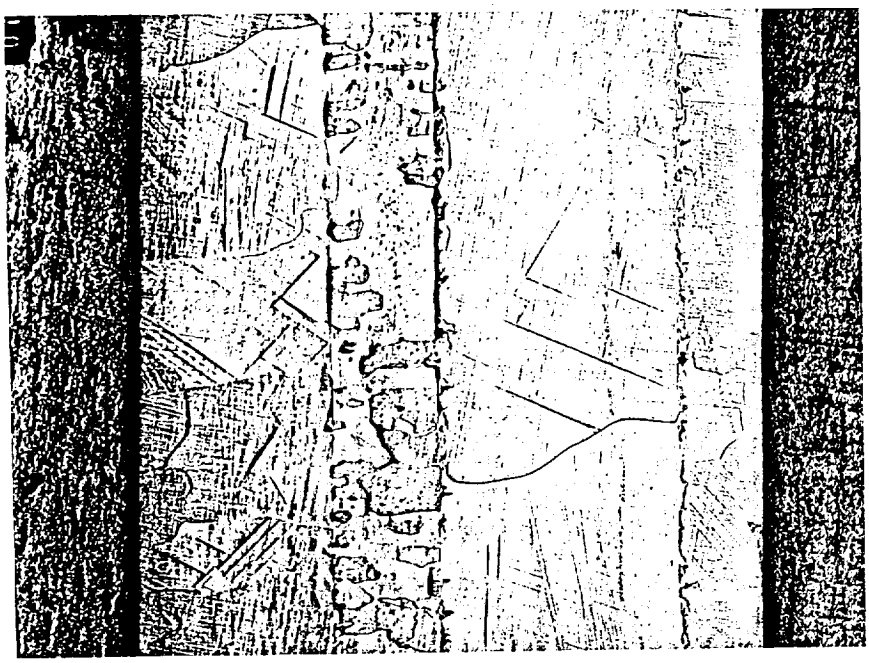

Figure 5.1.3-5. Micrograph of tensile specimen 1-10 showing combination of columnar and recrystallized. 50X.

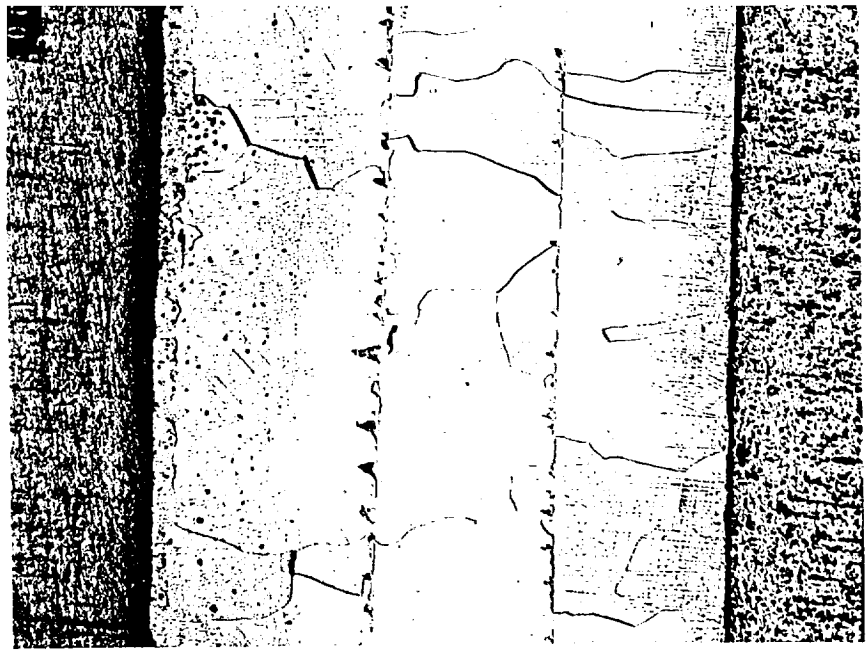

Figure 5.1.3-6. Micrograph of tensile specimen 1-13 showing completly recrystallized structure. 50X.

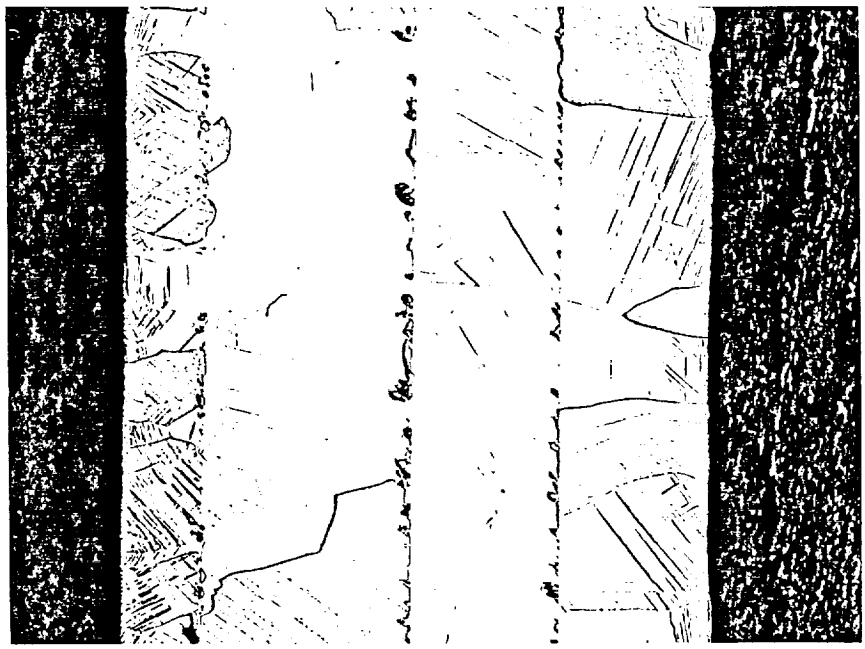

Figure 5.1.3-7. Micrograph of tensile specimen 1-15 showing completely recrystallized structure. 50X.

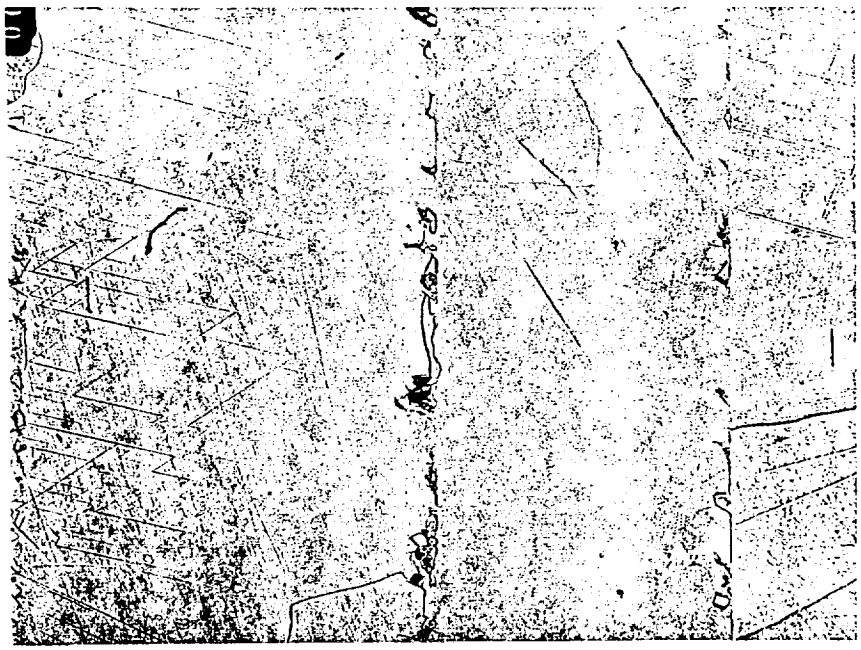

Figure 5.1.3-8. Detailed micrograph of tensile specimen 1-15 showing entrapped inclusions between layers. 100X.

There was an indication of low ductility suggesting a brittle failure at ultimate. Visual observation of the fracture faces suggested brittle failure. Scanning electron microscope (SEM) observation indicated titanium wetted the rhenium surface but failure was in a thin layer of titanium immediately adjacent to the rhenium. This indicates the brittle failure is not classic cleavage in the titanium but interlath failure (diffusion of rhenium into titanium in this thin layer to produce brittle phase). A bend test was also conducted on this concept. The results indicated a maximum bend strength of 86 ksi with only 1% fiber strain indicating brittleness. As a result, this EB titanium braze (intermolecular bond) was eliminated as a potential method of attachment.

5.2.1.2 Braze Investigations

Various investigations were conducted to evaluate braze materials which are candidates for attachment of the columbium injector to rhenium chamber and rhenium chamber to columbium nozzle extension. Table 5.2-1 shows candidate braze alloys. Samples of Palniro 1, Palniro 4 and Paloro were evaluated with Palniro 1 being the best, Palniro 4 being next best and Paloro the third best. In addition two Pd-Au brazes were evaluated: 35Pd-65Au demonstrating good wetting and 50Pd-50Au demonstrating good wetting.

Simulated joint configurations of rhenium-columbium (C103) were evaluated with four braze alloys. The four braze alloys evaluated were Palniro 4, 35Pd-65Au, 50Pd-50Au and titanium. Table 5.2-2 summarizes the results demonstrating that the Pd-Au braze alloys were the best.

The two Pd-Au and titanium braze samples were subjected to thermal aging tests where the samples were subjected to four hours at 2200°F and then cycled from room temperature to 2200°F for 20 cycles. The titanium showed a small crack at the braze to rhenium interface which indicated an embrittled phase at the crack. The 50Pd-50Au simulated joint showed void areas where there was poor flow of braze and shrinkage cracks. The 35Pd-65Au simulated joint was the best indicating only some small voids, no diffusion of braze into the rhenium or columbium but diffusion of columbium and hafnium into the braze.

As a result of this investigation, the 35Pd-65Au has been selected as the braze alloy.

5.2.1.3 Joint Configuration

Various joint configurations for attachment of the rhenium thrust chamber to the columbium (C103) injector and nozzle extension were examined and analyzed. Figure 5.2-5 shows the design to be pursued.

TABLE 5.2-1

Candidate Brazing Alloys For Cb to Re

Braze Alloy	Solidus(F)	Liquidus(F)
Nioro** 82Au,18Ni	1751	1751
	VISUAL- excellent wetting, no erosion	
Palniro 4*** 30Au,34Pd,36Ni	2075	2136
	VISUAL excellent wetting - no erosion	
Paloro*** 92Au,8Pd	2192	2318
	VISUAL excellent wetting, no erosion	
Palniro 1 50AU,25NI,25Pd	2016	2050
	VISUAL excellent wetting, no erosion	
Palni 60Pd,40Ni	2260	2260
	VISUAL excellent wetting, Cb erosion	
Palco 65Pd,35Co	2226	2226
	VISUAL excellent wetting, Cracks in braze line, Cb erosion	

TABLE 5.2-2

SIMULATED BRAZE JOINT TESTS

Braze Alloy	Solidus Temp(^{o}F)	Liquidus Temp(^{o}F)	Results
Palniro 4 30Au, 34Pd, 36Ni	2075	2136	Shrinkage cracks Cracks perpendicular to braze layer Diffusion of Ni into C103
35Pd-65Au	2589	2628	Shrinkage voids - no cracks No diffusion of Au or Pd into Re or Cb Diffusion of Cb and Hf into braze
50Pd-50Au	2679	2702	Same results as 35Pd-65Au More diffusion of Cb and Hf into braze
Titanium	3020	3020	Cracks parallel to braze layer Not shrinkage cracks Brittle phase No diffusion of Ti into Re or Cb Cb and Hf diffusion into Ti

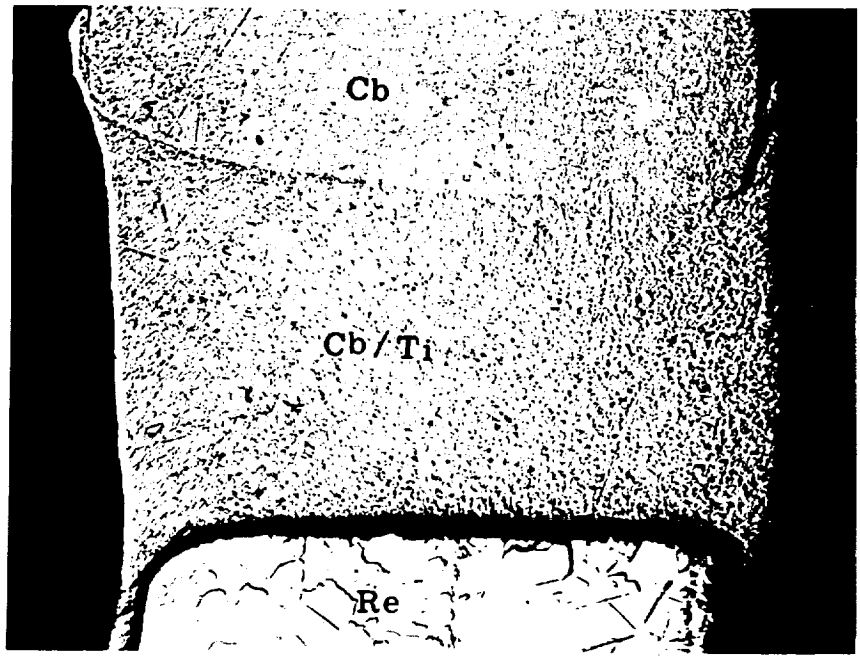

Figure 5.2-1. Microsection of weld sample 3. 50X.

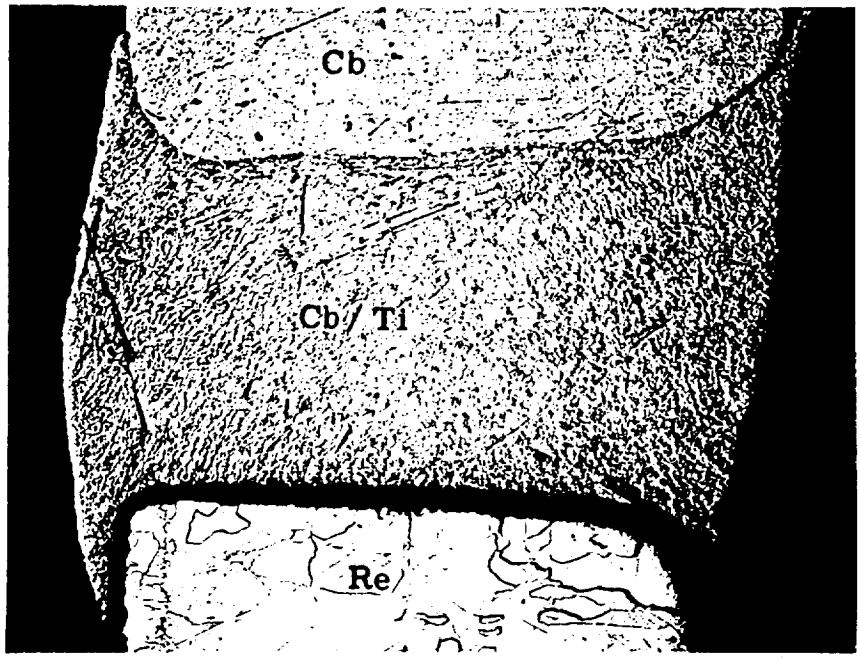

Figure 5.2-2. Microsection of weld sample 4. 50X.

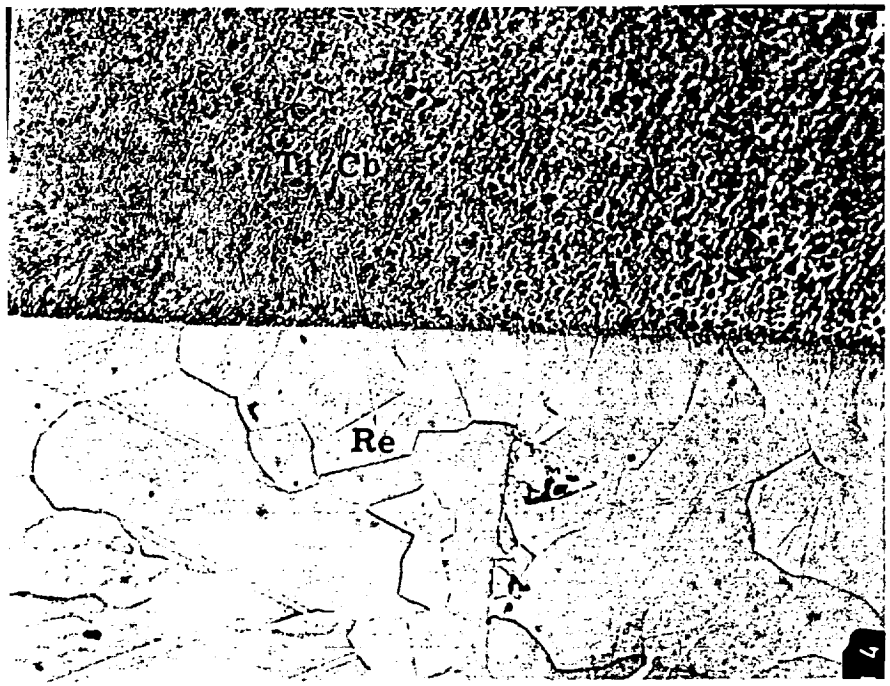

Figure 5.2-3. Detailed micrograph of weld sample 3 at the Ti/Re interface. 250X.

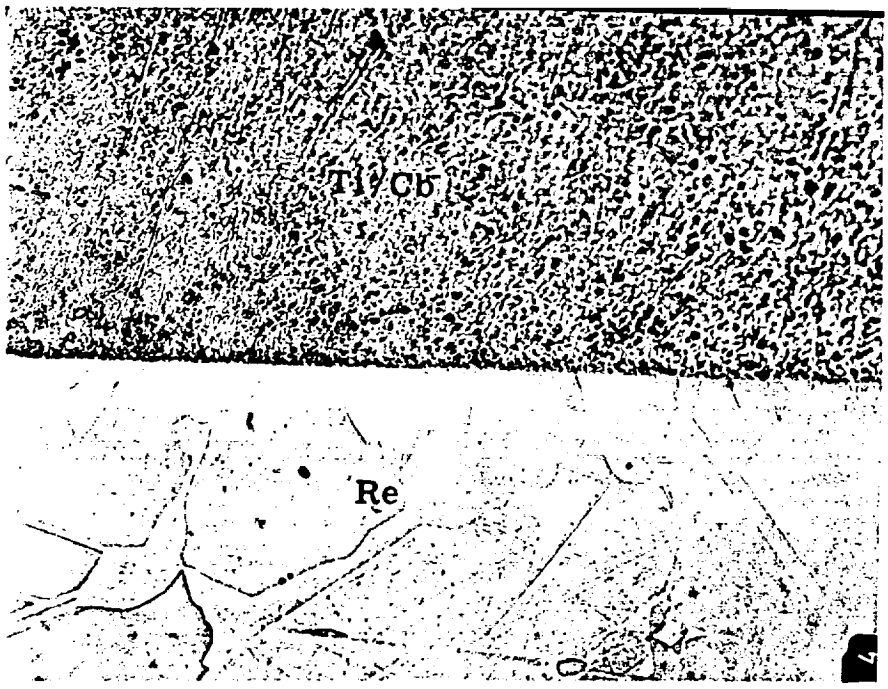

Figure 5.2-4. Detailed micrograph of weld sample 4 at the Ti/Re interface. 250X.

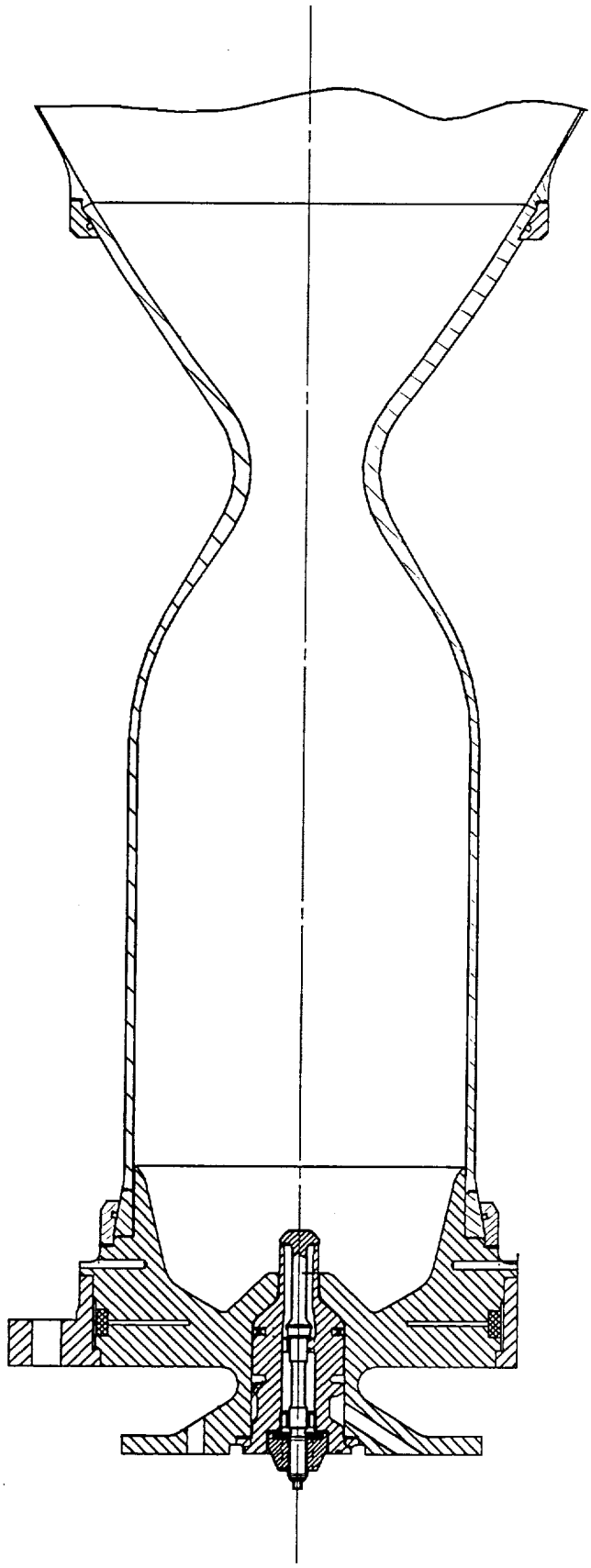

Figure 5.2-5. Thrust Chamber Joints.

6.0 CONCLUSIONS

Several conclusions can be drawn from the results of the SSRT program. With respect to the LO_2-N_2H_4 engine, performance of > 345 lbf-sec/lbm is feasible in a high temperature material thrust chamber (e.g., rhenium). However, the injector face must be protected to allow for operation without excessive temperatures. The thermal block concept without splash plate is the concept to be incorporated into the baseline injector for Option 2 Program. The injector element giving high performance which will be utilized for the baseline injector is the -11 hybrid which incorporates sixty slots.

The rhenium technology task generated several conclusions. Additional materials testing is required to obtain a better understanding of the materials properties. Other methods (non-CVD) of producing rhenium thrust chambers should be evaluated due to increasing material strength and the concern for multiple layers in the CVD process which have potential failure modes and potential problems with reproducibility.

7.0 RECOMMENDATIONS

The major recommendation based upon the Basic and Option 1 results is to continue the development of the Space Storable engine with Option 2. The emphasis on the Option 2 program is demonstrating an injector achieving high performance and dome temperatures compatible with the materials of construction and operability with LO_2-N_2H_4. The injector should them demonstrate operation in a high temperature material thrust chamber meeting the performance goal.

Another recommendation is to demonstrate operation of the injector in a high temperature material thrust chamber other than CVD rhenium.

The recommendation for Option 3 is to demonstrate an engineering model Space Storable engine (including valves) meeting high performance and thermal characteristics compatible with engine operation to allow verification and qualification beyond Option 3.

REPORT DOCUMENTATION PAGE

Form Approved
OMB No. 0704-0188

Public reporting burden for this collection of information is estimated to average 1 hour per response, including the time for reviewing instructions, searching existing data sources, gathering and maintaining the data needed, and completing and reviewing the collection of information. Send comments regarding this burden estimate or any other aspect of this collection of information, including suggestions for reducing this burden, to Washington Headquarters Services, Directorate for Information Operations and Reports, 1215 Jefferson Davis Highway, Suite 1204, Arlington, VA 22202-4302, and to the Office of Management and Budget, Paperwork Reduction Project (0704-0188), Washington, DC 20503.

1. AGENCY USE ONLY (*Leave blank*)	2. REPORT DATE	3. REPORT TYPE AND DATES COVERED
	5 August 1993	Final Contractor Report

4. TITLE AND SUBTITLE
Space Storable Rocket Technology
Final Report - Option 1 Program

5. FUNDING NUMBERS
WU-
Contract NAS 3-26246

6. AUTHOR(S)
Melvin L. Chazen
Thomas Mueller
Thomas Rust

7. PERFORMING ORGANIZATION NAME(S) AND ADDRESS(ES)
TRW Space & Technology Group
Applied Technology Division
One Space Park
Redondo Beach, CA

8. PERFORMING ORGANIZATION REPORT NUMBER
E- None

9. SPONSORING/MONITORING AGENCY NAMES(S) AND ADDRESS(ES)
National Aeronautics and Space Administration
Lewis Research Center
Cleveland, Ohio 44135-3191

10. SPONSORING/MONITORING AGENCY REPORT NUMBER
NASA CR- 191171

11. SUPPLEMENTARY NOTES
Project Manager - Mr. James A. Biaglow
Space Propulsion Technology Division
NASA-Lewis Research Center

12a. DISTRIBUTION/AVAILABILITY STATEMENT
Unclassified-Unlimited
Subject Category

12b. DISTRIBUTION CODE

13. ABSTRACT (*Maximum 200 words*)

The SSRT Option 1 Program has continued to establish a technology base for a new class high performance/long life LO2-N2H4 space storable engines. The Option 1 Program evaluated two new injector elements, two different methods of injector thermal protection, high temperature rhenium properties and methods of joining rhenium thrust chamber to columbium injector and nozzle. Additional critical experiments were conducted to evaluate the effects of GO2 injection into the chamber, GHe injection into the main LO2, splash plate effects and decreasing aspect ratio impact on the 120-slot element. Summarization of results follows: Decreasing the aspect ratio improved performance; however, the 60-slot hybrid injector was still best. Testing demonstrated LO2 conditions at injection was the performance driver. Both thermal block and film cooling adaptors demonstrated thermal stability but low performance due to low LO2 injection temperatures. GO2 injection downstream of LO2 injection and GHe injection into main LO2 demonstrated thermal stability but below maximum performance. Removal of splash plate improves performance. CVD rhenium properties were evaluated(70-3400F). Brazing was the effective method of joining rhenium to columbium. Performance >345 seconds(ϵ=204)was demonstrated-a 30-second improvement over best existing flight apogee engine.

14. SUBJECT TERMS
Rocket engines, Satellite propulsion, Bipropellant engines, Space storable, High performance engines, Long life engines.

15. NUMBER OF PAGES

16. PRICE CODE
A05

17. SECURITY CLASSIFICATION OF REPORT	18. SECURITY CLASSIFICATION OF THIS PAGE	19. SECURITY CLASSIFICATION OF ABSTRACT	20. LIMITATION OF ABSTRACT
Unclassified	Unclassified	Unclassified	SAR